DETERMINATION OF CURVED SURFACE SLIDER BEHAVIOR UNDER DIFFERENT LOADING CONDITIONS

PhD Dissertation

Esengül ÇAVDAR

Eskişehir 2025

DETERMINATION OF CURVED SURFACE SLIDER BEHAVIOR UNDER DIFFERENT LOADING CONDITIONS

Esengül ÇAVDAR

PhD Dissertation

Department of Civil Engineering

Programme in Mechanical

Supervisor: Prof. Dr. Gökhan ÖZDEMIR

Eskişehir

Eskişehir Technical University

Institute of Graduate Programs

April 2025

FINAL APPROVAL FOR THESIS

This thesis titled DETERMINATION OF CURVED SURFACE SLIDER BEHAVIOR UNDER DIFFERENT LOADING CONDITIONS has been prepared and submitted by Esengül ÇAVDAR in partial fulfillment of the requirements in "Eskişehir Technical University Directive on Graduate Education and Examination" for the Degree of PhD in Civil Engineering Department has been examined and approved on 10/04/2025.

Committee Members		Title, Name and Surname	Signature
Member	:	Prof. Dr. Gökhan ÖZDEMİR	
Member	:	Prof. Dr. Polat GÜLKAN	
Member	:	Prof. Dr. Uğurhan AKYÜZ	
Member	:	Prof. Dr. Beyhan BAYHAN	
Member	:	Dr. Öğr. Üyesi Fatih SÜTCÜ	

Prof. Dr. Harun BÖCÜK
Director of the Institute of Graduate Programs

10/04/2025

SUPERVISOR APPROVAL

PhD student Esengül ÇAVDAR, whom I supervise, has completed this thesis titled DETERMINATION OF CURVED SURFACE SLIDER BEHAVIOR UNDER DIFFERENT LOADING CONDITIONS. According to my inspections, the work is scientifically and ethically appropriate for the student to the thesis defense exam.

Supervisor
Prof. Dr. Gökhan ÖZDEMIR

ABSTRACT

DETERMINATION OF CURVED SURFACE SLIDER BEHAVIOR UNDER DIFFERENT LOADING CONDITIONS

Esengül ÇAVDAR

Department of Civil Engineering

Programme in Mechanical

Eskişehir Technical University, Institute of Graduate Programs, April 2025

Supervisor: Prof. Dr. Gökhan ÖZDEMIR

This study systematically investigates the variations in friction coefficient of both full-scale double-curved surface sliders and small-scale slider material under different loading conditions. First, wear tests were performed, and the corresponding friction coefficients obtained from full- and small-scale tests were compared. Second, full- and small-scale test results were used to assess the variations in static and dynamic friction coefficients under cyclic motions performed at both room- and low-temperature conditions. In the experimental program, not only the temperature and exposure time but also the normal stress level and the loading velocity were selected as parameters. Finally, a unified model was proposed to estimate the friction coefficient of full-scale isolator by means of small-scale test results. The key findings are as follows: (i) After 1000 m wearing tests, it seen that the hysteretic behavior of full-scale isolator remains unchanged. (ii) In low-temperature tests, due to formation of an ice layer at the sliding interface, which behaves like a lubricant, friction coefficients of both the isolator and the slider reduces substantially compared to ones obtained from room-temperature tests. (iii) Friction coefficients obtained from full- and small-scale tests (either wear or cyclic motion tests) results are very close to each other at room-temperature but not at low-temperature cases. (iv) The proposed formulation, which is calibrated based on small-scale test results, is accurate enough to estimate friction coefficients of full-scale isolator at room-temperature for a wide range of loading combinations.

Keywords: Curved surface slider, Friction coefficient, Wear tests, Low-temperature effects, Scale effects.

ÖZET

FARKLI YÜKLEME KOŞULLARI ALTINDA SÜRTÜNMELİ SARKAÇ TİPİ SİSMİK İZOLATÖR DAVRANIŞININ BELİRLENMESİ

Esengül ÇAVDAR

İnşaat Mühendisliği Anabilim Dalı

Mekanik Bilim Dalı

Eskişehir Teknik Üniversitesi, Lisansüstü Eğitim Enstitüsü, Nisan 2025

Danışman: Prof. Dr. Gökhan ÖZDEMIR

Bu çalışmada, farklı yükleme koşulları altında hem çift sürtünme yüzeyli kayıcı izolatörlerin hem de küçük ölçekli kayıcı malzemenin sürtünme katsayısındaki değişimler sistematik olarak incelenmiştir. İlk olarak, gerçekleştirilen aşınma testleri sonrasında izolatör testlerinden ve küçük ölçekli malzeme testlerinden elde edilen sürtünme katsayıları karşılaştırılmıştır. Daha sonra, izolatör ve küçük ölçekli malzeme test sonuçları, hem oda hem de düşük sıcaklık koşullarında gerçekleştirilen döngüsel hareketler altında statik ve dinamik sürtünme katsayılarındaki değişimleri belirlemek için kullanılmıştır. Gerçekleştirilen deneysel çalışmada, yalnızca sıcaklık ve maruz kalma süresi değil, aynı zamanda normal gerilme seviyesi ve yükleme hızı da birer parametre olarak seçilmiştir. Son olarak, küçük ölçekli malzeme test sonuçları vasıtasıyla sismik izolatöre ait sürtünme katsayısını tahmin edebilmek için bir model geliştirilmiştir. Bu çalışmadan elde edilen başlıca sonuçlar şu şekildedir: (i) 1000 m aşınma testlerinden sonra, sismik izolatörün histeretik davranışında bir değişiklik olmadığı görülmüştür. (ii) Düşük sıcaklık testlerinde, kayma arayüzünde oluşan buz tabakasının bir kayganlaştırıcı gibi davranması nedeniyle, hem izolatörün hem de küçük ölçekli malzemenin sürtünme katsayıları, oda sıcaklığında elde edilenlere kıyasla önemli ölçüde azalır. (iii) İzolatör ve küçük ölçekli malzeme testlerinden (aşınma veya döngüsel hareket testleri) elde edilen sürtünme katsayıları, oda sıcaklığında birbirine çok yakındır, ancak düşük sıcaklıklarda farklılık göstermektedirler. (iv) Küçük ölçekli test sonuçları kullanılarak kalibre edilen ve oda sıcaklığında izolatöre ait sürtünme katsayılarını tahmin etmek için önerilen formülasyon, geniş bir aralıktaki yükleme kombinasyonları için oldukça başarılı olmuştur.

Anahtar Sözcükler: Eğri yüzeyli kayıcı izolatör, Sürtünme katsayısı, Aşınma testleri, Düşük sıcaklık etkisi, Boyut etkisi.

ACKNOWLEDGEMENTS

This study was funded by the Disaster and Emergency Management Presidency (AFAD) National Earthquake Research Projects under grant number UDAP-Ç-21-35 to perform full-scale isolator tests. Additionally, I received a scholarship from the Turkish Scientific and Technical Research Council (TÜBİTAK) 2214-A International Research Fellowship Programme for PhD Students to perform small-scale experiments at Politecnico di Milano University. I gratefully acknowledge their support.

I would like to express my deepest gratitude to my supervisor, Prof. Dr. Gökhan Özdemir, for his unwavering support and guidance throughout my academic journey. His patience, dedication, and encouragement have greatly influenced my passion for research. I am grateful for his generosity in sharing his knowledge and experience, as well as his constant support, both academically and personally. I hold him in the highest regard and am profoundly thankful for all he has taught me, both professionally and personally.

I am also deeply grateful to the distinguished members of my thesis committee Prof. Dr. Polat Gülkan, Prof. Dr. Uğurhan Akyüz, Prof. Dr. Beyhan Bayhan, and Dr. Öğr. Üyesi Fatih Sütcü for their invaluable insights and contributions.

I would like to sincerely thank Prof. Dr. Virginio Quaglini his invaluable guidance and mentorship during my time at Politecnico di Milano, Italy.

I would like to express my heartfelt thanks to my colleagues, Osman Altuncu at Eskişehir Technical University in Türkiye and Daniele Ribolla at Politecnico di Milano in Italy, who worked alongside me in both laboratories. Their support, collaboration, and dedication were essential in completing the experiments and overcoming the challenges I encountered. I deeply appreciate their hard work and the valuable insights they provided throughout this process.

I would like to thank TIS Technological Isolation Systems for their valuable assistance in providing the materials necessary for conducting my experiments.

I would like to express my deepest gratitude to my family, —my mother, father, and sister— for their unwavering love, support, and encouragement throughout my academic journey. Their belief in me has been a constant source of strength and motivation

Esengül ÇAVDAR

10/04/2025

STATEMENT OF COMPLIANCE WITH ETHICAL PRINCIPLES AND RULES

I hereby truthfully declare that this thesis is an original work prepared by me; that I have behaved in accordance with the scientific ethical principles and rules throughout the stages of preparation, data collection, analysis and presentation of my work; that I have cited the sources of all the data and information that could be obtained within the scope of this study, and included these sources in the references section; and that this study has been scanned for plagiarism with "scientific plagiarism detection program" used by Eskişehir Technical University, and that "it does not have any plagiarism" whatsoever. I also declare that, if a case contrary to my declaration is detected in my work at any time, I hereby express my consent to all the ethical and legal consequences that are involved.

Esengül ÇAVDAR

CONTENTS

Page

LIST OF TABLES

Page

LIST OF FIGURES

GLOSSARY OF SYMBOLS AND ABBREVIATIONS

CSS	:	Curved Surface Slider
DCSS	:	Double Curved Surface Slider
FPS	:	Friction Pendulum System
HDPE	:	High-Density Polyethylene
LDPE	:	Low-Density Polyethylene
MDPE	:	Medium-Density Polyethylene
PA	:	Polyamide
PE	:	Polyethylene
PTFE	:	Polytetrafluorethane
TCSS	:	Triple Curved Surface Slider
UHMWPE	:	Ultra-high-molecular-weight polyethylene
EDC	:	Energy dissipated per cycle
u_1	:	Displacement of top plate
u_2	:	Displacement of bottom plate
2d	:	Total displacement of both top and bottom surfaces
d	:	Maximum displacement capacity of a single concave surface
d_{max}	:	Displacement amplitude of the horizontal motion for sliding material tests
D_{max}	:	Maximum displacement value on the F-D curve
D_{min}	:	Minimum displacement value on the F-D curve
F_h	:	Horizontal force acting on the sliding material
F	:	Horizontal force acting on a sliding body
F_v	:	Vertical force acting on the sliding material
f	:	Frequency of loading
F_1	:	Horizontal force acting on the top surface of isolator
F_2	:	Horizontal force acting on the bottom surface of isolator
F_{dyn}	:	Lateral force recorded during sliding
F_f	:	Frictional force
F_{f1}	:	Friction force at the top contact interface
F_{f2}	:	Friction force at the bottom contact interface
Fr	:	Restoring force

F_{st}	:	Lateral force measured at motion reversals
h_1	:	Half of the slider's height
h_2	:	Half of the slider's height
k_{eff}	:	Horizontal stiffness of the isolation system
N	:	Axial load applied to the specimen
p	:	Applied contact pressure
q	:	Heat flux
R_1	:	Radius of curvature of the top concave surface
R_2	:	Radius of curvature of the bottom concave surface
R_{eff}	:	Effective radius of curvature
R_a	:	Arithmetic Mean Roughness of stainless steel surface
R_z	:	Surface roughness of stainless steel surface
S_1	:	Vertical force component of the axial pressure
S_x	:	Sliding path
T_{iso}	:	Period of the isolated structure
W	:	Vertical load
α	:	Radius of the slider
ΔT	:	Temperature rise at the mating surface
λ	:	Property modification factor
μ	:	Friction coefficient
μ_1	:	Friction coefficient of the top contact interface
μ_2	:	Friction coefficient of the bottom contact interface
μ_{ave}	:	Average dynamic friction coefficient
μ_B	:	Breakaway friction coefficient of sliding material
μ_{LV}	:	Dynamic friction coefficient of sliding material at low velocity region
μ_{HV}	:	Dynamic friction coefficient of sliding material at high velocity region
μ_{dyn}	:	Dynamic friction coefficient
μ_{eff}	:	Effective coefficient of friction of isolation device
μ_M	:	Friction coefficient of sliding material
μ_{reff}	:	Reference friction coefficient
μ_{pv}	:	The friction coefficient of the sliding material, calculated in the first cycle using the proposed formula

μ_{st}	:	Static friction coefficient
u	:	Total displacement of slider
v	:	Velocity of the slider
β_1	:	A transition rate parameter relating the transition between the low velocity and the high velocity regimes
β_2	:	A transition rate parameter relating the transition between the static to dynamic regimes
$c(ED)$	:	Degradation function
γ	:	A parameter that controls the rate of degradation of the coefficient of friction

1. INTRODUCTION

1.1. Seismic Isolation

Seismic isolation systems are among the most effective methods for protecting structural and non-structural components, as well as equipment housed within buildings, from potential earthquake-induced motions (Constantinou 1994; Naim and Kelly 1999; Ozdemir and Constantinou 2010; Calvi et al. 2017; Quaglini et al. 2019). The basic concept behind seismic isolation involves a system that mitigates the effects of ground acceleration by using low horizontal stiffness devices placed between the superstructure and its foundation. This application results in the isolated structure effectively shifting the fundamental period away from the dominant periods of the ground motions (see Figure 1.1), thereby significantly minimizing the floor accelerations, interstory drifts and seismic forces. The reduced seismic forces result in a superior performance of the superstructure during a seismic action compared to its fixed-base counterpart.

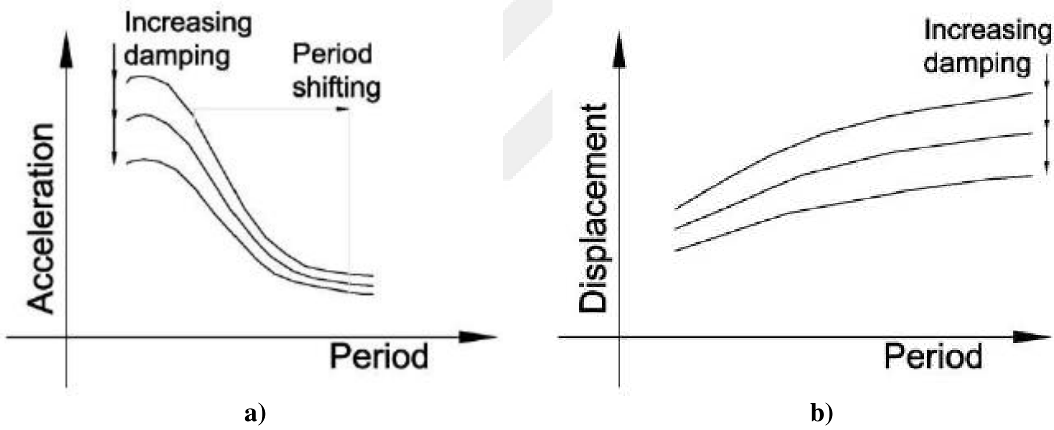

Figure 1.1. *Basic concept of seismic isolation: a) shifting the fundamental period of the structure to a longer period range, b) controlling excessive displacement through increased damping (adapted from Skinner et al. 1993)*

The primary design consideration in structures with a seismic isolation system is the maximum displacement that will occur at the isolation level. This displacement value is crucial for determining the shear force transferred from the superstructure, the necessary seismic gap around the structure to allow free movement, and the geometric properties of the isolators to be used. An increase in the period and the corresponding increase in flexibility result in larger displacements at the isolation level. However, as shown in Figure 1.1, increasing the damping ratio helps to mitigate excessive horizontal movements.

Seismic protection techniques date back to early historical periods, with the first recorded applications found in Ancient Greece around 440 BC. Over time, advancements in construction and material technologies have evolved the concept of seismic protection. Initially focused solely on protecting structural members, the modern approach has expanded to encompass the protection of non-structural components as well. New construction techniques, such as seismic isolation, now integrate both structural and non-structural protection into the design phase.

Today, one of the most widely utilized types of isolation devices is elastomeric bearings, which may or may not include a lead core (Pavese et al. 2019; Ponzo et al. 2021; Yaşar et al. 2023a; Yasar et al. 2023b). In addition to elastomeric bearings, sliding bearings with curved surfaces have become increasingly popular (Calvi and Calvi, 2018; Barone et al., 2019). Among these isolation devices, the Curved Surface Slider (CSS) stands out due to its simplicity and widespread use.

1.2. Curved Surface Slider

The Curved Surface Slider (CSS), first introduced in the 1980s in North America as the Friction Pendulum System® (FPS) by Victor Zayas (Zayas et al. 1987a), represents a significant advancement in seismic isolation technology. A patent application was submitted on December 12, 1985, and granted on February 24, 1987 (Zayas et al. 1987b). Zayas clarified the operational principles, design methodology, modeling techniques, and testing procedures for this system in a comprehensive report and article (Zayas et al., 1987a; Zayas et al 1990).

In its basic form, the CSS comprises an articulated slider and two concave plates that create two sliding surfaces. The primary surface handles horizontal displacements, while the secondary surface accommodates rotational movements (Figure 1.2). A self-lubricating thermoplastic material (filled Polytetrafluorethane-PTFE) lines the slider's contact area with the primary surface, facilitating energy dissipation during sliding. Due to the sliding taking place on a single surface (the primary surface), this type of isolation unit is referred to as a Single CSS. Furthermore, the patent proposed by Zayas involves the use of filled Polytetrafluorethane (PTFE with reinforcing fiber and lead-filled porous bronze) (Evans and Senior 1982) for the isolation device. Such material was chosen for its high load bearing capacity and energy dissipation capacity, while providing a low friction coefficient. A number of self-lubricating materials with enhanced sliding properties have been later proposed, like, e.g. Ultra-high-molecular-weight polyethylene (UHMWPE), polyethylene (PE) and polyamide (PA) (Calvi and Calvi 2018; Barone et al. 2019). Details on self-lubricating materials, specifically, are provided in subsequent sections.

CSSs are designed to integrate four essential functions of an isolation system within a compact design: supporting vertical loads from the superstructure, accommodating lateral displacements, dissipating seismic energy, and enabling re-centering capability. Advanced versions of CSSs, such as the Double CSS (Fenz and Constantinou 2006; Bao et al 2017), which doubles the displacement capacity of the single-surface version, and the Triple CSS (Becker and Mahir 2012; Sarlis, et al. 2013; Becker et al 2017), featuring adaptive stiffness and damping based on excitation intensity, follow the same fundamental mechanical principles despite their enhanced features.

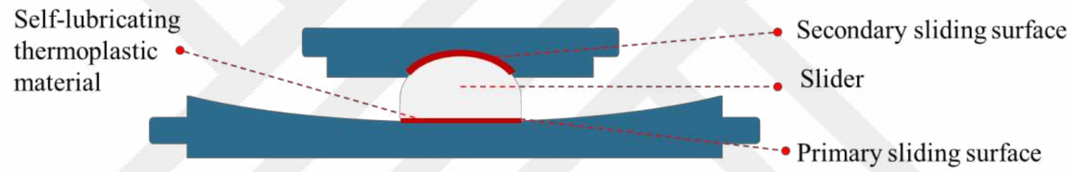

Figure 1.2. *Structure of a Single CSS*

The design of a CSS is relatively simple, based on two key parameters: the radius of the concave plate and the friction coefficient at the sliding interface. The radius of the concave plate defines the isolation period of the system, while the friction coefficient governs the energy dissipation of the isolation unit. Consequently, the hysteretic behavior of CSSs is primarily influenced by any parameter that changes the friction properties at the sliding interface of the isolation unit. Key factors include axial pressure, sliding velocity, temperature, environmental effects, wear, and contamination (Campbell et al. 1993; Constantinou et al. 1999; Dolce et al. 2005; Quaglini et al. 2009; Quaglini et al. 2012; Quaglini et al. 2014; Furinghetti et al. 2019; De Domenico et al. 2019). To accurately predict the hysteretic behavior of CSSs, it is essential to conduct tests under representative load and displacement conditions that align with the isolator's intended purpose and design.

The practical implementation of single CSS systems exhibits limitations in specific areas or ground motion scenarios (Pranesh and Sinha 2000; Shakib and Fuladgar 2003; Fenz and Constantinou 2008). These limitations are primarily related to the system's displacement capacity and energy dissipation effectiveness under various seismic conditions. As a result, there has been a need for more effective and adaptable isolation units that can perform better across a wider range of ground motions.

To address these limitations, researchers have developed isolators featuring multiple sliding surfaces, such as the Double Curved Surface Slider (DCSS). This system is designed to increase the displacement capacity and improve the energy dissipation capabilities compared to the single CSS. The Triple Curved Surface Slider (TCSS), which includes three sliding surfaces, also follows similar principles but is not the primary focus of this study.

The DCSS, with its double concave friction surfaces, provides a more effective solution to the limitations of single CSS units. The following subsection provides a comprehensive analysis of the DCSS system, highlighting its mechanical principles, advantages, and performance.

1.2.1. Double curved surface slider (DCSS)

Over a century ago, seismic isolators featuring double curved surface sliders were conceived and patented in the United States (Touaillon 1870; Bechtold 1907) and Europe (Barucci 1990). Nevertheless, the contemporary DCSS required substantial time for development, implementation, and testing. The initial DCSS was created, evaluated, and successfully employed in a Japanese building in 2001 (Hyakuda et al 2001). The primary goal in developing the DCSS was to achieve almost double the sliding capacity of traditional CSSs. To achieve this, Hyakuda et al (2001) designed a non-articulated slider with concave sliding surfaces possessing identical radii and friction coefficients, effectively attaining the desired high displacement capacity. However, it is to be noted that when friction coefficients at two sliding interfaces of the DCSS, the articulation becomes essential (Zhang and Ali 2021). An articulated slider facilitates the synchronization of upper and lower isolator component rotations, preventing excessive wear by evenly distributing forces across the surfaces. Similarly, Tsai et al (2003; 2006) conducted additional experimental and numerical investigations of the same isolation concept, though these studies were limited to isolators with equal friction coefficients and radii. Fenz et al. (2008) conducted a more extensive investigation that focused on the cyclic behavior of DCSSs, considering various factors that influence the force-displacement relations of isolators. Their study encompassed the effects of varying radii of curvature, unequal friction coefficients on the contact surface, the height of the articulated slider, and the impact of the articulated slider's friction coefficient. The primary advantage of DCSS systems over their CSS counterparts is the cost reduction resulting from their more compact size, as smaller bearings directly translate to lower expenses. Figure 1.3 shows modern DCSS isolators and their key components currently employed in engineering practices.

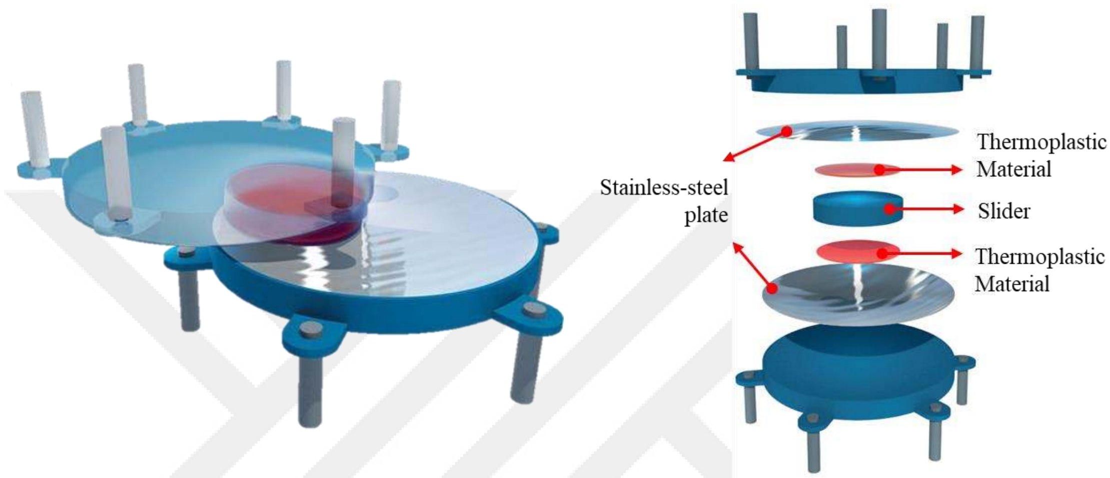

Figure 1.3. *DCSS and its basic components (http-1, http-2)*

1.2.1.1. Hysteretic behavior of DCSS

This section presents the hysteretic behavior of double curved surface slider, which is the primary focus of the experimental studies in this PhD thesis. The mathematical formulations presented here are adaptable to other CSSs.

Double curved surface slider, as shown in Figure 1.3, consist of two concave stainless-steel surfaces and a slider. The radius of curvature of the concave surfaces are R_1 and R_2, whereas the friction coefficients at the contact interfaces with the sliding surface are μ_1 and μ_2, which can be either identical or different. Figure 1.4 illustrates cross-sections corresponding to various displacement regimes of a DCSS. Specifically, Figure 1.4.a shows the cross-section of the isolator in its initial position (zero displacement), while Figure 1.4.b depicts the isolator at its maximum displacement. Here, d represents the maximum displacement capacity of a single concave surface, and the total displacement of both top and bottom surface is calculated as 2d. To derive the force-displacement relationship for a DCSS, free-body diagram of top and bottom concave plates is analyzed separately. Then, the overall relationship for the isolator is established based on equilibrium and compatibility conditions. Figure 1.5 presents a free-body diagram of the slider considering the displaced position of top concave plate. In Figure 1.5, forces acting on the slider include the vertical load W, acting on the center of the slider, the horizontal force F_1, the friction force at the contact surface F_{f1}, and the vertical force component of the axial pressure S_1.

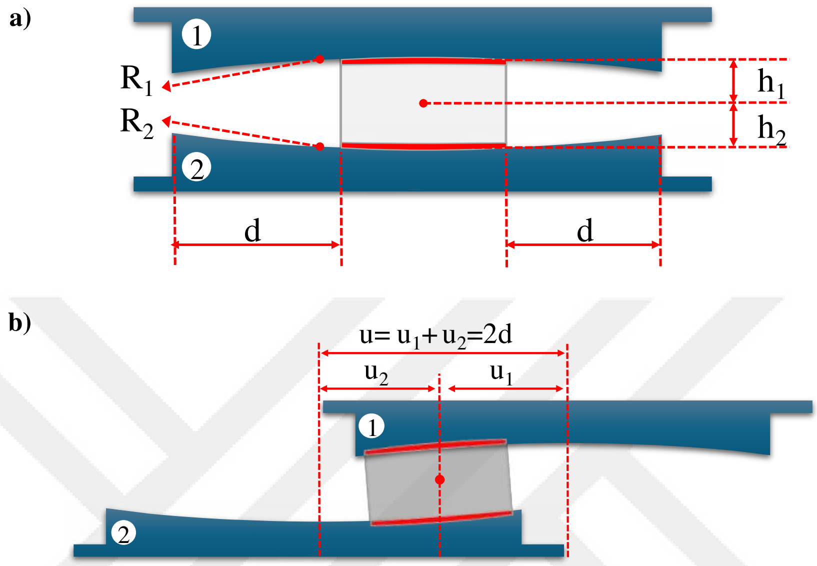

Figure 1.4. *Theoretical relationship for double curved surface slider*

Considering the force equilibriums in both horizontal ($\sum F_x = 0$) and vertical ($\sum F_y = 0$) directions yields the following mathematical expressions:

$$F_1 - S_1 \sin\theta_1 - F_{f1} \cos\theta_1 = 0 \tag{1.1}$$

$$W - S_1 \cos\theta_1 + F_{f1} \sin\theta_1 = 0 \tag{1.2}$$

As a consequence of geometric compatibility, the slider's movement on the top plate:

$$u_1 = (R_1 - h_1) \sin\theta_1 \tag{1.3}$$

In Eqn. (1.3), R_1-h_1 represents the distance between the center of the concave surface and the center of the slider.

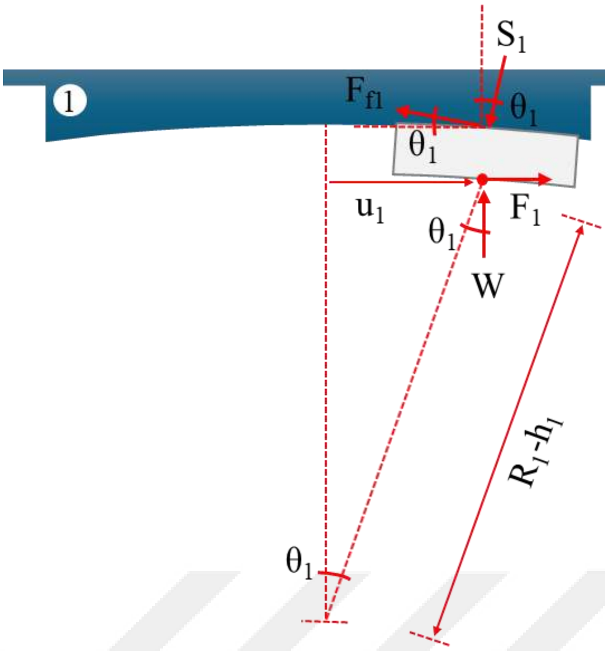

Figure 1.5. *Free body diagram of the top plate of a double curved surface slider*

The force-displacement relationship for the top plate is derived by combining Eqns. (1.1), (1.2), and (1.3). Following a similar process for the bottom plate, Eqns. (1.4) and (1.5) are established for the entire double curved surface slider.

$$F_1 = \frac{W}{R_1 - h_1} u_1 + F_{f1} \tag{1.4}$$

$$F_2 = \frac{W}{R_2 - h_2} u_2 + F_{f2} \tag{1.5}$$

Since the total displacement, u, of the isolator is equal to sum of the displacements of both top and bottom plates:

$$u = u_1 + u_2 \tag{1.6}$$

where

$$u_1 = \left(\frac{F - F_{f1}}{W}\right)(R_1 - h_1) \tag{1.7}$$

$$u_2 = \left(\frac{F - F_{f2}}{W}\right)(R_2 - h_2) \tag{1.8}$$

The friction coefficient at each contact surface is calculated by dividing the friction force by the vertical load.; $\mu_1 = F_{f1}/W$ and $\mu_2 = F_{f2}/W$. On the other hand, considering the equilibrium of the forces ($F = F_1 = F_2$) acting on the slider in the horizontal direction, the force-displacement relation for the entire isolator will be as follows:

$$F = \left(\frac{W}{R_1 + R_2 - h_1 - h_2}\right) u + \left(\frac{F_{f1}(R_1 - h_1) + F_{f2}(R_2 - h_2)}{R_1 + R_2 - h_1 - h_2}\right) \quad (1.9)$$

In the above equation, the term $(R_1 + R_2 - h_1 - h_2)$ is defined as the effective radius of curvature R_{eff} of the sliding surfaces. The second part of Equation 1.9, divided by the vertical load, W, gives the effective coefficient of friction (μ_{eff}) of the isolator.

$$\mu_{eff} = \frac{\mu_1 R_1 + \mu_2 R_2}{R_1 + R_2 - h_1 - h_2} \quad (1.10)$$

Equation 1.11 provides the terms that define the force-displacement relation of the isolator unit. In Eqn. (1.11), the first term represents the restoring force (F_r) provided by the concave surface based on the pendulum mechanism, and the second term denotes the frictional force (F_f) activated at the sliding interface.

$$F = F_r + F_f = \frac{W}{R_{eff}} u + \mu_{eff} W \cdot sgn\,(v) \quad (1.11)$$

where v and sgn(·) are velocity of the slider and the signum function, respectively. In Eqn. (1.11), W/R_{eff} is equal to the horizontal stiffness (k_{eff}) of the isolation system. Thus, period of the isolated structure will be $T_{iso} = 2\pi\sqrt{\frac{R_{eff}}{g}}$. Figure 1.6 illustrates the correspondence of the terms defined in Eqn. (1.11) on the force-displacement relationship of a DCSS.

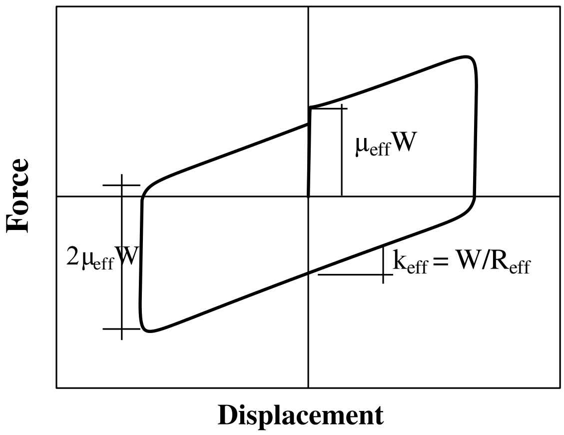

Figure 1.6. *Representative bi-linear force-displacement curve of DCSS*

1.2.2. Self-lubricating thermoplastic materials used in CSSs

Friction represents a nonconservative force that dissipates energy in various forms. This energy dissipation can occur through mechanisms such as heat generation, material wear, and molecular interactions, which are influenced by factors including the coefficient of friction and loading conditions. To address this issue, researchers have developed self-lubricating polymeric materials that prevent wear-related failures caused by insufficient lubrication, enhance wear resistance, reduce friction, and adapt to extreme conditions, thereby improving overall performance (Ozdemir et al 2024). These materials are developed by incorporating solid lubricants into various matrices, including metal, polymer, and ceramic, for applications that require lubrication (Evans and Seniro 1982). The solid lubricant component in these materials forms a lubricating layer through tribo-chemical reactions, ensuring a constant supply of lubricant at the interface (John and Menezes 2021). Self-lubricating materials not only offer superior lubrication properties but are also characterized by their ability to withstand potential damage, such as cold welding, scratching, and adhesion, which may occur during friction between two surfaces without lubrication. Furthermore, these materials exhibit excellent tribological properties under extreme conditions, including high speeds, high temperatures, and heavy loads (Kasar et al 2024).

Polytetrafluoroethylene (PTFE) is a well-known self-lubricated material used to provide low friction at the sliding interfaces of CSSs. It is made up of carbon and fluorine atoms. PTFE is preferred because of its low friction coefficient, low surface tension and the absence of stick-slip motion (Evans and Senior 1982). Practical application temperatures range from -100°C to 250°C. However, unfilled PTFE does not have a higher load-bearing capacity or durability compared to other alternatives, and it wears out quickly under dry conditions. Low thermal conductivity of unfilled PTFE prevents heat dissipation, potentially leading to premature failure due to melting (Menezes et al 2018). As a result, its use is limited to low-velocity sliding applications. On the other hand, by adding various filler materials, mechanical properties (such as load-bearing capacity, wear rate, etc.) can be improved without compromising its friction characteristics. This is the reason behind the use of filled PTFE in curved surface sliders, rather than unfilled PTFE.

Polyethylene (PE), a type of plastic, comprises a mixture of similar polymers of ethylene (Whiteley et al 2000). The mechanical properties and strength of polyethylene are associated with its molecular weight, the type of bonding of atoms and the presence of long chain molecular structures (Kaiser 2023). It is available in various forms: Low-Density Polyethylene (LDPE), Medium-Density Polyethylene (MDPE), and High-Density Polyethylene (HDPE). Each type exhibits different melting points (LDPE 105°C, MDPE 120°C, HDPE 130°C) and mechanical properties. Consequently, the selection of an appropriate type of PE is crucial, depending on its intended application. Ultra-High-Molecular-Weight Polyethylene (UHMWPE) is a variant of polyethylene with a molecular weight ranging from 3.5 to 7.5 million atomic mass units (amu) (Kurtz 2015). Due to its high molecular weight, it is characterized as an exceptionally durable material. As a result, its properties, such as resistance to cutting, wear, and chemicals, make it suitable for CSS applications.

Polyamides (PA) represent an additional category of plastics utilized for sliding surfaces in CSS. These materials exhibit superior characteristics, including high tensile strength, hardness, high melting points, and resistance to chemicals, which make them adaptable for numerous applications (Palmer 2001). Similar to other thermoplastics, the properties of PA can fluctuate based on several factors, such as molecular weight, moisture content, temperature, and the incorporation of additives (Kang and Park 2010; Touris et al 2020).

The fundamental properties of these thermoplastic materials are provided in Table 1.1 (Calvi and Calvi 2018). However, even though some of them proved to be operational under extreme conditions (Calvi and Calvi 2018), the selection of viable sliding material is still a critical task. The sliding material for CSSs shall fit different requirements related to both service and seismic conditions. It shall provide low sliding resistance combined with high wear endurance at low velocities in order to accommodate service movements. Furthermore, it shall ensure a stable coefficient of friction at high velocities necessary to provide the required level of damping (Quaglini et al. 2017a; Quaglini, et al. 2012a).

Table 1.1. *Properties of thermoplastic materials utilized for CSS (adapted from Calvi and Calvi 2018)*

	PTFE	PE	UHMWPE	PA
Unit mass (kg/mm^3)	2200	900	950	1100
Melting Temperature (°C)	335	120	130-136	200-350
Unconfined compression strength (MPa)	25	12-33	38-50	55-220
Friction coefficient on polished steel (%)	5-10	15	5-10	10-20

1.3. Friction Phenomena

Friction is a force defined as the resistance experienced when one object moves across another. This comprehensive explanation covers two primary categories of relative motion: sliding and rolling. Although it is beneficial to differentiate between sliding and rolling friction, these two phenomena are not entirely separate, and even seemingly 'pure' rolling generally involves an element of sliding. As depicted in Figure 1.7, both ideal rolling and sliding scenarios require a tangential force F to move the upper body over the fixed surface. The coefficient of friction, typically denoted by μ, is defined as the ratio between this frictional force and the normal load W:

$$\mu = \frac{F}{W} \tag{1.12}$$

The coefficient of friction is used to quantify the strength of frictional forces. This value can range significantly, from as low as 0.001% in a lightly loaded rolling bearing to exceeding 10% for identical clean metal surfaces sliding in a vacuum. However, for most common materials sliding in air without lubrication, the coefficient of friction typically falls between 0.1 and 1% (Hutching and Shipway 2017).

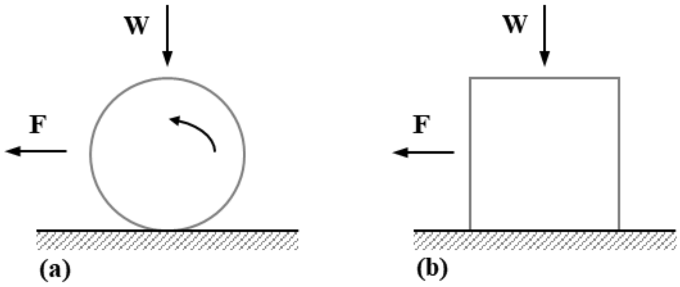

Figure 1.7. *Force, F, needed to overcome friction and start motion by a) rolling or b) sliding adapted from (Hutching and Shipway 2017)*

1.3.1. Dry friction: A basic overview

The earliest documented investigations on friction are credited to Leonardo da Vinci (1452-1519). These initial observations were later expanded upon by Amontons (1663-1706) (Amontons 1699). Then, Coulomb subsequently contributed that friction force remains unaffected by any change in velocity and provided theoretical models for friction (Dowson 1979). These fundamental observations, as documented by Amontons and Coulomb, can be summarized as follows:

- Frictional force is directly proportional to the normal force applied,
- The magnitude of friction is not influenced by the size of the contact area between surfaces,
- Friction force remains constant regardless of velocity (known as Coulomb friction).

However, friction is influenced by various parameters, including lubrication, elastic deformation, velocity, material heterogeneity, and contact area (Archard 1957; Hornbogen 1986; Narisawa 1993; Otsuki and Matsukawa 2012; Tiwari et al. 2018; Bai et al. 2021; Mirzaev et al. 2024). The general findings of these experimental studies indicate that Amontons' laws are valid under specific conditions, including dry friction, absence of elastic deformation, low-speed motions, homogeneous surfaces with ideal roughness, and macroscopic-scale contact (Gao et al. 2004). Because, real systems differ from Amontons' ideal conditions, indicating that ideal friction laws are only applicable under specific circumstances (Apostoli et al 2017). On the other hand, the third law of friction is less well-founded than the first two laws, and many studies have obtained results that contradict this law (discussed in the next section). Common observations demonstrate that the friction force needed to start sliding typically greater than the friction force required to continue sliding (Hutching and Shipway 2017). Consequently, friction is understood to have two distinct phases: *static friction* (μ_{st}) and *dynamic friction* (μ_{dyn}).

In the context of CSSs, static friction (μ_{st}) is defined as the friction at the initiation of motion, or at any instant when a temporary stop of sliding occurs (such as at motion reversal), while dynamic friction (μ_{dyn}) is activated during continuous sliding. Static friction is caused by the chemical bonds that form between the mating surfaces that stick to each other, in absence of relative motion. Since the number and strength of these bonds increase with the duration of sticking, the static friction coefficient (μ_{st}) at the breakaway is generally larger than the ones at motion reversal (Gandelli and Quaglini 2018). For CSSs at the motion reversal point, where the sliding velocity V ≈ 0, the frictional force reaches its maximum value, causing the contacting surfaces to temporarily adhere to each other. Following this, at V = 0, there is an instant stop, and as the frictional force changes direction, the surfaces continue to slide over each other. This phenomenon, where the sliding interface alternate between sticking and slipping, is referred to as *stick-slip behavior* in the literature.

While the static friction governs the transition from sticking to sliding at the breakaway, the operational performance of CSSs is determined by dynamic friction. Sliding is triggered when the horizontal force due to seismic action overcomes the resistance provided by the static friction; as long as the ground-motion acceleration is not able to overcome this resistance (as it may occur in case of low or mild intensity earthquakes, or high values of μ_{st}), the isolator remains in the sticking phase and the superstructure behaves like a fixed base structure (Gandelli and Quaglini 2018; Gandelli et al 2019; Gandelli et al 2020). Static and dynamic frictions are clearly shown on the isolator force-displacement curve in Figure 1.8, where HV and LV represent the value of the dynamic friction coefficient (μ_{dyn}) in the high and low velocity region respectively.

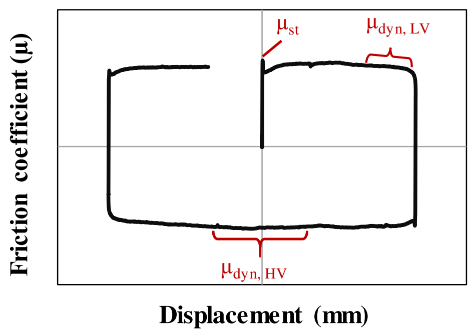

Figure 1.8. *Typical frictional behaviour of a CSS during cyclic motion*

1.3.2. The role of different parameters in friction coefficient – Previous research

The coefficient of friction at the interface between the slider and the mating concave surface controls the energy dissipation and affects the recentering capability of CSSs (Quaglini et al. 2017a; Quaglini et al. 2017b; Quaglini et al. 2019) and this phenomena is sensitive to a number of factors including axial pressure, sliding velocity, contact surface temperature, cycling, wear, low air temperature (Campbell et al 1993; Constantinou et al. 1999; Dolce et al 2005; Quaglini et al. 2009; Quaglini et al 2012a; Quaglini et al 2014; Furinghetti 2019; De Domenico 2019). This section provides a comprehensive examination of how these parameters affect the coefficient of friction, with a thorough review of previous studies conducted in this field under each topic.

1.3.2.1. Effect of axial pressure

Research studies on isolators with different sliding interface combinations have demonstrated that the dynamic coefficient of friction (μ_{dyn}) tends to decrease as axial pressure increases. This behavior can be explained by several interconnected mechanisms that affect material interactions at the contact surface. As pressure rises, changes in the real contact area and material properties contribute to a reduction in friction. Specifically, greater axial pressure increases the actual contact area between surfaces, enabling a more uniform load distribution and minimizing localized stress concentrations (Białas et al., 2021). Additionally, the deformation of surface asperities under higher pressures results in a smoother contact interface, further lowering friction (Białas et al., 2021). The role of lubricants is also significant; their performance often improves under increased pressure, leading to enhanced lubrication and a corresponding decrease in friction (Workel et al., 2000; Bijelić et al., 2017). Experimental investigations have provided valuable insights into these mechanisms, confirming the pressure-dependent variation in the coefficient of friction and highlighting the complex interplay of surface, material, and lubrication factors. Specifically, Tyler (1977) conducted experiments on small-scale PTFE and steel specimens under simulated earthquake conditions to evaluate the frictional properties of PTFE materials. Tests were performed at temperatures of 0°C and 20°C and pressures ranging from 15 to 31 MPa. The results showed that as normal pressure increases, the coefficient of friction decreases.

Another study conducted by Constantinou (1994) has examined the friction characteristics of PTFE and PTFE-based composites when in contact with polished stainless steel. The investigation differentiates between static (breakaway) and sliding friction coefficients, exploring their relationship with variables such as pressure, surface roughness, and temperature. The findings indicate that the friction coefficient decreases as bearing pressure increases across all sliding velocities.

Mokha et al. (1990) analyzed the friction properties of Teflon-steel interfaces in sliding bearings for base isolation systems. Their study focused on the effects of sliding velocity, bearing pressure, and Teflon type on friction. Laboratory tests conducted at pressures ranging from 6.9 to 44.8 MPa and sliding velocities between 2.54 and 500 mm/s demonstrated that friction decreases with increasing pressure. The unfilled Teflon exhibited lower friction than glass-filled Teflon, although this difference became less significant at higher pressures. The breakaway coefficient of friction was notably higher than the sliding coefficient.

Barone et al. (2019) performed over 1000 dynamic tests on 60 types of spherical friction-based isolation devices at the EUCENTRE laboratory, using polyamide (PA) and polyethylene (PE) materials. The study analyzed the impact of sliding velocity and contact pressure on the dynamic friction coefficient. Findings showed that normal force influences the friction coefficient by changing the contact pressure, especially during the transition from static to dynamic friction. Additionally, the breakaway friction coefficient, affected by normal force, plays a crucial role in the first loading cycle.

Lin et al. (2020) introduced a novel base isolation system, the bidirectional variable curvature friction pendulum bearing (BD-VCFPB), for large structures. Through dynamic cyclic testing, they investigated the performance of the sliding interface and the forces on the PTFE component. Their findings led to the development of a hysteretic model, which showed a strong correlation with both unidirectional and bidirectional experimental data. The study revealed that the friction coefficient of the curved surface slider is greatly influenced by the applied normal force and the contact pressure on the PTFE surface.

Pigouni et al. (2020) examined the friction behavior of full-scale DCSS isolators following the CEN 2009 standards. According to the author's results, the normal force (vertical load) applied has a substantial impact on the friction coefficient of curved surface sliders. The study found that vertical load has a more significant influence on the friction coefficient than sliding velocity, emphasizing the need to understand the interaction between the friction coefficient and vertical load for accurate performance evaluation of friction pendulum systems.

Furinghetti et al. (2021) focused on the behavior of CSSs under seismic activity, particularly when displacement demands exceed their maximum geometric capabilities. The study investigated the performance of CSS devices using PTFE-based materials with varying friction coefficients (5%, 3%, 1%) during cyclical testing. The research also developed computational models to simulate extra-stroke displacement characteristics, enhancing the understanding of CSSs' dynamic behavior. Findings showed that increased axial pressure reduces the friction coefficient by smoothing the polymeric surface, which affects the force-displacement behavior during seismic events.

Cavdar et al. (2022) focused on the effect of vertical force on the frictional properties of DCSS through displacement-controlled dynamic tests. The tests, simulating seismic conditions, assessed the friction coefficient degradation over three loading cycles, with varying vertical forces and loading velocities. The results revealed that vertical force significantly influences frictional heating, which in turn affects the overall hysteresis behavior of the isolator.

1.3.2.2. Effect of sliding velocity

Experimental studies highlighted that current sliding materials do not follow the classic Coulomb's law (i.e., constant friction) but are characterized by a more complex behavior (Constantinou et al. 1990; Berto et al. 2013; Quaglini et al. 2019). According to experimental research, the friction coefficient increases with increasing sliding velocities up to a certain threshold, beyond which it remains almost constant (Mokha 1990; Dolce 2005; Quaglini et al 2012). In terms of tribology, the increase in the friction coefficient of sliding materials with increasing velocity can be explained by various interrelated factors, such as the material's response to stress, thermal influences, and tribochemical reactions. As PTFE is subjected to increased velocities, it undergoes substantial deformation, causing larger polymer particles to be transferred between the sliding surfaces in contact (Makinson and Tabor, 1964). Moreover, the viscoelastic properties of PTFE result in increased viscous forces at higher speeds. These forces can exceed the strength of crystalline boundaries, leading to increased friction (Makinson and Tabor 1964; Steijn, 1968). Furthermore, an increase in sliding velocity often raises the temperature, which usually decreases friction; the accelerated motion amplifies the shear forces on the material, counteracting this effect and causing the friction coefficient to rise (Makinson and Tabor 1964; Guaii et al. 2021).

Numerous studies in literature have examined the effect of sliding velocity on the friction coefficient between Teflon and steel contact surfaces. Mokha et al. (1991a) examined the friction characteristics of Teflon-steel interfaces in sliding bearings, emphasizing the advantageous low friction coefficients for seismic base isolation systems. The authors observed that the sliding coefficient of friction increases with velocity but typically stays under 0.05, which is considered low and beneficial for base isolation. Additionally, the study investigated how prior high-velocity motion affects friction values, indicating that repeated tests may result in higher friction due to heat generated by friction and variations in the surface characteristics of Teflon.

Research conducted by Bondonet and Filiatrault (1997) has focused on the friction properties of PTFE sliding bearings at frequencies above 1 Hz. Their study focused on the dynamic behavior of PTFE-steel interfaces under varying frequencies and axial pressures, emphasizing the high-frequency seismic responses of PTFE bearings in bridge structures. The frictional properties were found to be influenced by the interaction of frequency, displacement amplitude, and axial pressure, with velocity-related changes in friction due to factors like heat, material deformation, and interface interactions.

Research conducted by Tsai et al. (2006) examined the efficiency of the multiple friction pendulum system (MFPS) as an advanced seismic protection method. Their study utilized full-scale component testing and shaking table experiments to evaluate the MFPS's performance in mitigating earthquake-induced effects. The study emphasizes that the friction coefficient of the lubricant material, particularly the Teflon composite applied to the sliding surface, varies based on the sliding velocity, with values ranging from 0.03 to 0.12. Results from the component testing reveal that the sliding interface maintains its durability even after 2000 cycles of sliding movements, suggesting the MFPS isolator's long-term reliability.

A novel seismic isolation bearing that combines a Teflon sliding mechanism with helical springs has been introduced by Xue et al. (2009). The authors highlighted that sliding velocity, vertical pressure, and seismic excitation characteristics significantly affect the friction coefficients between the Teflon and stainless-steel plate. The research findings indicate that these factors are essential in determining the hysteresis behavior of bearing when subjected to dynamic pressure.

Research conducted by Zeng et al. (2013) examined the factors affecting the friction coefficient between stainless-steel and PTFE in sliding isolation bearings (SIB), with a specific focus on the velocity of sliding. The research findings indicate that the dynamic friction coefficient is proportional to the sliding velocity up to 150 mm/s. After this point, the friction coefficient remains constant regardless of further increases in velocity. The results suggest that controlling the velocity of sliding is essential for reducing the coefficient of friction and improving SIB efficiency.

A model addressing the deterioration of friction properties in friction-based devices during seismic events has been developed by Lomiento et al. (2013). Their research specifically examines how velocity impacts the coefficient of friction in these scenarios. They reported that as the sliding distance increases, particularly during complete motion reversals, the friction coefficient gradually decreases. This observation suggests a notable connection between velocity and frictional performance. The model includes a term for load impact and highlights that cycling and velocity effects can modify frictional characteristics, especially at increased velocities.

A study by Messina and Miranda (2022) studied the friction characteristics of eight different polymers sliding against galvanized steel surfaces, examining the friction performance at velocities up to 350 mm/s. The research explores the relationship between velocity and the friction coefficient at steel-polymer interfaces, providing insights for seismic isolation systems. In a later study (2024), they introduced a model for the friction coefficient in steel-PTFE interfaces used in seismic isolation bearings. The model accounts for factors like sliding velocity, normal force, stick-slip behavior, and heat generation. It successfully replicates experimental results, highlighting its effectiveness in modeling complex friction dynamics in these interfaces.

1.3.2.3. Effect of contact surface temperature

The relative motion of sliding surfaces generates frictional heat, causing an increase in temperature at the sliding interface. Several studies have shown that this temperature increase can lead to a decrease in the friction coefficient (Mokha et al. 1991b; Quaglini et al. 2012a; Trovato 2013; Kumar et al. 2015; De Domenico et al, 2019; Gandelli et al. 2021; Keikha and Amiri 2021). From a tribological perspective, this phenomenon can be explained by considering three main factors: i) *viscosity of lubricant*: As lubricants lose their viscosity due to increased temperatures, they allow for smoother sliding and reduced friction coefficients (Smith 1962), ii) *material properties*: The high contact temperature can alter the mechanical characteristics of the utilized polymeric material, potentially leading to a decrease in the effective contact area and friction (Sakurai et al. 1971), and iii) *the surface interactions*: As materials heat up and expand, their contact geometry can be changed, which in turn affects their frictional properties (Bhushan 1971).

Several studies have explored the impact of frictional heating on the performance of seismic isolation systems. Al-Hussaini et al. (1994) examined spherical sliding isolation systems in multi-story frame structures, focusing on the effects of heating on the friction coefficient. They emphasized that the heating effect can significantly influence the performance of isolation systems during seismic events, highlighting the importance of including this factor in isolator design and analysis. In a similar context, Mosqueda, et al. (2004) investigated the effects of frictional heating in PTFE/steel interface isolators. They observed a 20% reduction in the friction coefficient after three cycles of loading at peak velocities greater than 127 mm/s, attributing this change to the heating of the sliding surfaces.

Constantinou et al. (2007) conducted an experimental study on the heating effects in sliding bearings used for seismic isolation and damping systems. They demonstrated that frictional heating can significantly change the friction coefficient, which affects the performance of these bearings under seismic conditions, highlighting the need to account for thermal effects in the design of isolation systems.

The impact of temperature on friction coefficients was further explored by Quaglini et al. (2014). Their research revealed that the friction coefficient decreases exponentially with increasing temperature, stressing the importance of understanding the thermal stability of bearing materials to improve seismic response predictions. They also developed a numerical model to assess the temperature rise at the sliding interface, providing valuable insights into the design properties affected by heating.

Kikuchi and Ishii (2018) focused on the thermal-mechanical coupled behavior of sliding bearings under long-duration ground motions. They observed that cyclic deformations in the bearings led to an increase in contact surface temperature, which reduces the friction coefficient, highlighting the necessity of considering thermal effects when analyzing the seismic response of isolation bearings.

De Domenico et al. (2018) investigated the thermo-mechanical response of friction concave isolators, particularly the degradation of the friction coefficient due to heating during seismic events. Their study revealed that the variability in the friction coefficient is influenced by factors such as contact pressure, sliding velocity, and temperature rise, which can lead to unconservative estimations of displacements and energy dissipation. They proposed a finite element model to predict the minimum expected friction coefficient under seismic conditions.

In the study by Furinghetti et al. (2019), the researchers examined the frictional response of CSS devices, focusing on the heating effects during both unidirectional and bidirectional motions. They found that bidirectional motion typically results in a higher friction coefficient at low vertical loads, while at high loads, the friction behavior becomes similar for both motion types due to the energy dissipation and heating at the sliding interface. The authors proposed that the degradation of the friction coefficient could be more accurately modeled as a function of dissipated energy rather than temperature.

Gandelli et al. (2019) developed a mathematical formulation for the friction behavior of curved surface sliding bearings, which accounts for the heating effects associated with energy dissipation at the sliding surface. This model allows for parameter estimation from mechanical quantities, avoiding the need for temperature measurements. They demonstrated that the model improves the predictive capability of the bearings' behavior, particularly in estimating the increase in displacement demand due to friction coefficient degradation during sustained motion.

Finally, Cavdar et al. (2022) explored the effects of normal stress and sliding velocity on the reduction of the friction coefficient in CSSs with a PTFE/steel interface. They found that the friction coefficient could be reduced by up to 30% depending on the normal stress and sliding velocity, emphasizing the importance of considering these factors in the design and analysis of friction-based isolation systems.

1.3.2.4. Effect of cycling

The impact of cycling on the friction coefficient of sliding isolators is influenced by factors such as temperature, accumulated sliding distance, and mechanical variables (Lomiento et al. 2013; Domenico et al., 2018). Full motion reversal results in a gradual reduction of the friction coefficient for PTFE-steel sliding interfaces (Mokha et al. 1991b, Chang et al. 1990). Considering thermodynamic principles, frictional heating from a moving heat source creates a sharp temperature gradient in the depth of the sliding surfaces (Jaeger 1942). Nakahara (2005) demonstrated that this temperature distribution leads to a sharp decrease in hardness near the surface due to material softening. This significant reduction in hardness is reported as the source of a thin, soft layer on the surface that functions as a solid lubricant. Sextro (2002) proposed a simplified theory of this phenomenon, assuming a linear correlation between surface material shear strength and temperature. Blok (1963), and Carlsaw and Jaeger (1959) primarily provided the foundation for the theoretical examination of temperature rise at mating surfaces. The equations developed by these researchers have been extensively examined and implemented in studying friction-induced temperature rises by Archard (1959) and Rabinowicz (1995). The theoretical analysis of temperature increase at contact surfaces generally builds upon the work of Blok (1963) and Carlsaw and Jaeger (1959). Archard (1959) and Rabinowicz (1995) have discussed and applied the relationships derived by these authors to friction-induced temperature rise problems. These theories were applied by Constantinou et al. (2007) to PTFE sliding isolators for calculating the temperature rise at the sliding interface, resulting in a strong agreement between experimental results and theoretical predictions. Through these studies, the increase in temperature is associated with the heat flux produced by friction, which is equivalent to the power dissipated per unit area. For sliding isolators, the source of heat is the interface between the slider and the concave sliding surface, with the heat flux (q) expressed as:

$$q = \frac{\mu \cdot W \cdot |\nu|}{\pi \cdot \alpha^2} \tag{1.13}$$

Here, μ is the friction coefficient, W is the vertical force, ν is the sliding velocity and α is the radius of the slider (Constantinou et al. 2007). The generated heat flux is assumed to be equally transferred and distributed to the stainless steel of DCSS. Therefore, it is expected to have an amplification in temperature rise proportional to axial load level. However, in accordance with the concept of thermal control of friction, the corresponding temperature rise is not scaled proportionally with the heat flux (Ettless 1986). Another observation regarding the contact surface temperature is that, during cyclic motion, there is a fluctuation in the temperature rise rather than a steady increase. This behavior is identified as *flash temperature* by Stachowiak and Batchelor (2005).

1.3.2.5. Effect of wear

The results of wear tests on sliding materials of isolators reported in the literature are very few. Long-term sliding tests are expensive and are usually carried out by manufacturers specifically for qualification purposes. The findings of these tests are proprietary and kept confidential. Among the few papers on this subject, Quaglini et al. (2012a) and Quaglini (2012b) disclosed the results of a wear test conducted on a PTFE matrix with metal filler over a total sliding distance of approximately 2400 m. The test was performed at a sliding velocity of 2 mm/s and a temperature of 20°C. During the wear test, the coefficient of friction of the sliding material decreased from 7.8% (measured on the virgin specimen), to about 6% after 1200 mm and then held substantially stable, showing a value of 6.5% at 2400 m. At the end of the test a film made of large flakes of PTFE adherent to the mating steel surface was noticed. This transfer film was suggested to be the main reason for the decrease in friction during the test. The dependency of the friction coefficient temperature was also assessed in their study. The test revealed a decrease in the friction coefficient at low temperatures (from 0°C to −20°C) between 0 and 1600 m, and the return to the initial values after 2400 m. In contrast, at ambient temperature and at very low temperature (−35°C), the coefficient of friction remained constant regardless of the accumulated distance.

1.3.2.6. Effect of low temperature

The behavior of the friction coefficient at low temperatures and its fundamental tribological causes is highly influenced by factors such as hardness, young's modulus, and viscoelasticity. As temperature decreases, materials typically experience an increase in stiffness, which can result in higher friction coefficients (McCook et al., 2005; Buckle, et al. 2006). These changes lead to enhanced resistance of polymers to deformation under load (Opałka et al. 2020; McCook et al. 2005) and not to slide as easily against steel surfaces (Ptak and Kowalewski 2018). To illustrate this behavior, Figure 1.9, adapted from (Buckle et al. 2006), shows the variation of the friction coefficient at low temperatures.

According to Figure 1.9, the coefficient of friction tends to increase significantly as the temperature decreases. Specifically, at temperatures below 0°C, the friction coefficient for sliding bearings shows a marked increase.

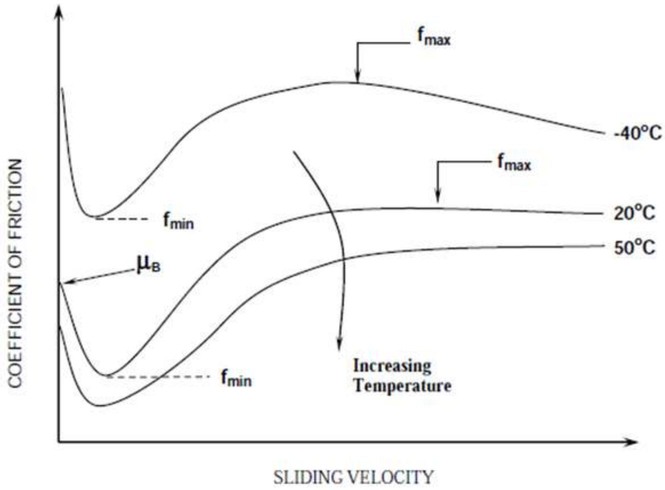

Figure 1.9. *Temperature-dependent frictional properties of PTFE-steel interfaces adapted from (Buckle, et al. 2006)*

There are very few studies that examine the effects of low ambient temperatures on PTFE-steel interfaces for sliding bearings. One of these studies in this regard is the experimental research conducted by Dolce et al. (2005), which investigates the variation of the coefficient of friction between small-scale PTFE and steel interfaces. The experimental parameters included several normal stress levels (9.4, 18.7, and 28.1 MPa), displacement amplitudes (10, 25, and 50 mm), and loading velocities (0.05, 0.2, 0.5, and 1 Hz, with a maximum speed of 314 mm/s). A key novelty of the study conducted by Dolce et al. (2005), compared to previous works, is the integration of the effect of ambient temperature as a parameter. Specifically, tests were conducted under varying ambient temperatures of -10, 20 and 50°C. Dolce et al. (2005) reported that at lower temperatures, particularly at -10°C, the friction coefficient is significantly higher than the ones at higher temperatures, indicating a greater resistance to sliding. This finding highlights the importance of considering the effect of low temperature in the design and performance evaluation of steel-PTFE sliding bearings for seismic isolation applications. In addition, another study conducted by Dolce et al. (2007) investigating the seismic isolation of bridges using steel-PTFE sliding bearings revealed that low ambient temperature has a considerable impact on the mechanical behavior of isolation systems. Specifically, approximately 10% increase in force was observed for every 10°C decrease in temperature. Moreover, the equivalent damping of the isolation system was found to decrease by about 13% for every 10°C drop in temperature. These findings showed that low ambient temperature can significantly rise friction coefficients, potentially affecting the performance of isolation systems during seismic events.

Another study in this field, performed by Quaglini et al. (2012a), investigates the effect of low air temperature on the friction coefficient of self-lubricating materials used in seismic isolation systems. Using 75 mm diameter specimens and normal stress values of 20 MPa and 40 MPa, the experiments were conducted at temperatures ranging from -35°C to 35°C to examine how the coefficient of friction is affected by ambient temperature. The study concluded that low temperature significantly increases both the static and dynamic coefficients of frictions for self-lubricating materials, which can impact their performance in seismic isolation systems. This information is crucial for the design and performance assessment of materials in seismic isolation applications, especially in colder climates.

1.4. Research Motivation

The reviewed literature reveals that numerous investigations have concentrated on the variables influencing the friction coefficient between PTFE and stainless-steel surfaces in CSSs. Among these studies, normal stress and sliding velocity are the most frequently emphasized factors. Additionally, researchers have examined other parameters, including the temperature rise on the mating surface and the effects of low ambient temperature. Based on the reviewed studies, the key findings and limitations can be summarized as follows:

- The majority of previous research outputs depend on experimental data using small-scale samples. This approach is primarily due to constraints in loading capabilities of test setups. However, these studies are in lack of presenting the correlation between the small- and full-scale behaviors of the tested materials. Thus, there is a need to investigate the efficacy of using small-scale test results to represent the behavior of full-scale specimen.
- The normal stress levels considered in previous experiments range from 20 MPa to 45 MPa. On the other hand, in most of the seismic isolation applications, these values are very low and do not represent the typical range of normal stresses acting on CSSs. Isolation units are generally designed to operate under normal stresses significantly higher than these values. Thus, the existing experimental data is in lack of representing the behavior of CSSs.

- The previous research studies that focused on the effect of loading velocity on friction coefficient at the sliding interface have typically considered maximum loading velocities up to 50 mm/s. This is basically due to inability to perform tests at higher velocities in the experimental program. Nevertheless, due to extreme seismic events, the sliding may take place at higher velocities up to 500 mm/s or even beyond. The existing data also represents combinations of normal stresses and loading velocities which are unrealistically low considering the existing seismic isolation applications.
- In literature, the effect of low ambient temperature on friction coefficient of CSSs has been examined by only a limited number of studies. These investigations primarily focused on temperatures at or above 0ºC. And, none of these studies were conducted with full-scale specimens. Moreover, in studies that investigated the effect of temperature below 0ºC, either the normal stress level or the sliding velocity was considerably low.
- None of the studies that focused on the effect of low temperature (temperatures below 0ºC) did not consider the duration of exposure to low temperature as a parameter in the experimental program. The lack of experimental data that can be used to show the compatibility between small- and full-scale test results is even more pronounced for parameters such as low temperature and exposure time.

Thus, there is a need to conduct a systematic research program to assess the effect of different loading conditions on hysteretic properties of CSSs. This dissertation investigates the variation in frictional properties of CSSs due to wear of the sliding material by means of accumulated sliding distance, change in normal stress level and sliding velocity for different low temperatures and exposure times. This thesis also includes a comprehensive investigation to demonstrate the success of using the data obtained from small-scale tests to determine sliding properties of a full-scale CSS behavior.

1.5. Scope and Objectives of the Research

In design of seismic base-isolated structures, the primary consideration is the displacement value at the isolation level. This value is crucial for dimensioning both the superstructure and the isolators. Consequently, accurately determining the maximum isolator displacements during the design phase is essential for the proper design of all components of a seismically isolated structure. However, in the boundary analysis method, which is predicated on several assumptions and defined in the earthquake specification, the variables whose effects on isolator displacements are indirectly considered include the climatic conditions, aging, and temperature effects in the geographical location where the structure will be constructed. To reflect how these factors affect the mechanical properties of the seismic isolator in the design phase, the lower and upper bound modification coefficients defined by the specifications are utilized. This approach aims to determine the most unfavorable seismic demands that will affect the seismic isolator and the structure. However, the coefficients suggested by the specifications are obtained either by considering unrealistic climatic conditions (e.g., -35ºC and 24 hours exposure time) or from specimens tested under displacements that are inconsistent with the design. Therefore, it is necessary to critically evaluate the efficiency of these coefficients in reflecting the observed change in curved surface sliders properties under repeated cyclic motions, particularly at low ambient temperatures.

The first objective of this study is to investigate the response modification of a CSS due to accumulated service movements that may occur during the working life of the device, through complementary investigations performed on both a small-scale specimen of the slider and the double curved surface slider (DCSS) system. In these tests, both small-scale specimen of the slider and full-scale DCSS were tested over a 1000 m accumulated sliding distance. Comparison of friction properties obtained from small-scale slider and full-scale DCSS tests is presented and discussed in order to substantiate the use of small-scale results to estimate the characteristics of the full-scale sliding isolation system. Eventually, the observed changes in friction coefficient due to temperature and cumulative sliding distance are compared to the relevant λ factors suggested in the European codes (CEN 2005, CEN 2009).

The second objective of this study is to provide an insight into the static friction coefficient of CSSs in icing conditions, considering a full-scale sliding isolator exposed to low temperature, and subjected to the formation of ice on the sliding surface. Cyclic displacement-controlled tests were performed on the DCSS after exposure to temperatures of 20, 0, and -20°C for periods of 3, 12, and 24 hours. The experiments were conducted under varying conditions, including normal stresses of 40, 60, and 80 MPa and maximum sliding velocities of 250, 500, and 750 mm/s, to assess their influence on the static friction coefficient. The force-displacement curves generated from these tests were analyzed to determine the static friction coefficients, clarifying the effect of ice formation on the sliding interface.

The third objective of this study is to examine the influence of ice on the dynamic friction coefficient of CSSs. Additionally, the effect of exposure time to low temperatures on the dynamic friction coefficient of a full-scale CSS was investigated for the first time in the literature. In the experimental program conducted within the scope of this study, a double CSS was subjected to various levels of normal stresses (40, 60, 80 MPa) and loading velocities (50, 250, 500, and 750 mm/s) after being conditioned at different low temperatures (20, 0, and -20°C) and exposure times (3, 12, 24). During the tests, a CSS was subjected to displacement-controlled cyclic motions, and the corresponding dynamic friction coefficients were presented comparatively.

The fourth objective of this study is to evaluate whether small-scale test results can accurately reflect the frictional characteristics of a full-scale CSS at room temperature. Initially, the sliding material's frictional properties were assessed using small-scale tests conducted at room temperatures (20°C), under varying normal stresses (20, 40, and 60 MPa) and sliding velocities (5, 25, 50, 100, 200, and 250 mm/s). Following these tests, a unified model was developed to characterize the material's friction coefficient. Finally, to determine the reliability of small-scale tests in predicting the performance of the isolator, the estimated friction values from small-scale tests were compared with the effective friction coefficient of a full-scale isolator that incorporates the same material.

Finally, the fifth objective of this study is to evaluate the ability of small-scale test results to represent the frictional properties of a full-scale CSS under icing conditions. For this purpose, the frictional properties of the sliding material were initially investigated through small-scale tests conducted at low ambient temperatures (0°C and -20°C) for 3, and 24 hours, applying various normal stresses (20, 40, and 60 MPa) and sliding velocities (50, 100, 200, and 250 mm/s). The results of these small-scale tests were then compared with the friction coefficients calculated for a full-scale CSS, assessing the effectiveness of small-scale tests in representing the behavior of full-scale CSS.

1.6. Organization of the Dissertation

This dissertation comprises of six chapters with the following brief summaries:

Chapter 1: A general overview of Curved Surface Sliders and basic principles of friction phenomena, along with a review of previous studies that investigate the response of sliding materials under different loading conditions.

Chapter 2: An experimental program and corresponding test results aimed at the investigation of wear effects on the friction coefficient of a curved surface slider and the comparison of small- and full-scale test results.

Chapter 3: An investigation on the static friction coefficient of Curved Surface Sliders in icing conditions. For different levels of low temperatures and exposure times, an ice layer forms at the sliding interface.

Chapter 4: A detailed discussion on the dynamic friction coefficient of Curved Surface Sliders subjected to different loading conditions with an emphasis on prolonged exposure at temperatures below 0ºC.

Chapter 5: Proposing a unified model to estimate the friction coefficient of the sliding material under different loading conditions and assessing the success of the estimated values by comparing with the effective friction coefficient of a full-scale CSS.

Chapter 6: An assessment on the accuracy of using frictional properties obtained from small-scale tests to determine frictional properties of a full-scale Curved Surface Slider, especially in case of low temperature exposure.

Chapter 7: A concise summary and conclusions are presented.

2. EXPERIMENTAL INVESTIGATION OF WEAR EFFECTS ON THE FRICTION COEFFICIENT OF A CURVED SURFACE SLIDER: COMPARISON OF SMALL- AND FULL-SCALE TESTS

2.1. Introduction

Current codes prescribe to test isolation systems to assess the reference properties to be used in design, and to check, in quality control testing, the actual properties of manufactured devices. For sliding isolators, the standards (ASCE/SEI 7 2016; AASHTO 2014; CEN 2009) recommend to test full-scale prototypes under displacement-controlled dynamic motions to assess the friction behavior during earthquakes. The number of cycles in these tests is generally three for most of the loading conditions representative of seismic situations. On the other hand, the friction coefficient in service conditions, characterized by frequent but small amplitude motions, is assessed by performing cyclic tests on small-scale samples of the slider (not the isolator) considering very large accumulated sliding distances such as 1000 m for use in buildings, and 10,000 m for use in bridges (CEN 2009). In these tests, effect of change in environmental temperature is also considered.

However, two issues that are still unsettled among both the researchers and the manufacturers, and in standardization committees as well, concern (i) the viability of the small-scale tests to estimate the sliding behavior of a full-scale sliding system during service movements and (ii) the possible change in the "seismic" coefficient of friction (i.e. the high-speed coefficient of friction) of the CSS due to wear occurred in service situations. In conventional tribotesting, small-scale tests performed on unidirectional rotating pin-on-disc, block-on-ring or reciprocating cylinder-on-plate test rigs are mainly used because of their cost- and time-effectiveness and ease of handling small samples (Samyn et al. 2006). Several studies (Cardone et al. 2022; O'reilly et al. 2022; Quaglini et al. 2022; Quaglini et al. 2012a) support the claim that small-scale procedures can estimate the coefficient of friction of isolators with an accuracy of ±20% (and in most cases better than ±10%) at sliding velocities higher than 100 mm/s and normal stresses between 30 and 60 MPa, which represent practical design applications for sliding isolation bearings. However, test conditions can strongly differ from real application; for example, the duration of the motion is an important parameter for the establishment of kinematic similarity between small-scale and full-scale tests, because of the temperature rise during the thermal transient (Quaglini et al. 2022).

In addition, prototype tests are generally performed on virgin devices. In such a case the possible influence of wear on the high-speed coefficient of friction, in the event that the earthquake hits the isolated structure after several years of service of the isolators, is disregarded. To the best of the authors' knowledge, the effect of wear on the seismic performance of sliding isolators has never been investigated in detail. To consider any probable changes in the friction coefficient due to wearing of the sliding surfaces, especially pronounced for large sliding distances, European (CEN 2005, 2009) and North American (AASHTO 2014) codes suggest the use of property modification factors (λ factors) for upper and lower bound values. For unlubricated PTFE/steel interfaces, the coefficient of friction is assumed to remain unchanged (λ_{max} = 1) for cumulative sliding distances less than 1.0 km. On the other hand, for sliding distances between 1.0 and 2.0 km, a 20% increase in the coefficient of friction is assumed (λ_{max} = 1.2). In the case of lubricated interfaces, the coefficient of friction is assumed to remain unchanged for cumulative distances up to 2000 m. For distances longer than 2000 m, for both unlubricated and lubricated PTFE interfaces, the codes recommend to establish the actual variation in the coefficient of friction by test. However, it has to be noted that such λ_{max} values are mainly empirical and are available only for PTFE. It is also interesting to observe that the influence of wear on the friction coefficient is overlooked in the recent version of ASCE/SEI 7 (2022).

This study aims at investigating the response modification of a CSS due to the accrual of service movements that may occur during the working life of the devices, through complementary investigations performed on both a scaled specimen of the slider and the double curved surface slider (DCSS) system. The experimental program was carried out by joint efforts of two research facilities established in Politecnico di Milano and Eskişehir Technical University. The small-scale tests were performed at the Material Testing Laboratory of Politecnico di Milano according to the procedure established in the European standard EN 15129 (CEN 2009) for assessing the coefficient of friction at low velocity, as due to service movements of the superstructure. In these tests, a small-scale specimen of the slider was tested over a 1000 m accumulated sliding distance. During the tests, the effects of normal stress and ambient temperature on the friction properties of the slider material were investigated too. Full-scale DCSS tests were performed at the Seismic Isolator Test Laboratory of Eskişehir Technical University. The investigated DCSS was subjected to cyclic motion where the total sliding distance is 1000 m.

Comparison of friction properties obtained from small-scale slider and full-scale DCSS tests is presented and discussed in order to substantiate the use of small-scale results to estimate the characteristics of the full-scale sliding isolation system. Moreover, the change in hysteretic properties of the DCSS at different cumulative sliding distances was also assessed experimentally under the effect of ground motion excitations representative of different levels of seismicity. Eventually, the observed changes in friction coefficient due to temperature and cumulative sliding distance are compared to the relevant λ factors suggested in the European codes (CEN 2005, 2009).

2.2 Test Program

2.2.1. Small-scale slider test

2.2.1.1. Specimen

The slider specimen consists of a circular pad made of a proprietary sliding material (TIS Technological Isolation Systems SA, Ankara, TR) consisting of filled PTFE (Fig. 2.1a); the composition of the material is confidential. The pad has a diameter of 75 mm and a thickness of 7 mm, and is recessed by 4.5 mm into a steel plate, leaving a sliding gap of 2.5 mm. The specimen is combined with a stainless-steel mating surface mirror finished to $R_a \leq 0.2$ μm and $R_z \leq 1$ μm roughness, in order to replicate the same sliding interface of the full-scale isolator.

2.2.1.2. Test setup

The scaled model of slider is placed in the testing machine at Politecnico di Milano (Quaglini et al. 2012a). The machine consists of a four-column steel frame equipped with two servo-hydraulic jacks aligned at 90 degrees to each other (Fig. 2.2) and driven in closed-loop by servovalves to ensure accurate control of load and velocity. The vertical jack (item A in Fig. 2.2a), rated 300 kN, imposes a compression force to the specimen. The horizontal jack (item B in Fig. 2.2a), rated 50 kN, drives a sledge (item C) that carries the pad of sliding material. The stainless-steel mating plate is fixed to the rod of the vertical jack (item A). Load cells and inductive displacement transducers are used to measure the loads and the movements applied to the slider.

A thermal chamber (item D) operating between −70°C and 90°C encloses the specimen. The temperature within the chamber is adjusted within a tolerance of ± 1°C by a digital controller coupled with a thermal sensor embedded in the stainless-steel plate.

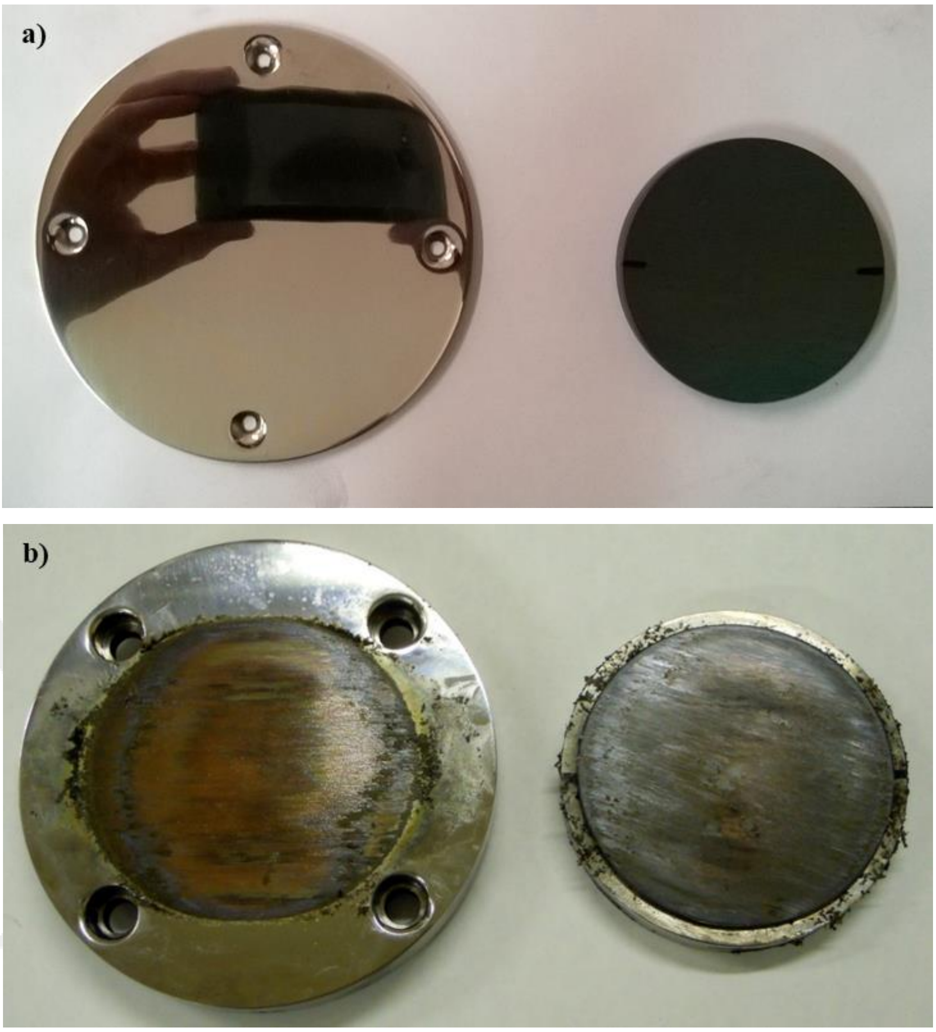

Figure 2.1. *Small-scale slider specimen and stainless-steel mating plate: before the test (a), and after the travelled distance of 1000 m (b).*

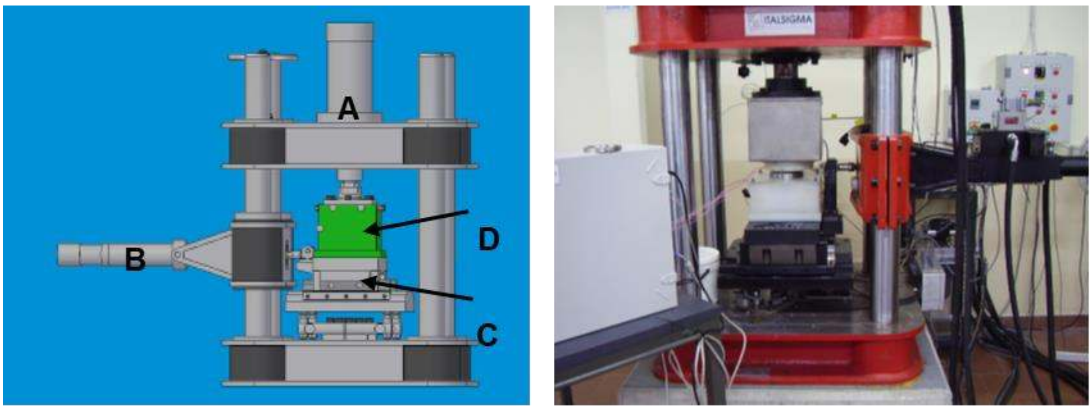

a) b)

Figure 2.2. *Sketch of the testing apparatus for small-scale slider test (a), and the apparatus at the Materials Testing Laboratory of Politecnico di Milano (b) (Quaglini et al. 2012a)*

2.2.1.3. Loading protocol

The tests are performed in accordance with the "Long Term Friction Test" procedure prescribed in the European Standard on Anti-Seismic Devices EN 15129 (CEN 2009), adapted to include temperatures up to +70°C.

The slider specimen is subjected to the concurrent application of an axial load reproducing the design normal stress acting on the sliding interface of the full-scale isolation system, and a concurrent back-and-forth sliding motion in lateral direction.

The test program consists of four variable-temperature phases complemented with one constant-temperature phase, in accordance with Table 2.1. In variable-temperature phase 1, the static and dynamic coefficients of friction are measured at different temperatures between −35°C and+70°C for a sliding velocity of 0.4 mm/s. The constant-temperature phase is then performed at 2 mm/s and 21°C over a total sliding distance of 1000 m, with the aim of promoting the wear of the sliding materials (slider and mating stainless steel). After the wear phase, the coefficient of friction is evaluated again in a variable-temperature test program (phases 3, 4, and 5) performed at 45, 30, and 15 MPa, respectively, to account for the effect of the normal stress. Test parameters are given in Table 2.2, while the temperature profile of the variable-temperature program is shown in Fig. 2.3.

Table 2.1. *Long term friction test program*

Phase Number	1	2	3	4	5
normal stress on the slider	45 MPa	45 MPa	45 MPa	30 MPa	15 MPa
Distance	22 m	S_t = 1000 m	22 m	22 m	22 m

Table 2.2. *Long term friction test parameters in accordance with Figure 2.3*

Variable-Temperature program (phases 1, 3, 4 and D)			
Normal stress on the slider	p	Type A: 45 MPa $^{+3}_{0}$ Type C:- 30 MPa $^{+3}_{0}$ Type D: 15 MPa $^{+3}_{0}$	MPa
Temperature	T	0/-10/-20/-35/+35/+48/+70/+21 (±1)	°C
Temperature gradient		0,5 ± 1,0	°C/min
Preload time	t_{pl}	1	h
Sliding distance (per stroke)	s_A	10 $^{+0.5}_{0}$	mm
Dwell time at the end of the strokes	t_0	12±1	s
Number of cycles (two strokes)	n	1500	
Sliding distance (per phase)	S_A	30	m
Sliding speed (constant)	v	0.4 MPa $^{+0.5}_{0}$	mm/s
Dwell between phases	t_0	1	h
Constant-temperature program (phase 2)			
Normal stress on the slider	p	45 MPa $^{+3}_{0}$	MPa
Temperature	T	21 ± 1	°C
Temperature gradient		0,5 ± 1,0	°C/min
Sliding distance (per stroke)	s_B	8 $^{+0.5}_{0}$	mm
Number of cycles (two strokes)	n	62500	
Sliding distance (per phase)	S_B	1000	m
Sliding speed (constant)	v	2 (± 0,1)	mm/s

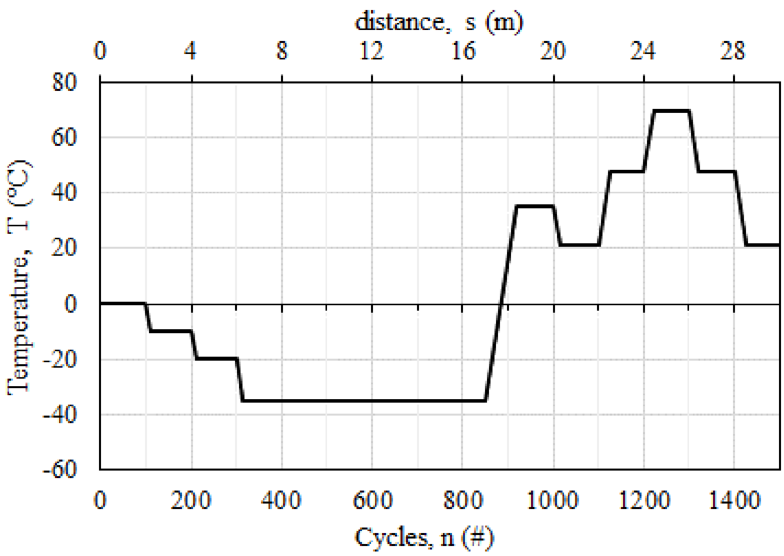

Figure 2.3. *Temperature profile vs. number of cycles and sliding distance of the variable-temperature program (phases 1, 3, 4 and 5)*

2.2.2. Curved surface slider test

2.2.2.1. Specimen

The tested seismic isolator is a DCSS consisting of two concave plates and a slider with a convex sliding pad (sketched in red in Fig. 2.4b) made of a proprietary filled PTFE (section 2.2.1) at either interface. The energy dissipation capacity of the isolation system is proportional to the friction coefficient triggered between the slider and the mating stainless-steel surfaces during the movement of top and bottom plates with respect to each other (Fig. 2.4b). The DCSS tested in this study was used in seismic protection of Bitlis Viaduct in Turkey as shown in Fig. 2.5. The Bitlis Viaduct has 12 piers, and its total length is 900 m. At each pier, there are four DCSSs manufactured by Technological Isolation Systems (TIS). The DCSSs are 700 mm in diameter and the radii of curvature of both top and bottom concave surfaces are identical and equal to 1800 mm; the diameter of the two sliding pads is 280 mm. The design displacement of the DCSS is 300 mm.

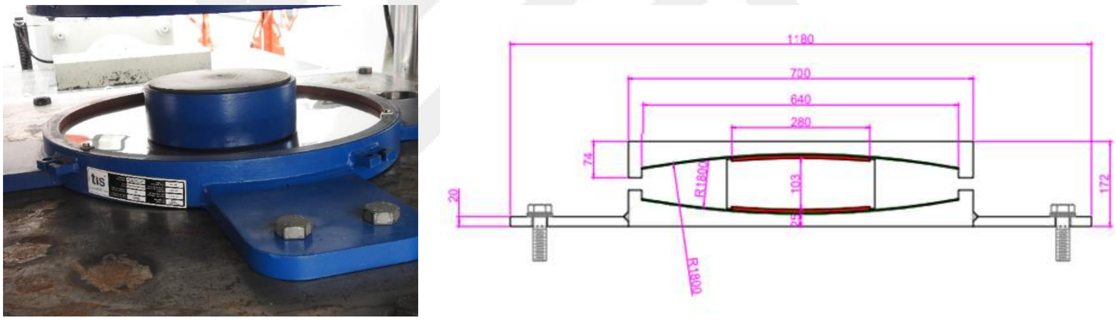

a) b)

Figure 2.4. *Picture of the tested DCSS (a), and main geometrical properties (b).*

a) b)

Figure 2.5. *View from the construction site of Bitlis Viaduct (a), and installation of a friction pendulum on top of the pier (b)*

2.2.2.2. Test setup

To determine the change in friction coefficient of the DCSS due to the accumulated sliding distance, different loading cases were applied to the specimen at the Seismic Isolator Test Laboratory of Eskişehir Technical University. The test setup shown in Fig. 2.6 can apply force and displacement-controlled dynamic motions in both horizontal and vertical directions. The maximum loading capacities are 2000 kN and 20,000 kN in horizontal and vertical directions, respectively. In the horizontal direction, the maximum stroke is ±600 mm and the maximum velocity is 1000 mm/s.

a) b)

Figure 2.6. *Seismic isolator test set-up (a), and accumulator sets used in Seismic Isolator Test Laboratory of Eskişehir Technical University (b).*

2.2.2.3. Loading protocol

The loading protocol was established based on the design properties of the DCSS under investigation. The amplitude of the motion of the isolation system due to service movements was assumed to be 70 mm during the design of Bitlis Viaduct. Thus, the amplitude of the cyclic motion imposed to the DCSS specimen was chosen as 70 mm. The loading velocity was 5 mm/s and the accumulated sliding distance applied to the DCSS through the cyclic motion was 1000 m. The loading protocol is sketched in Fig. 2.7, where the triangular waveform was chosen to provide a constant velocity over the whole stroke. It is necessary to emphasize that, even though for bridge applications the standard (CEN 2009) prescribes to assess the material of the slider over 10,000 m, in the current test the sliding path was limited to 1000 m to reduce the experimental costs. The test program consisted of 20 blocks of 50 m sliding distance each, with a dwell period of not less than 40 min between two consecutive blocks. In accordance with the design loads, the vertical force applied to the DCSS during the cyclic motion was 3500 kN corresponding to an average normal stress of 57 MPa on the slider. The ambient temperature of the laboratory was 21.3°C at the beginning of first set of cyclic motion and ranged between 21.1°C and 27.1°C throughout the whole test.

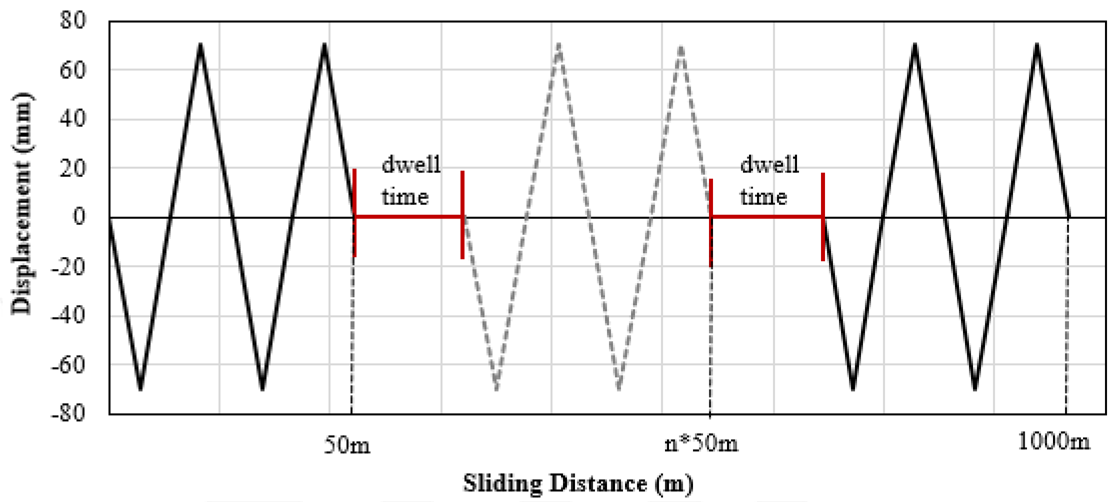

Figure 2.7. *Loading protocol applied to the tested DCSS*

To investigate the change in the hysteretic behavior of the DCSS due to wear, after accumulated sliding distances of 250, 500, 750, and 1000 m, the DCSS was subjected to scaled down displacement histories of the strong motion component of Kocaeli Yarımca record. The original ground displacement time history of Kocaeli Yarımca record was downloaded from PEER strong motion database (http-3). Then, in order to obtain displacement histories with different amplitudes and to mimic the effect of ground motion excitations with different seismicity levels, modified versions of Kocaeli Yarımca record were considered (Fig. 2.8). Scale factors used to modify the original displacement history are 0.2, 0.3, 0.4, and 0.5 which correspond to maximum displacements of 100, 150, 200 and 250 mm, respectively. The displacement histories were applied to the DCSS in order of increasing amplitude with a 15 min dwell period between two tests.

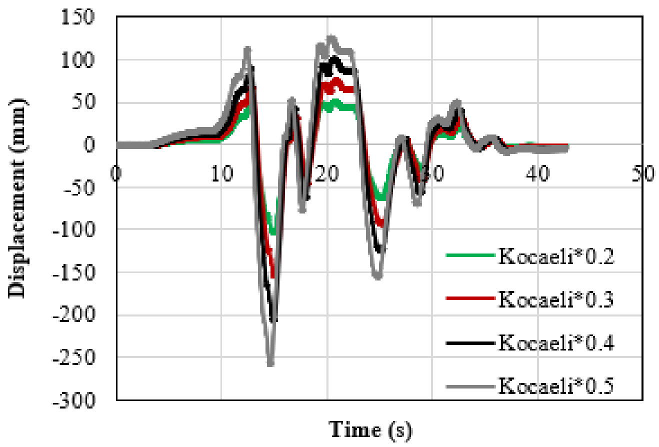

Figure 2.8. *Displacement histories assumed to mimic the effect of ground motion excitations with different seismicity levels*

2.3. Results

2.3.1. Small-scale slider test

From the values of axial and lateral loads measured during test phases 1, 3, 4, and 5, the temperature-dependent static coefficient of friction $\mu_{st(T)}$ and dynamic coefficient of friction $\mu_{dyn(T)}$ at low velocity are calculated at each cycle according to equations 2.1a and 2.1b:

$$\mu_{st(T)} = \frac{F_{st(T)}}{N} \tag{2.1a}$$

$$\mu_{dyn(T)} = \frac{F_{dyn(T)}}{N} \tag{2.1b}$$

where $F_{st(T)}$ is the lateral force measured at motion reversals (after each stop-and-start), $F_{dyn(T)}$ is the lateral force recorded during sliding, and N is the axial load applied to the specimen (Fig. 2.9).

Fig. 2.10 summarizes the results of the test by reporting the maximum values of $\mu_{st(T)}$ and $\mu_{dyn(T)}$ assessed at various temperatures, different normal stress levels and accumulated sliding distances. By comparing the plots in Fig. 2.10a,b, it is apparent that at each temperature, the static and dynamic coefficients of friction are very close to each other. This behavior, which is ascribed to the effect of the embedded fillers, represents a valuable feature of the sliding material under investigation. In fact, for most of the available sliding materials, a substantial difference exists between static and dynamic

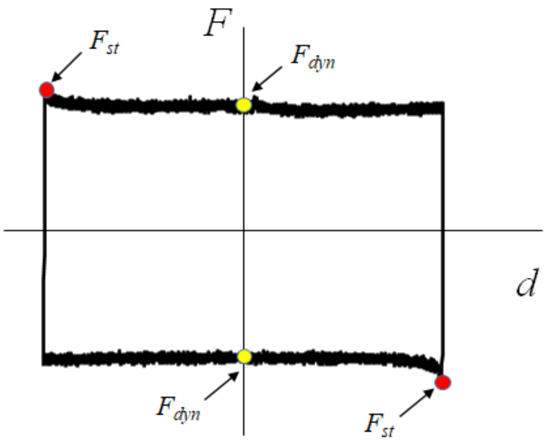

Figure 2.9. *Static and dynamic forces considered for the evaluation of the coefficient of friction.*

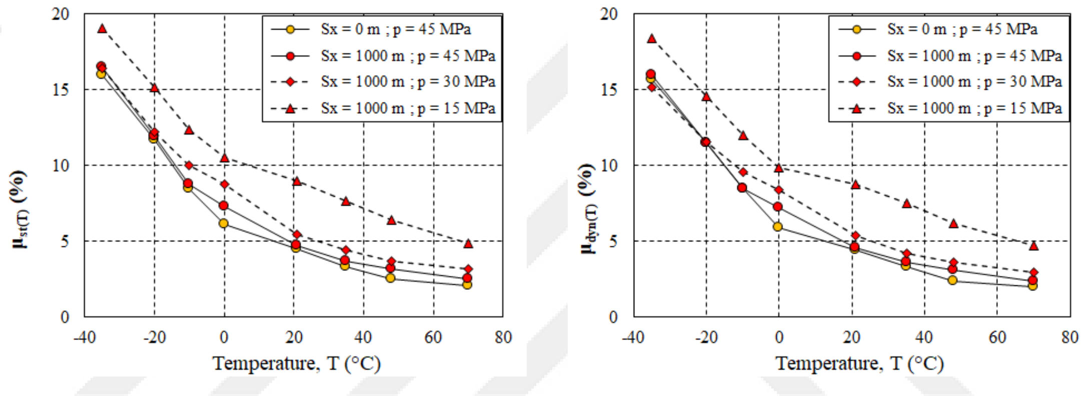

Figure 2.10. *Coefficients of friction assessed in small-scale slider test on the virgin specimen (S_x=0m) and after the travelled distance of 1000 m (S_x=1000m) at various temperatures and stress levels (p): (a) static coefficient of friction, (b) dynamic coefficient of friction.*

friction coefficients: depending on the examined material, $\mu_{st(T)}$ can be 1.5–4.5 times larger than $\mu_{dyn(T)}$ (Mokha, Constantinou, and Reinhorn 1990; Fagà et al. 2015). It is indeed noted that in CSSs characterized by a high $\mu_{st(T)}/\mu_{dyn(T)}$ ratio sliding is triggered only by high-intensity ground motions and that, therefore, such isolators can be not effective in case of weak or moderate earthquakes (Gandelli and Quaglini 2018; Gandelli et al. 2019, 2020). Another important outcome of the tests is that the accumulated sliding distance has a very limited effect on the low-velocity coefficient of friction, which shows only a small rise at the end of the 1000 m sliding path in comparison to the values computed at the initial loading step of the test (the increase is smaller than 0.5% at every temperature considered in the loading protocol but at 0°C where the variation is about+1.2%). However, it should be taken into account that, according to the procedure recommended in the standard (CEN 2009) and implemented in the present study, invariable-temperature phases the first temperature step is always performed at 0°C; therefore, the value of the coefficient of friction assessed at T = 0°C in phase 3 may be biased by the sudden switch from the constant-temperature program (phase 2) to the variable-temperature program.

Pictures of the scaled slider and the stainless-steel mating plate are shown in Fig. 2.1b. The stainless-steel plate was coated by an adherent film made of worn slider material that preserved the underlying steel from abrasion during motion. This transfer film was indeed similar to that observed for a metal-filled PTFE compound investigated by one of the authors (Quaglini et al. 2012a; Quaglini 2012b). After removal of this adherent film, it was noticed that the steel surface was free from scratches and signs of wear. A few debris of the friction material in the form of flakes also accumulated outside the sliding region. Despite these flakes, the wear of the slider was very small and almost uniform over its surface. The average change in thickness of the sliding pad at the end of the 1000 m path was 0.33 mm only out of the initial value of 7 mm, and was mostly due to the lateral deformation of the slider material rather than to loss of material. The decrease in thickness was uniform over the whole surface, with no significant differences between the edges and the center of the specimen. By referring to the test at p = 45 MPa, the low-velocity coefficient of friction of the virgin material (sliding path S_x = 0 m) counts about 7% at T = +21°C, and is significantly affected by the change in temperature, rising ranging between 2.1% at T = +70°C and about 16% at T = −35°C. In this regard, it is worth noting that the rate of increase in friction coefficient vs. temperature has a steep change below 0°C, switching from 0.073% (°C^{-1}) between 0°C and+70°C, to 0.287% (°C^{-1}) between 0°C and −35°C. To highlight the influence of temperature, Fig. 2.11 shows the ratios between the static and dynamic friction coefficients at various temperatures $\mu_{st(T)}$ and $\mu_{dyn(T)}$ and the reference values $\mu_{st(+21°C)}$ and $\mu_{dyn(+21°C)}$ determined at + 21°C. Both coefficients of friction have a huge variation over the examined temperature range, with $\mu_{st(T)}/\mu_{st(+21°C)}$ and $\mu_{dyn(T)}/\mu_{dyn(+21°C)}$ ratios rising from about 0.5 at T = +70°C to more than 2 at T = −35°C (more precisely, the ratio counts 1.7–2.0 at p = 15 MPa, 2.0–2.1 at p = 30 MPa, and about 3.5 at p = 45 MPa). This behavior is typical of available thermoplastic sliding materials, including virgin and filled PTFE (Dolce et al. 2005; Quaglini et al. 2012a), UHMWPE (Braun and Butz 2010) and PET (polyethylene terephthalate) (Quaglini et al. 2012a).

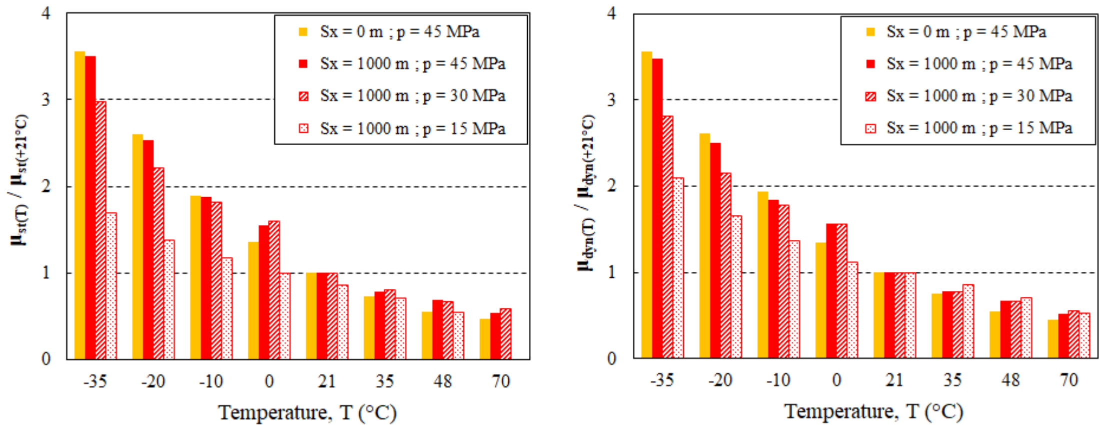

a) b)

Figure 2.11. *Variation of friction coefficient with temperature: (a) static coefficient of friction, and (b) dynamic coefficient of friction.*

The influence of the normal stress *p* was assessed at the end of the total sliding distance of 1000 m (Fig. 2.12). As experimentally observed on current sliding materials (Constantinou et al. 2007; Quaglini et al. 2009; Quaglini et al. 2012a; Barone et al. 2019;), both $\mu_{st(T)}$ and $\mu_{dyn(T)}$ increase as the normal stress *p* is reduced; in general, the effect is more significant at low stress levels (*p* = 15MPa), while the variation is smaller when *p* increases from 30 to 45 MPa, especially at low temperatures.

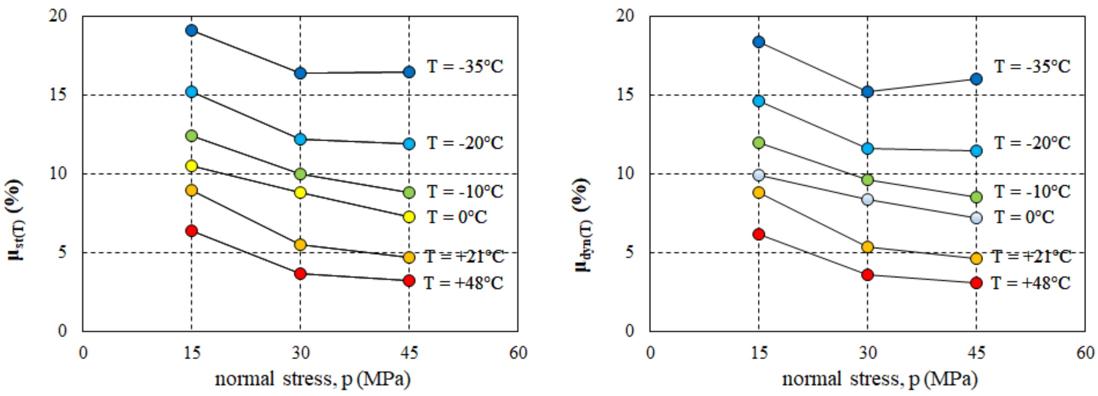

a) b)

Figure 2.12. *Coefficient of friction vs. normal stress p at different temperatures T: (a) static coefficient of friction, and (b) dynamic coefficient of friction.*

2.3.2. Curved surface slider test

The physical conditions of the sliding surfaces of the DCSS after 1000 m accumulated distance are shown in Fig. 2.13. The surfaces were cleaned before taking the pictures, and the transfer film of sliding material on the steel plate was removed. However, some debris of worn sliding material which melted and sticked on the surface of the pad is still visible. Similar to the findings for the small-scale specimen, the wear of both surfaces is low. The decrease in thickness of the pad of sliding material is on the order of 0.3 mm, and only shallow scratches are noticeable on the steel plate. The friction coefficient μ of the tested DCSS based on experimental force–displacement curves is computed by Eq. (2.2). The term N of Eq. (2.2) stands for the axial force acting on the seismic isolator, EDC is the energy dissipated per cycle (corresponding to the area enclosed by the hysteretic force–displacement loop) and D_{max} and D_{min} represent the amplitudes of cyclic motion in positive and negative directions, respectively.

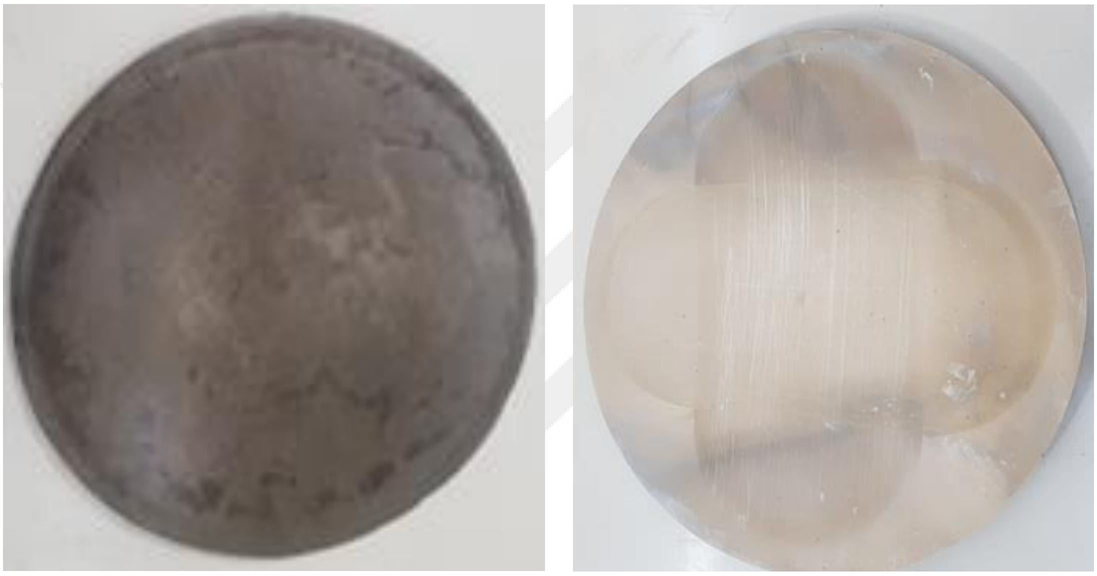

Figure 2.13. *Sliding surfaces of the DCSS: pad of sliding material (left) and stainless-steel sheet (right) at the bottom side of the specimen*

$$\mu = \frac{EDC}{2(D_{max} - D_{min})N} \tag{2.2}$$

In Fig. 2.14a-d, force–displacement curves recorded at the first and last cycle corresponding to accumulated distances of 0–250, 250–500, 500–750, and 750–1000 m, respectively, are presented. As evident from the plots, a reduction in the strength of the DCSS occurs during each 250 m path, with a decrease in the maximum force of the DCSS between the last and the first cycle of the path. The energy dissipation per cycle (EDC) computed for the first and last cycle are 52–40 kNm for the 0–250 m path, 48–37 kNm for the 250–500 m path, 48–39 kNm for the 500–750 m path and 48–37 kNm for 750–1000 m path, respectively. Such decrease in force and ensuing reduction in EDC may be ascribed to the heating of the sliding interface. This behavior is indeed consistent with the decreasing trend of friction with temperature observed on the scaled model (Fig. 2.10).

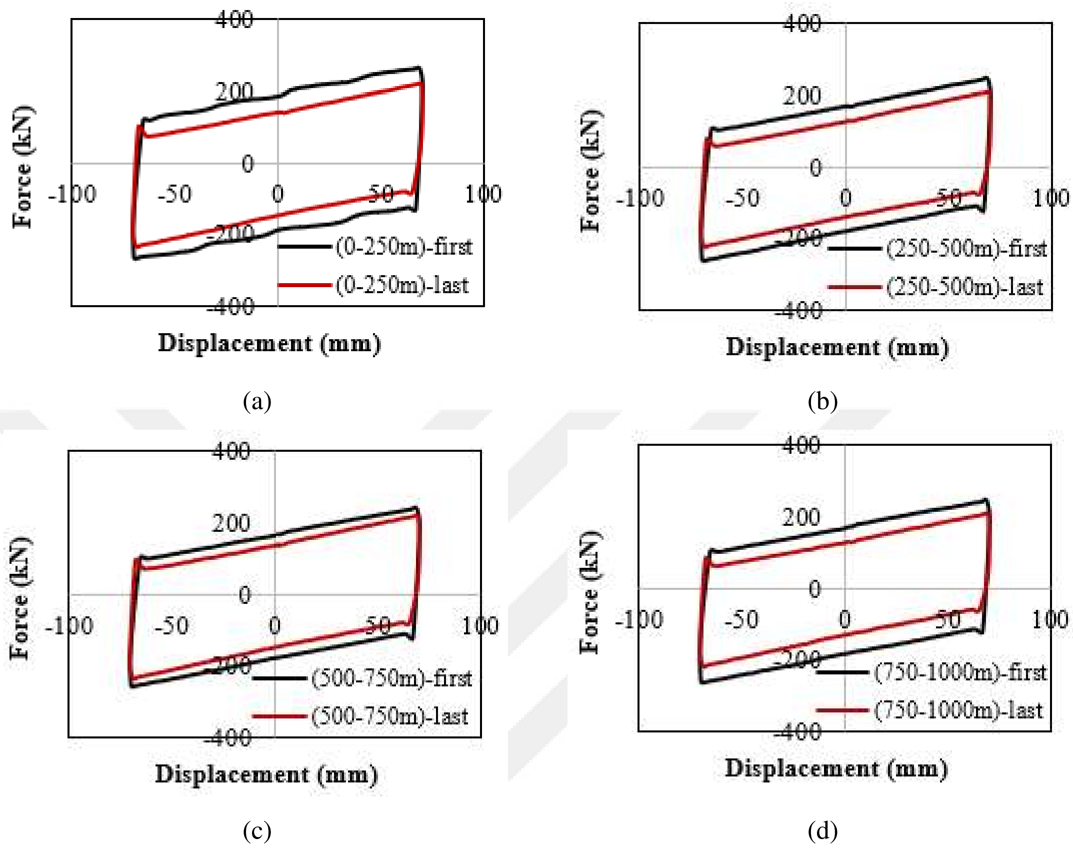

Figure 2.14. *Force-displacement curves recorded at the first and last cycles of each path of 250 m, sliding speed: 5 mm/s.*

However, it must be recalled that in the small-scale test, the friction variation was due to a controlled change of the environmental temperature within the thermal chamber of the testing machine, while in the tests on the DCSS the heating is an effect of the dissipation of mechanical energy by friction. Such inference is supported by the plot shown in Fig. 2.15 where the friction coefficient is reported against the sliding distance accumulated in the test. Within each block of 50 m, the coefficient of friction gradually decreases as the traveled distance increases, approaching a steady value at the end of the block. On the other hand, at the beginning of a new block, a steep increase in μ is observed with respect to the value recorded at the end of the previous block, e.g. the friction coefficient is 5.4% at the beginning of the 200–250 m block, decreases to 4.0% at the end of the block, and rises to 4.9% at the beginning of the next one (see Fig. 2.15). This is due to the dwelling between two consecutive blocks: the temporary stop of the motion allows the cooling down of the sliding surface and leads to a recovery in the friction coefficient.

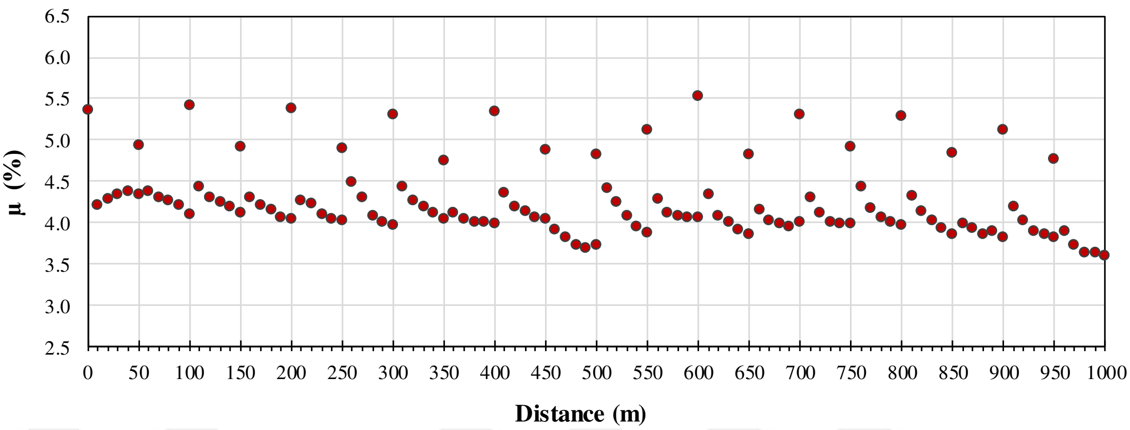

Figure 2.15. *Variation of friction coefficient with sliding distance. The total sliding path of 1000 m is divided into 20 blocks of 50 m each, with a dwell time between any pair of sets.*

To further highlight this effect, Fig. 2.16 shows the variation of μ observed from 200 to 450 m. In the Figure, green and blue dots represent μ values computed at the last and first cycle of each block of 50 m, respectively. As illustrated in Fig. 2.7, dwell periods were introduced between blocks, and the corresponding durations are reported in Fig. 2.16. Short dwell periods (<1.5 h) result in a partial recovery of the value of coefficient of friction measured at the beginning of the previous block, e.g. with dwell periods of either 40 or 50 min the recovery is on the order of 50% (μ increases from 4.1% to 4.8%) or 64% (μ increases from 4.0% to 4.9%), respectively. On the other hand, a dwell period of 18 h or longer, i.e. 66 h, leads to full recovery of the friction resistance (μ increases from 4.0% to 5.4%). Such behaviour supports the assumption that the reduction in μ is due to heating at the sliding interface (Cavdar and Ozdemir 2021; Quaglini et al. 2014). The correlation between the increase in friction and the dwell period, during which the sliding interface cools down, is well evident. As the dwell time increases, the amount of recovery increases. However, too long dwell periods do not carry a substantial improvement: after 18 h, the sliding interface is likely to have completely cooled down to ambient temperature, and there is no further recovery with longer dwells. It is to be noted that Fig. 2.16 and the corresponding observations on the effect of dwell time apply to the examined DCSS and loading protocol. Larger isolators may need more time to cool down, and the same is likely to occur when the isolators are tested at higher speeds or normal stress levels, which entail the introduction of a larger amount of energy that must be dissipated by friction (and consequently, a higher temperature rise).

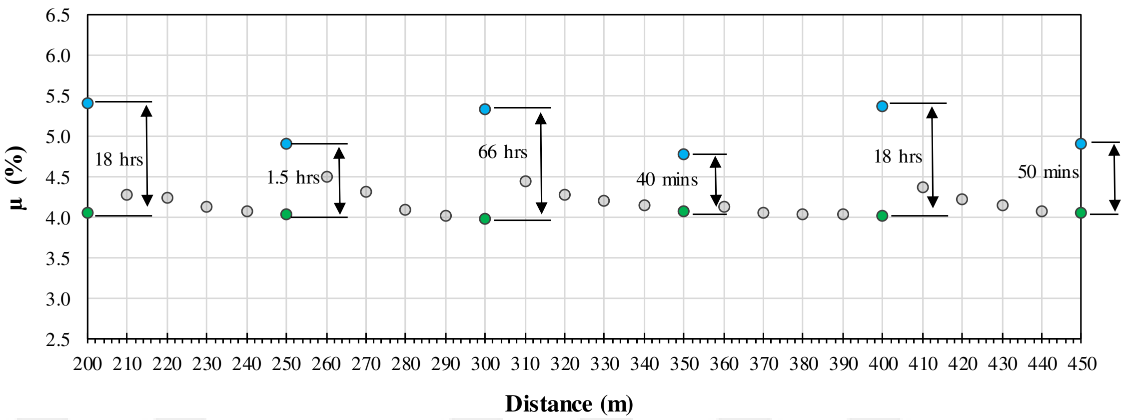

Figure 2.16. *Effect of dwell time between consecutive loading blocks.*

Figure 2.17 presents the force–displacement curves of the DCSS subjected to the displacement histories defined in Fig. 2.8 after accumulated distances of 250, 500, 750, and 1000 m. In Fig. 2.17a, relevant to an amplification of 0.2 times the displacement history of Kocaeli Yarımca record, the hysteresis loops evaluated at different distances are almost identical. However, by referring to the test result at 0 m, a slight increase in the isolator force is noticed. After 250 m, the amplification in the maximum isolator force is 23 kN which corresponds to an increase of +6.8%. Similar comparisons for the data presented in Fig. 2.17b-d result in +5.2%, +4.3% and +3.0% increments, respectively. This indicates that as the amplitude of the ground motion excitation increases, the amplification of the isolator force decreases and the hysteresis loops get closer to the ones obtained in the reference tests.

Table 2.3 presents the amplifications in maximum isolator force computed for every loading condition. It is interesting to observe that the general trend in amplifications is to increase up to 500 m and then to decrease as the accumulated sliding distance further increases. However, it is necessary to underline that considering a different displacement history (i.e. with a considerable number of high amplitude cycles or with a large number of small-amplitude cycles prior to large amplitude motion) may lead to different results, due to different heating of the sliding interface. In this respect, the current research suggests further studies to investigate this behaviour and propose adequate and realistic testing protocols.

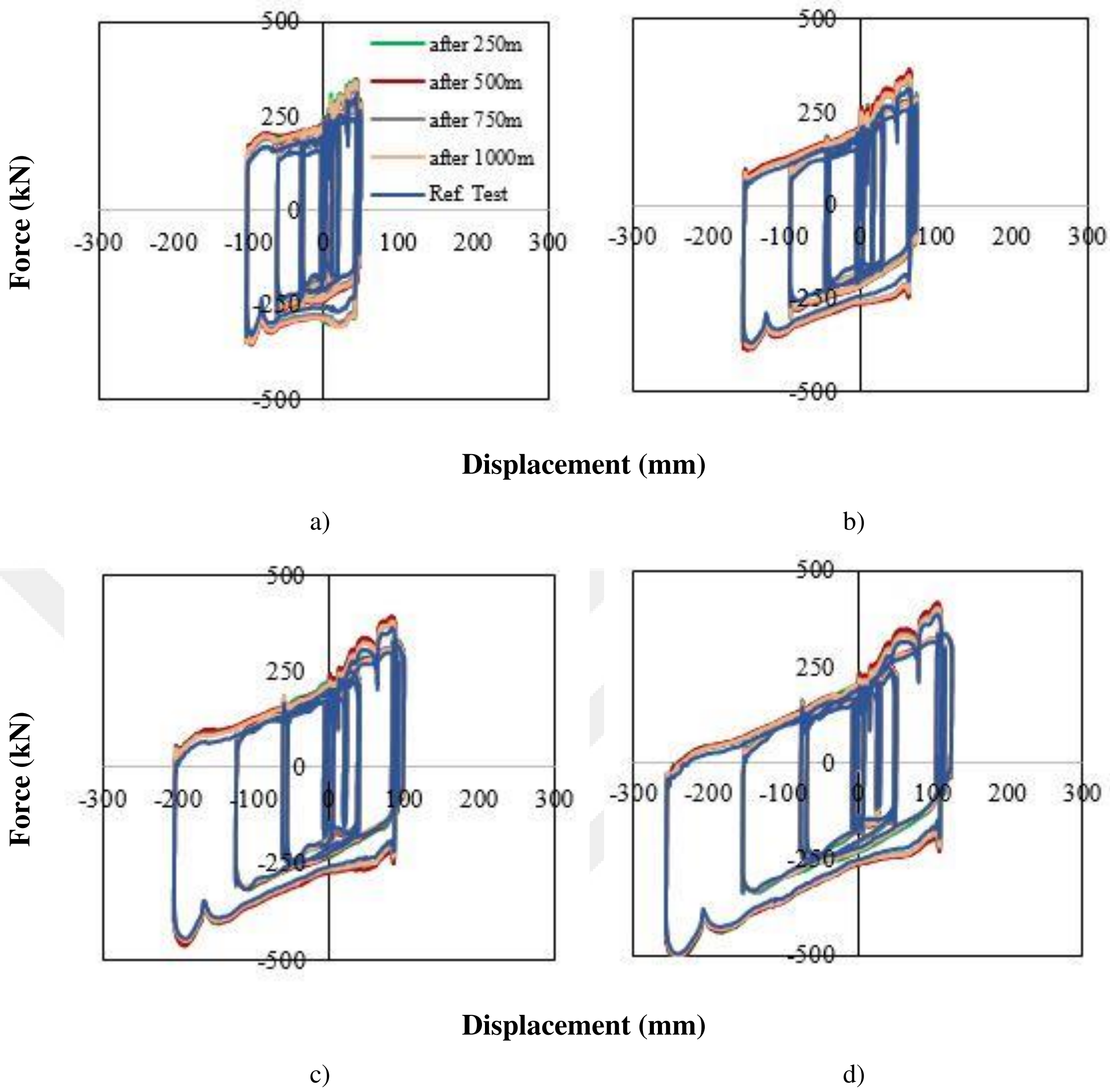

Figure 2.17. *Force-displacement curves obtained from ground motion excitations using modified displacement histories of Kocaeli Yarımca record by scale factors of (a) 0.2, (b) 0.3, (c) 0.4 and (d) 0.5.*

Table 2.3. *Amplification of the maximum isolator force due to accumulated sliding distance (in percent).*

		Scale factor of the input displacement history			
		0.2	**0.3**	**0.4**	**0.5**
Accumulated sliding distance	**250 m**	4.2	4.1	3.3	3.4
	500 m	6.8	5.2	4.3	3.0
	750 m	5.1	3.0	1.4	1.9
	1000 m	5.6	2.9	1.4	1.0

2.4. Discussion

Small-scale tests according to EN 15129 (CEN 2009) are aimed at assessing the coefficient of friction of sliding surfaces exposed to low-velocity service movements, in order to derive design values for non-seismic conditions, accounting also for the effects of ambient temperature, normal stress, and accumulated sliding distance. On the other hand, the full-scale tests on CSS prototypes recommended in the standards are performed to assess the coefficient of friction at high speeds due to seismic actions, in an attempt to derive design values in earthquake conditions. In the present study, to the best of the authors' knowledge, full-scale tests are performed for the first time to investigate the effect of the accumulated sliding distance on both the low-velocity and the high-velocity coefficient of friction of the CSSs, by assessing the relevant changes over a path of 1000m.

Figure 2.12 shows that as the normal stress increases, the coefficients of friction calculated from small-scale tests tend to level out (a further increase in normal stress level does not result in significant change in friction coefficient). Specifically, in Fig. 2.12b, friction coefficients determined at 30 and 45 MPa are sufficiently close to suggest that at 45 MPa a steady value has been achieved for temperatures of 21°C and 48°C. Therefore, even though the normal stress applied in small-scale and in DCSS tests is not the same (45 vs 57 MPa, respectively), it is believed that such difference has no practical effect on the assessed friction coefficients. On the other hand, the test on the DCSS was conducted at a speed 2.5 times higher than the test on the scaled model of slider (5 vs. 2 mm/s, respectively) in order to reduce the duration of experiment. In this respect, the standard EN 15129 (CEN 2009) prescribes only that the speed during the wear phase is not less than 2 mm/s. As already shown, at the end of the 1000 m path the sliding surfaces of both the small- and the full-scale specimens exhibit very similar conditions in terms of (small) decrease in thickness of the sliding material, creation of a transfer film of sliding material, and appearance of shallow scratches on the steel surface. Therefore, it is argued that, at least for the considered range, the effect of speed is negligible on the wear of the sliding surfaces.

By comparing Figs. 2.10–2.15, a discrete agreement is found between small- and full-scale test results. The coefficients of friction at 21°C of the small-scale slider are $\mu_{st(+21°C)} = 4.5\%$ and $\mu_{dyn(+21°C)} = 4.4\%$ at the beginning of the long-term friction test, and rise to $\mu_{st(+21°C)} = 4.7\%$ and $\mu_{dyn(+21°C)} = 4.6\%$ after 1000 m, respectively. For the DCSS, the friction coefficient determined experimentally at ambient temperature is μ = 4.3% after about 20 m (equivalent to the path at which $\mu_{dyn(+21°C)}$ is assessed during phase 1 of the small-scale friction test), and μ = 3.6% after 1000 m. Interestingly, it is observed that after 1000 m the friction coefficients of the small-scale slider at + 35°C ($\mu_{st(+35°C)}$ = 3.7%, $\mu_{dyn(+35°C)}$ = 3.6%) are similar to those of the DCSS. Although the DCSS test was performed at ambient temperatures ranging between 21°C and 27°C, the continuous cyclic motion leads to an increase in temperature at the sliding interface where the instantaneous temperature may be higher than the environmental temperature, and close to 35°C. In conclusion, the small-scale slider test seems to provide conservative estimates of the low-velocity friction coefficient of a full-scale DCSS, and this may be due to the different thermodynamical behavior associated to the size of the pad of sliding material, as well as to the thermal capacity of the steel plates of the DCSS.

Both small- and full-scale DCSS tests show that, for the examined slider material, the effect of the accumulated sliding distance on the coefficient of friction at low velocity is small (Figs. 2.10–2.15). This is consistent with the limited wear of the sliding surfaces occurred during the test (Figs. 2.1, 2.13). On the other hand, test results highlighted a gradual reduction in the friction coefficient of the DCSS under the effect of a large number of small-amplitude cycles at moderately low speeds. It is found that such reduction has nothing to do with wear but instead it is due to the heating of the sliding interface. Figure 2.16 clearly supports this deduction by showing the recovery in friction coefficient as a result of the dwell period (at which the sliding interface cools down) between consecutive sets of cyclic motion.

The full-scale test demonstrated that the travelled distance has a negligible effect also on the coefficient of friction at seismic velocities. The force–displacement curves recorded under the effect of displacement histories representative of different seismicity levels revealed that the hysteretic response of the DCSS remained almost unchanged, and the friction properties of the isolator were just marginally affected when exposed to sliding distances up to 1000 m.

The effect of ambient temperature is typically assessed by means of small-scale tests, as technically more feasible and less expensive than controlling the temperature of a full-scale isolator embedded in a massive testing equipment. At low temperatures, the coefficient of friction can be more than 3 times higher than the value assessed at 21°C which is assumed to be the ambient temperature in the test laboratory. Therefore, performing the design of the isolation system based on friction coefficients assessed in laboratory conditions on full-scale isolators can lead to underestimate the maximum resistance of the isolator for service movements occurring at very low temperatures. It is worth recalling that the effect of ambient temperature is relevant mainly to the estimation of the forces produced under the effect of non-seismic actions. Indeed, during an earthquake, once sliding is triggered, the large amount of energy dissipation occurring at high speeds will result in a substantial heating of the sliding interface, leading to a temperature at the sliding interface much higher than the ambient temperature.

It is useful to compare the variations in the coefficient of friction due to temperature and travel distance to the relevant λ-factors defined in the codes (AASHTO 2014; CEN 2005, 2009) for estimation of upper-bound design properties. Tables 2.4 and 2.5 report the values of λ_{max} for sliding isolators associated with changes in temperature and cumulative travel for unlubricated PTFE, together with the relevant values $\lambda_{max,exp}$ determined in small- and full-scale tests, respectively.

Table 2.4. *Property modification factor λ_{max} for changes in friction coefficient of unlubricated PTFE due to temperature (CEN 2005; CEN 2009) and values $\lambda_{max,exp}$ determined in small-scale tests on slider specimen at two different sliding distances*

		$\lambda_{max,exp}$	
T_{min}	λ_{max}	**0-22 m**	**1022-1044 m**
20°C	1.0	1.0	1.0
0°C	1.1	1.9	1.9
-10°C	1.2	2.6	2.5
-30°C	1.5	3.2[(a)]	3.2[(a)]

[(a)] obtained from linear interpolation of values at T = -20°C and T=-30°C

For the investigated sliding material, the low-velocity friction coefficient increases 1.9 times from 20°C to 0°C, 2.6 times at −20°C, and 3.2 times at −30°C. It is interesting to note that the variation is independent of the accumulated sliding distance, i.e. for each temperature the same $\lambda_{max,exp}$ is measured both for the virgin specimen and after 1000 m (Table 2.4). However, these figures are largely underestimated by relevant λ_{max} -values established in the codes (AASHTO 2014; CEN 2005, 2009). Namely, the difference is −42% at 0°C and −53% at −20 and −30°C.

The effect of the cumulative travel on the coefficient of friction at high velocities is summarized in Table 2.5. To be conservative, the maximum force amplification derived from Table 2.3 has been assumed for estimating $\lambda_{max,exp}$. The high-velocity coefficient of friction seems to be scarcely affected from the accumulated sliding distance, and in line with the estimation provided by the λ_{max-} value for unlubricated PTFE established in the codes (deviation+7%). As already mentioned, this is ascribed to the small wear of the investigated sliding material, and the creation of a transfer film of sliding material on the mating steel surface, which reduces wear and promotes a stable friction coefficient (Quaglini et al. 2009). The formation of the transfer film is typical of "soft" thermoplastics such as PTFE and UHMWPE (Quaglini et al. 2009; Quaglini and Dubini 2011; Quaglini et al., 2012a; Quaglini 2012b), and further investigation is needed to extend the conclusion on the limited effect of the cumulative travel to "hard" thermoplastic sliding materials.

Table 2.5. *Property modification factor λ_{max} for changes in friction coefficient at high speeds of unlubricated PTFE due to cumulative travel defined in codes (CEN 2005; CEN 2009) and values $\lambda_{max,exp}$ determined in large-scale tests on DCSS*

		$\lambda_{max,exp}$
Cumulative travel (km)	λ_{max}	**0-22 m**
≤ 1.0	1.0	1.07
1.0 < S ≤ 2.0	1.2	NA

2.5. Conclusion

Code specifications suggest different methodologies to determine the friction properties of Curved Surface Sliders in seismic and non-seismic conditions. Accordingly, for seismic situations, full-scale seismic isolators must be tested, whereas small-scale slider tests are addressed for service operations. In particular, in order to assess the effects of ambient temperature and accumulated sliding distance, performing small-scale tests will be the only feasible way. The present study compares the friction coefficients evaluated on both a full-scale DCSS and a scaled model of the slider subjected to a long-term friction over a total path of 1000 m in order to investigate the effect of the accumulated distance on the coefficients of friction at both low- and high-velocities. To the best of the authors' knowledge, such a comparison and corresponding discussions are presented for the first time in literature.

The main results of the study can be summarized as follows:

- At low velocity, at the very first cycles of the motion, the coefficient of friction computed from small-scale tests is slightly lower than that of the full-scale DCSS. However, small- and full- scale tests provide almost the same friction coefficients at the end of 1000 m accumulated path, with slightly smaller values for the DCSS device. This indicates that employing a small-scale test to estimate the coefficient of friction of a full-scale specimen is a practical, reliable, and feasible method when low-velocity friction is of concern. Small-scale isolator tests can also provide an affordable evaluation for the effect of ambient temperature on the coefficient of friction. It is therefore apparent that the full-scale tests should be complemented with small- scale slider tests to fully understand the behavior of isolators and investigate the actual properties to be considered in the design of seismically isolated structures;
- The effect of temperature on the low-velocity coefficient of friction can be huge, especially at low temperatures, and can endanger the operation of sliding isolation systems during their service operation. In this regard, the study has shown that a dedicated experimental investigation is needed to estimate suitable upper-bound design properties of the coefficient of friction, while property modification factors suggested by the codes (CEN 2005; CEN 2009; AASHTO 2014) can be highly non-conservative, especially at low temperatures;
- For the proprietary sliding material consisting of filled PTFE assessed in the study, the accumulated sliding distance has a not substantial effect on the coefficient of friction at high velocity to be considered in the seismic design. This result is in line with the relevant property modification factor established in the codes (CEN 2005; CEN 2009; AASHTO 2014). However, while it could be interpreted as a safety achievement, this outcome can be indeed ascribed to the small wear of the examined sliding material, and the creation of a transfer film of polymer on the mating steel surface. The effect of the cumulative travel on the seismic coefficient of friction of other sliding materials requires further investigation.

3. FRICTION COEFFICIENT OF SLIDING ISOLATORS IN ICING CONDITIONS

3.1 Introduction

According to European and North American standards (CEN 2009; AASHTO 2014), prototype tests on full-scale isolators are performed at ambient temperature. To account for the changes in the friction coefficient due to temperature, codes (CEN 1998; CEN 2009; AASHTO 2014) suggest the use of property modification factors (λ factors) for upper and lower bound values. Accordingly, for unlubricated PTFE/steel interfaces, the coefficient of friction is assumed to increase, in comparison to the value assessed at 21°C, by 10% (λ_{max} = 1.1) at 0°C, by 20% (λ_{max} = 1.2) at -10°C and by 50% (λ_{max} = 1.5) at -30°C, whereas for lubricated PTFE the corresponding amplifications are 30% (λ_{max} = 1.3), 50% (λ_{max} = 1.5) and 300% (λ_{max} = 3.0), respectively. It must be noted that λ_{max} values recommended in the codes are mainly empirical or derived from laboratory tests conducted on small-scale specimens and are available only for PTFE.

Experimental studies conducted on small-scale specimens of various sliding materials, including PTFE and UHMWPE (Tyler 1977; Braun and Butz 2010; Quaglini et al. 2012a; Becker et al. 2017) demonstrated that both μ_{dyn} and μ_{st} increase at low temperature, due to stiffening of the thermoplastic polymer, in accordance with the code recommendations. In the cited studies, specimens were cooled down and tested under controlled conditions (usually within a conditioning chamber). However, laboratory conditions are very different from the real environment where sliding isolators are supposed to operate in outdoor applications, e.g., in case of seismically isolated bridges in cold regions. Freezing winds strike the bridge above and below and on both sides, so it loses heat from every side. The sliding plates of the CSS are made of steel that is a good heat conductor and freezes shortly after temperature in the atmosphere hits the freezing point, resulting in the formation of an ice layer on the sliding surface. Such layer behaves as a lubricant, with a contrary effect on the friction coefficient than the one promoted by the stiffening of the slider lining material. Dry friction indeed describes the solid-solid sliding contact between two surfaces without any intermediate layer, and dry friction coefficient is typically high. However, in presence of ice, dry friction is extremely rare in practice because a thin liquid-like lubricating layer with a thickness of a few molecules is always present on the ice surface even at very low temperatures (Petrenko and Whitworth 1999; Rosenber 2005). Therefore, friction coefficient on ice is typically lower than in dry condition, and this mechanism is well known and exploited in ice sports such as skying and skating.

The effect of ice on the sliding behavior of CSSs has been generally disregarded up to now, as laboratory tests on small-scale samples generally focused on the characterization of the dry-friction coefficient of sliding materials (and generally the formation of ice on the mating steel surface was prevented in order to preserve the dry friction condition). In order to deepen knowledge of this aspect, which can have practical implications for applications in cold and very cold regions, and provide an insight for the static friction coefficient of CSSs in icing conditions, an experimental investigation was undertaken at Seismic Isolator Test Laboratory of Eskişehir Technical University, considering a full-scale sliding isolator exposed to low temperature, and subjected to the formation of ice on the sliding surface. The results of the investigation are presented in this study. The paper is arranged as follows. In Section 3.2 the basic mechanisms of friction on ice are recalled and presented in a way to help the reader understand the rationale of the study and its main findings. Section 3.3 describes the CSS under investigation and the experimental protocol implemented in the tests. The results of the experiments are presented in Section 3.4, while in Section 3.5 they are discussed and interpreted considering the practical implications related to the behavior of sliding isolators in icing conditions. Finally, the conclusions of the study are presented.

3.2. Friction on Ice

Since the exposure of the CSS to low temperatures results in the formation of an ice layer on the surface of the stainless-steel sheet as shown in Fig. 3.1, physics of friction in case of ice is addressed here. In literature, there has been a great effort to understand the mechanism of friction on ice (Colbeck 1994; Colbeck 1995; Petrenko and Whitworth 1999; De Koning et al. 2000; Kietzig et al. 2010; Bhushan 2013). The coefficient of friction between ice and most materials is universally recognized to be very low, and as it is exploited in sports such as skating, skiing, curling, etc. Although most of the previous studies that focused on ice friction were conducted with the aim of improving the performance in ice sports, the concept of friction between two solids with an interposed ice layer can be applied also to the case under investigation.

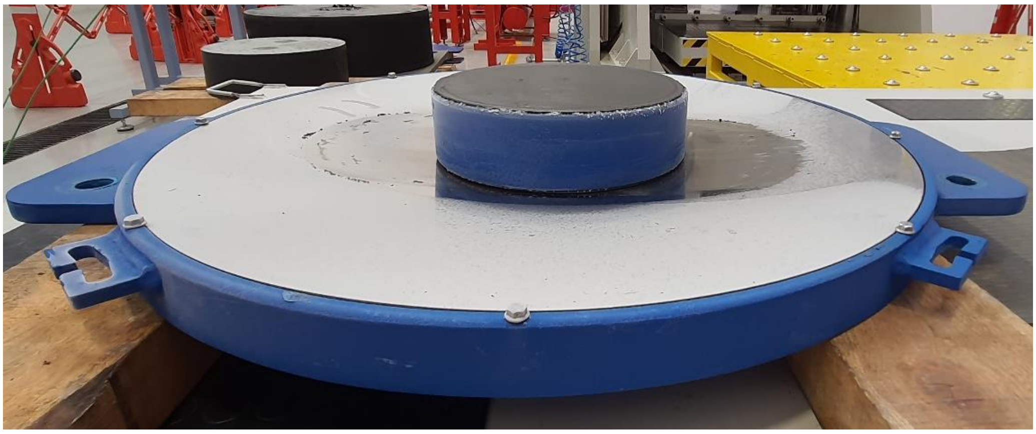

Figure 3.1. *Formation of ice layer on the surface of stainless-steel due to low temperature exposure*

Several theories have been proposed to account for the very low friction of ice (Pounder 1965). The two oldest ascribe it to the transient presence of a lubricating film of liquid water. Joly (1899) suggested that this film was produced by the pressure applied by the sliding surface which induces temporary melting of ice. On the other hand, Bowden and Tabor (1950) calculated that feasible pressures are unable to cause melting unless the ice temperature is very close to 0ºC, and suggested that the temporary liquid film is generated by frictional heating at the asperities: heat generated by friction during sliding increases the temperature at the contacting points to the melting temperature of ice, causing the ice surface to melt locally at the contacting asperities, resulting in a noncontinuous melt water film. This hypothesis has found considerable acceptance between researchers, but some objections still remain (Pounder 1965). A third theory (McConica 1950) therefore proposed water vapor as the lubricating film. Another theory (Niven 1959) considered molecular rotation on the surface of ice crystals as the leading mechanism. These water molecules lack a complete set of hydrogen bonds to lock them into place, so they could act in the manner of roller bearings to reduce friction. It is of course possible that more than one of these mechanisms come into play to produce the mechanism of friction on ice.

Regardless of its origin, the parameter influencing friction on ice is acknowledged to be the presence of a liquid-like layer on the ice surface. It has been suggested that, depending on current temperature, surface contact pressure and sliding velocity, different mechanisms can prevail, resulting in different friction regimes depending on the thickness of the liquid-like layer in relation to the roughness of the two mating surfaces, as summarized in Fig. 3.2 (Kietzig et al. 2010).

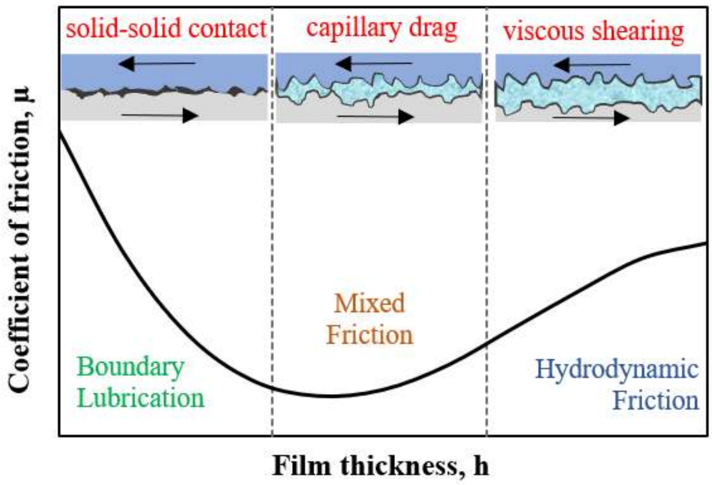

Figure 3.2. *Regimes for friction on ice (adapted from Kietzig et al. 2010)*

The boundary lubrication regime is characterized by the temperature in the contact zone being everywhere below the melting temperature of ice, and the thickness of the lubricating liquid-like film being on the order of few molecular layers. As the thickness of the liquid-like layer is substantially smaller that the roughness of the mating surfaces, friction is still governed by the contact between the asperities of the surfaces like in solid-solid friction, though the lubricating layer reduces the resistance of the solid-solid contact.

Mixed friction occurs when at some points within the contact zone the surface temperature rises above the melting temperature of ice, but the thickness of the liquid-like layer is still lower than the roughness of the surfaces. In this regime the load of the slider is partially supported by the surface asperities and partially by the lubricating layer. As the increased thickness of the lubricating layer reduces solid-solid adhesion and enhances the lubrication, a substantial decrease in friction force compared to boundary lubrication is achieved. However, at the same time the lubricant promotes the build-up of capillary water bridges between the mating asperities; such capillary bridges act as bonds between the slider and ice surfaces, resulting in an additional frictional resistance.

If everywhere in the contact zone the temperature is above the melting temperature of ice, and the thickness of the liquid-like lubricating layer between the two surfaces is greater than the height of the asperities, a hydrodynamic regime is triggered. In hydrodynamic friction it’s the lubricating layer, not the surface asperities, that carries the applied load and no solid-solid contact occurs during the sliding movement. Consequently, shearing of solid-solid adhesive bonds as in dry friction no longer contributes to the friction force. In the hydrodynamic regime friction coefficient increases with the liquid-like layer thickness due to increased viscous friction of the lubricant. Past researches (Fowler and Bejan 1993) concluded that the lubricating film under a slider on ice becomes thicker toward the trailing end. Consequently, friction mechanisms on ice can include all types of friction but for pure dry friction.

3.3. Tested Isolator and Experimental Program

An experimental campaign was performed to investigate the coefficient of friction of sliding isolators in icing conditions. The seismic isolator investigated in this research is a Double Curved Surface Slider (DCSS) having concave plates at top and bottom with a non-articulated slider in between. The slider houses two sliding pads (both are 260 mm in diameter) in contact with the two mating stainless-steel concave plates having surface roughness $R_z \leq 1$ μm (see Fig. 3.3a). The isolator was manufactured by Technological Isolation Systems (TIS) and sliding pads are made of filled PTFE. The top and bottom concave plates have the same radius of curvature R = 2500 mm. The height of the non-articulated slider is 73 mm. Thus, the effective radius of curvature of the tested DCSS is 4927 mm. Fig. 3.3b presents the geometrical properties of the tested DCSS.

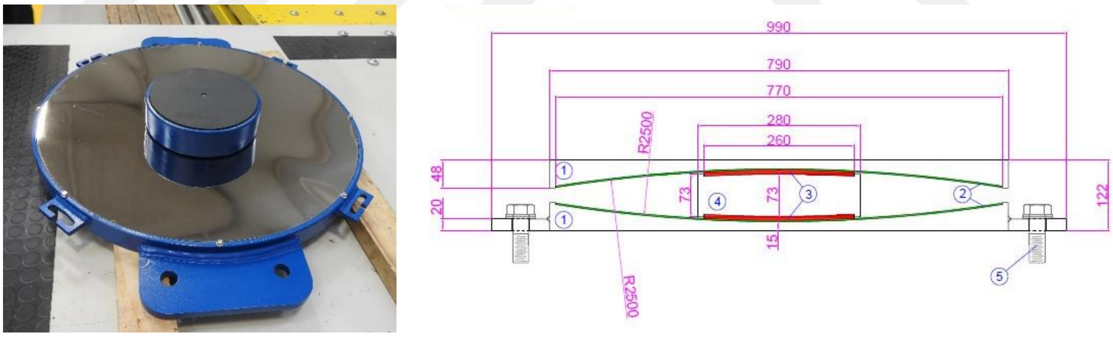

a) b)

Figure 3.3. *(a) View of the tested full-scale DCSS and (b) its geometrical properties*

The experimental campaign aims at assessing the variation in static friction coefficient of the DCSS introduced in Fig. 3.3, when subjected to low temperature. Accordingly, three different temperatures (20, 0, and -20ºC) and three different exposure times (3, 12 and 24 hrs) were considered in the tests. Additionally, in order to evaluate the effects of both axial pressure and loading velocity on static friction coefficient, the testing protocol also encompassed various axial pressures (40, 60 and 80 MPa) and loading frequencies (corresponding to maximum loading velocities of 250, 500 and 750 mm/s). Table 3.1 lists the testing protocol considered in the experiments.

Table 3.1. *Applied loading protocol for the full-scale DCSS tests*

Temperature (°C)		-20, 0, 20	
Exposure Time (hours)		3, 12, 24	
Axial Pressure (MPa)		40-60-80	
Maximum Velocity (mm/s)	250	500	750

The full-scale isolator tests were conducted at Seismic Isolator Test Laboratory of Eskişehir Technical University, and the test set-up of laboratory is presented in Figure 2.6. In the experimental program, a series of sinusoidal displacement histories, with an amplitude of D = 300 mm, were applied to the tested DCSS. The displacement histories shown in Fig. 3.4 have the form of $d(t) = D \cdot \sin(2\pi \cdot f \cdot t)$ where f is the frequency of loading and t is the time. In this form, the maximum loading velocity, V_{max}, will be equal to $2\pi \cdot f \cdot D$. For the considered maximum loading velocities (250, 500 and 750 mm/s) and the maximum amplitude of the motion (300 mm), the corresponding loading frequencies are computed as 0.133, 0.265 and 0.398 Hz.

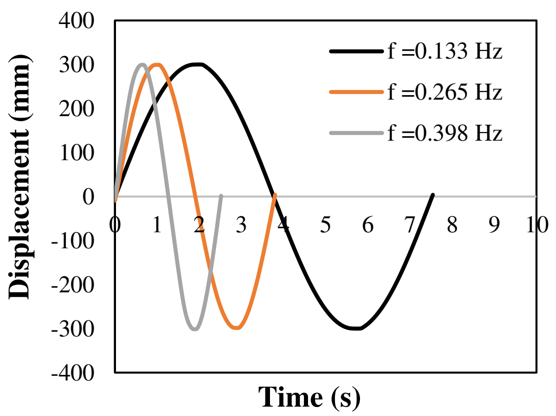

Figure 3.4. *Sinusoidal displacement histories applied in the tests.*

The temperature of the sliding surface was monitored by means of K-type thermocouples encased in the plate of the DCSS. For this purpose, a total of ten thermocouples with a temperature range of -200ºC to 1200ºC were used to record the temperature at the sliding surface. Eight of these thermocouples (labeled from 1 to 8) were embedded into the top plate of the isolator through drilled holes as shown in Fig. 3.5.a so that their probes were in contact with the back side of the concave stainless-steel plate. Fig. 3.5.b depicts the configuration of the holes drilled on the top plate of the isolator. These thermocouples were used to monitor the temperature of the area of the sliding surface crossed by the slider during its movement. The remaining two thermocouples (labeled as 9 and 10) were attached to the surface of the concave stainless-steel sheet (see Fig. 3.5.c) to record the temperature of the surface outside the area crossed by the slider, not subjected to heating due to friction. These two thermocouples also served to check the temperature of the sliding surface of the isolator in compliance with the assigned levels as listed in Table 3.1. The connectors of the thermocouples embedded to the top plate of the isolator were carefully positioned through CNC (computer numerical control) machined channels (see Fig. 3.5.d). Fig. 3.6 shows the data acquisition system used to monitor temperature readings by means of the ten thermocouples.

Prior to perform the tests, the DCSS was conditioned in the environmental chamber shown in Fig. 3.7.a according to the temperatures and exposure times given in Table 1. The controller unit (see Fig. 3.7.b) of the environmental chamber enables to keep the temperature at the desired level within a range of ±1ºC. After the conditioning at the rated temperature for the assigned period, the specimen was removed from the environmental chamber, immediately mounted on the test set-up and subjected to the application of the loading protocol. The tests were performed at laboratory temperature (20 ± 1 ºC), therefore care was paid for completing the test in the shortest possible time, in order to limit the heating of the specimen once removed from the environmental chamber. It took, at most, 8 min from the removal of the DCSS from the chamber to the end of the sinusoidal motion. Fig. 3.8 presents the temperature readings throughout the time elapsed from the removal of the DCSS to the end of test for two representative cases, namely after conditioning at 0ºC for 24 h (Fig. 3.8.a) and after conditioning at -20ºC for 24 h (Fig. 3.8.b).

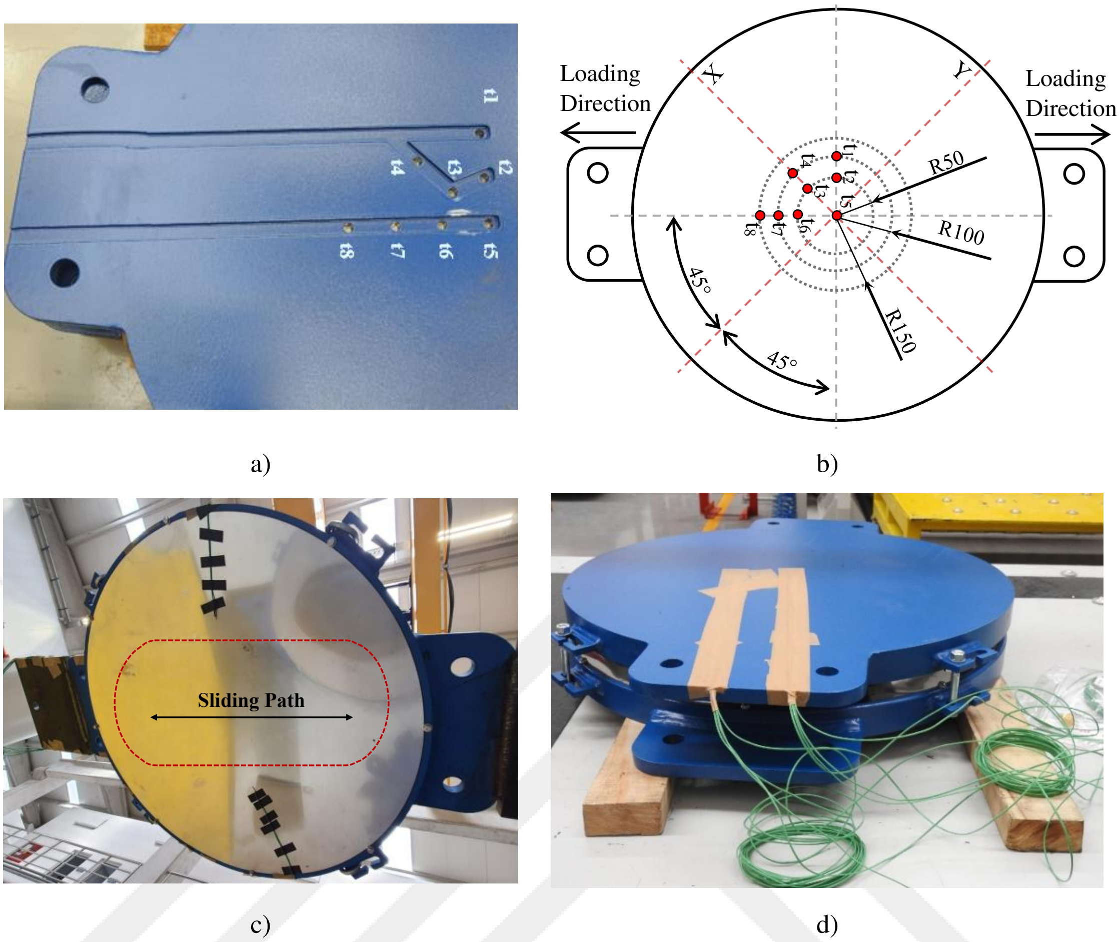

Figure 3.5. *(a) holes drilled on the top plate of DCSS to insert thermocouples, (b) configuration of the thermocouples, (c) thermocouples attached to the surface of concave stainless-steel sheet, (d) layout of the connectors of thermocouples.*

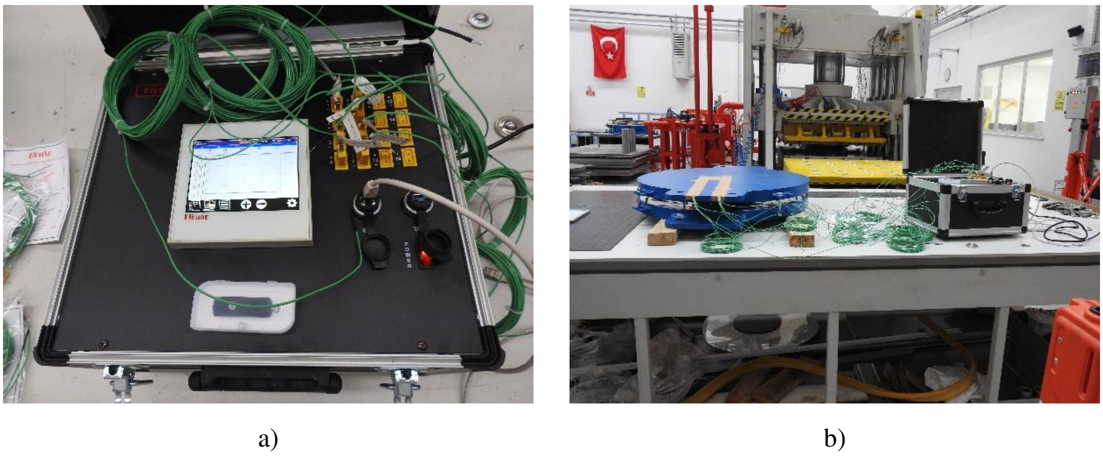

Figure 3.6. *(a) Data acquisition system used to monitor temperature and (b) its connections to the DCSS.*

a) b)

Figure 3.7. *(a) The environmental chamber and (b) its controller.*

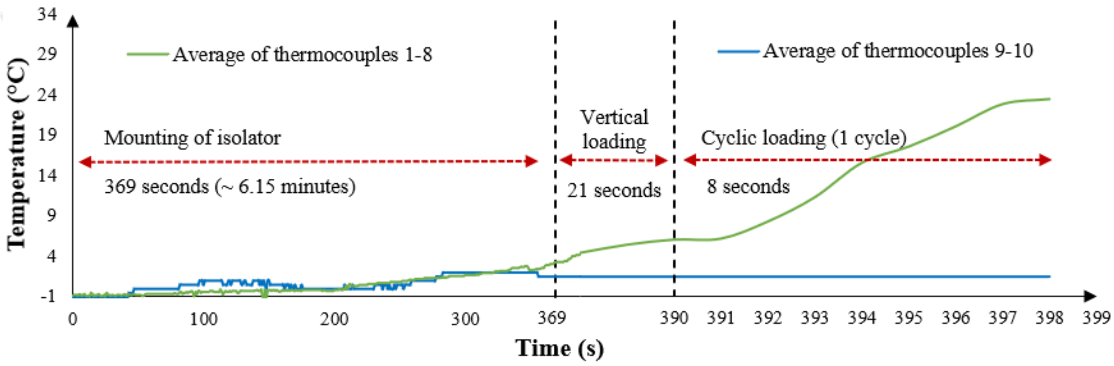

a)

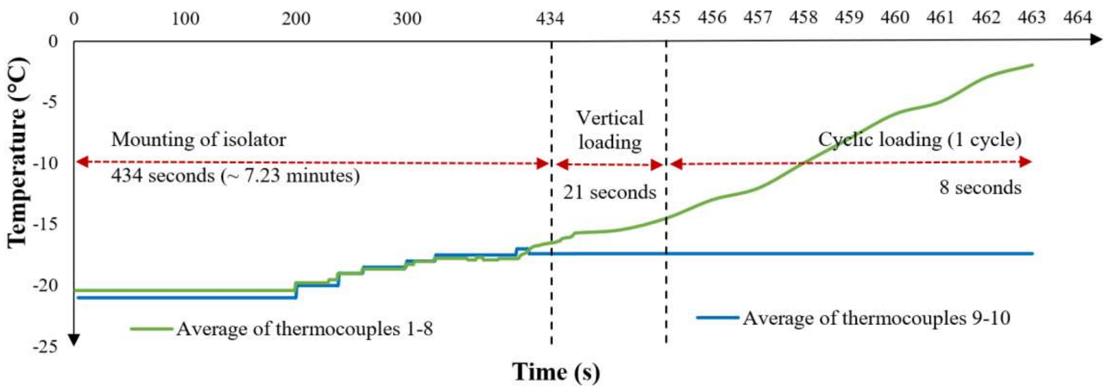

b)

Figure 3.8. *Temperature histories of the sliding surface of the CSS, inside and outside the contact area of the slider, from the removal of DCSS from the environmental chamber to the end of the test for an exposure time of 24 hrs at (a) 0°C and (b) -20°C.*

In the figure, the green line represents the average of temperatures recorded by the eight thermocouples embedded into the top plate, whereas the blue line stands for the average of temperatures recorded by the two thermocouples bonded on the surface of the stainless-steel sheet. The temperature of the sliding surface outside the area crossed by the slider remained almost constant, close to the assigned level, till the end of the test while the temperature of the area crossed by the slider gradually increased once the test was initiated. This observation confirmed that there was only marginal change in the temperature of stainless-steel surface (and, in general, of the CSS) even if the tests were performed at the laboratory conditions. As shown in Fig. 3.9, during the test, while the cyclic motion took place, the whole surface of the specimen was covered by a layer of ice. Only the temperature of the area of the sliding surface actually crossed by the back-and-forth motion of the slider increased due to the mechanism of frictional heating.

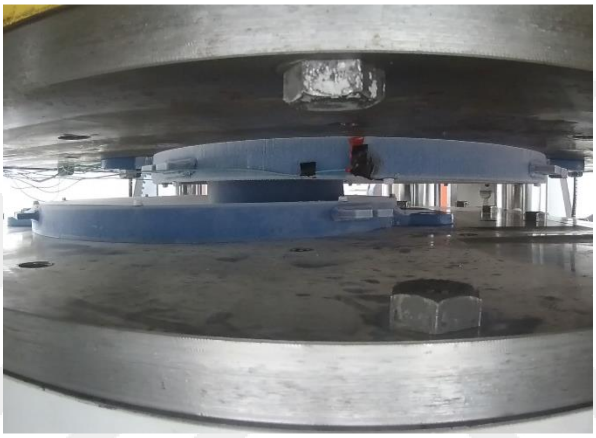

Figure 3.9. *Scene from the cyclic test of the DCSS exposed to low temperature.*

3.4 Test Results

In this section, force-displacement relations obtained from the tests performed in accordance with the loading protocol listed in Table 3.1 are illustrated. For instance, Fig. 3.10 shows the force-displacement diagrams for the tests carried out for different loading conditions at the temperatures of 20, 0 and -20ºC when the exposure time to low temperatures is 24 hrs. From these diagrams, the friction coefficient versus displacement plots can be calculated according to the procedure presented by Gandelli et al. (2019). An example of such plots, relevant to the tests performed at 80 MPa normal stress, 500 mm/s maximum loading velocity and 24 h exposure time is shown in Fig. 3.11.

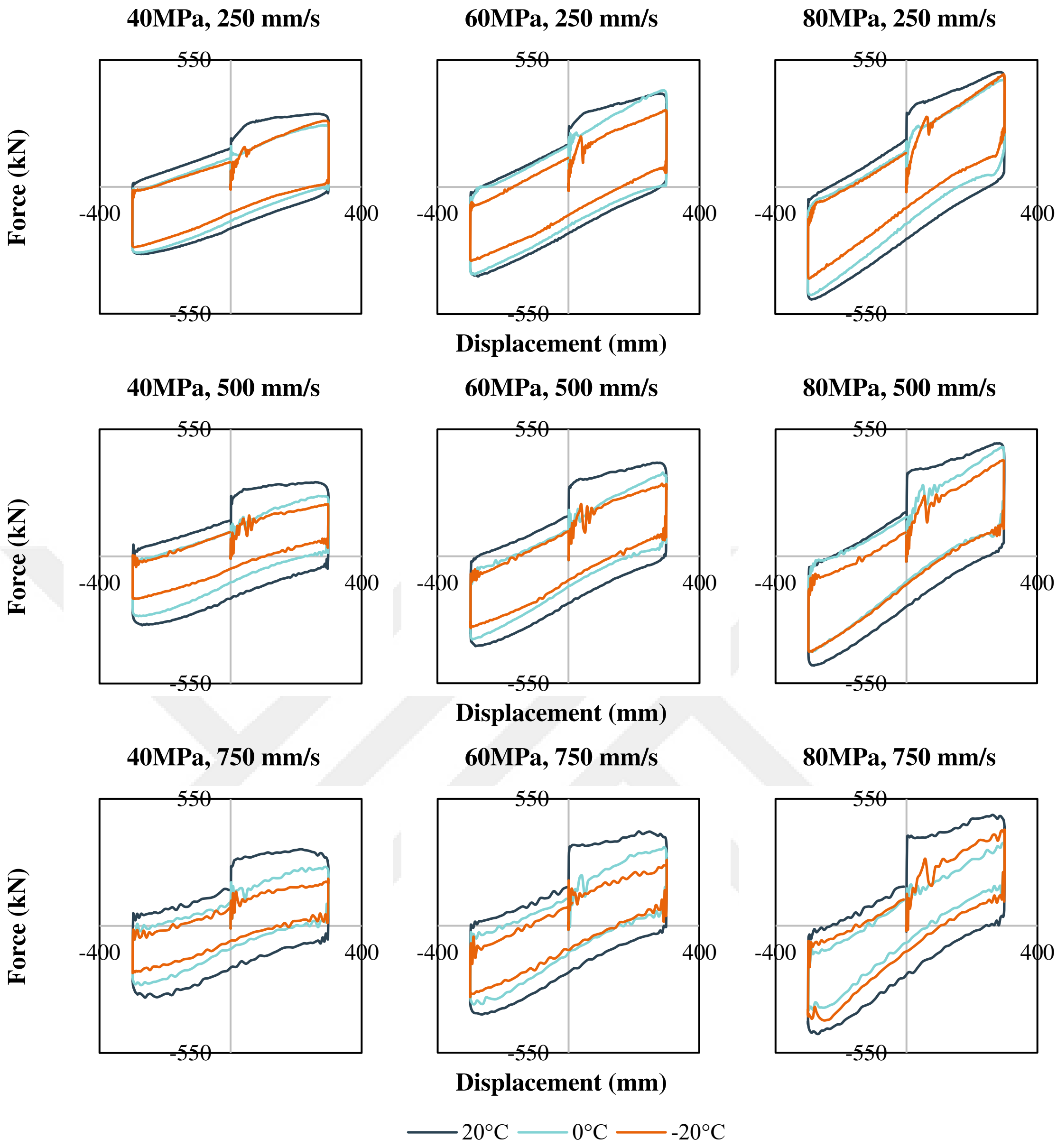

Figure 3.10. *Comparison of force-displacement diagrams obtained from tests after exposure to low temperature for 24 hrs with the corresponding reference diagrams (tests after exposure to 20°C).*

In the test at 20ºC the coefficient of friction shows the typical behavior of solid-solid contact, with a peak value at the initiation of motion, corresponding to the static friction, followed by a decrease to the dynamic value. On the contrary, in the tests performed after exposure to low temperatures, the friction coefficient shows an irregular behavior, consisting of a sequence of brief increases and drops until a peak value is achieved; friction coefficient then drops to a constant value which is maintained during sliding. It is worth noting that the achievement of the peak value of friction does not corresponds to the starting of motion like in the test at 20ºC, but to a not negligible displacement (in Fig.

3.11, at about 60 mm, corresponding to about 30 mm sliding on both curved surfaces). This phenomenon will be explained later. Anyway, the static coefficient of friction is taken as the maximum value achieved in the first half of the cycle, regardless if it is activated at the breakaway or in a displaced configuration.

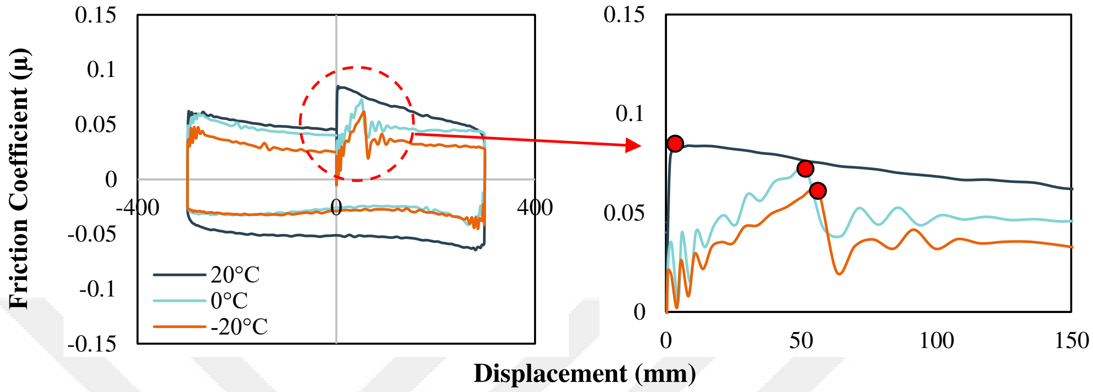

Figure 3.11. *Friction coefficient versus displacement diagrams for different exposure temperatures (normal stress: 80 MPa; maximum loading velocity: 500 mm/s; exposure time: 24 hrs).*

The static friction coefficients, μ_{st}, calculated for each loading case of Table 3.1 are presented in a comparative way to highlight the effects of temperature, exposure time, axial pressure and loading velocity. In the upcoming discussions and graphs, friction values obtained from tests conducted at 20ºC will be taken as the reference.

In Fig. 3.12, variation of static friction coefficient due to change in exposure time is presented for various axial pressures and loading velocities. The first observation in Fig. 3.12 is that static friction coefficient after exposure to -20ºC, $\mu_{st,-20^oC}$, is always smaller than the reference value $\mu_{st,20^oC}$ regardless of the exposure time, whichever the axial pressure and the velocity. On the other hand, the static friction coefficient after exposure to 0ºC, $\mu_{st,0^oC}$, may be either greater or smaller than its reference counterpart depending on the exposure time and axial pressure. For instance, for 24 hrs exposure time, $\mu_{st,0^oC}$ is always smaller than $\mu_{st,ref}$, but for exposure times of 3 and 12 hrs, $\mu_{st,0^oC}$ is greater than $\mu_{st,ref}$ for axial pressures of 40 and 60 MPa, and smaller for pressure of 80 MPa. To better highlight the effect of exposure time on the static friction coefficient, μ_{st} values calculated at low temperatures are normalized over the ones computed for reference tests; the normalized values are presented in Fig. 3.13. For 0ºC, $(\mu_{st,0^oC})/(\mu_{st,ref})$ ratios of Fig. 3.13a show that the general tendency of $\mu_{st,0^oC}$ is to decrease with increasing exposure time, with a maximum reduction of 50% for exposure time of 24 h. On the other hand, for exposures at 0ºC of 3 and 12 h the $(\mu_{st,0^oC})/(\mu_{st,ref})$ ratios are close to (and even larger than) unity. Increasing the conditioning time will promote the formation of a thicker ice layer; on the other hand, when the exposure time is short, a thin ice layer will form which will melt very quickly after the specimen is taken out from the conditioning chamber, even during the installation of the testing machine.

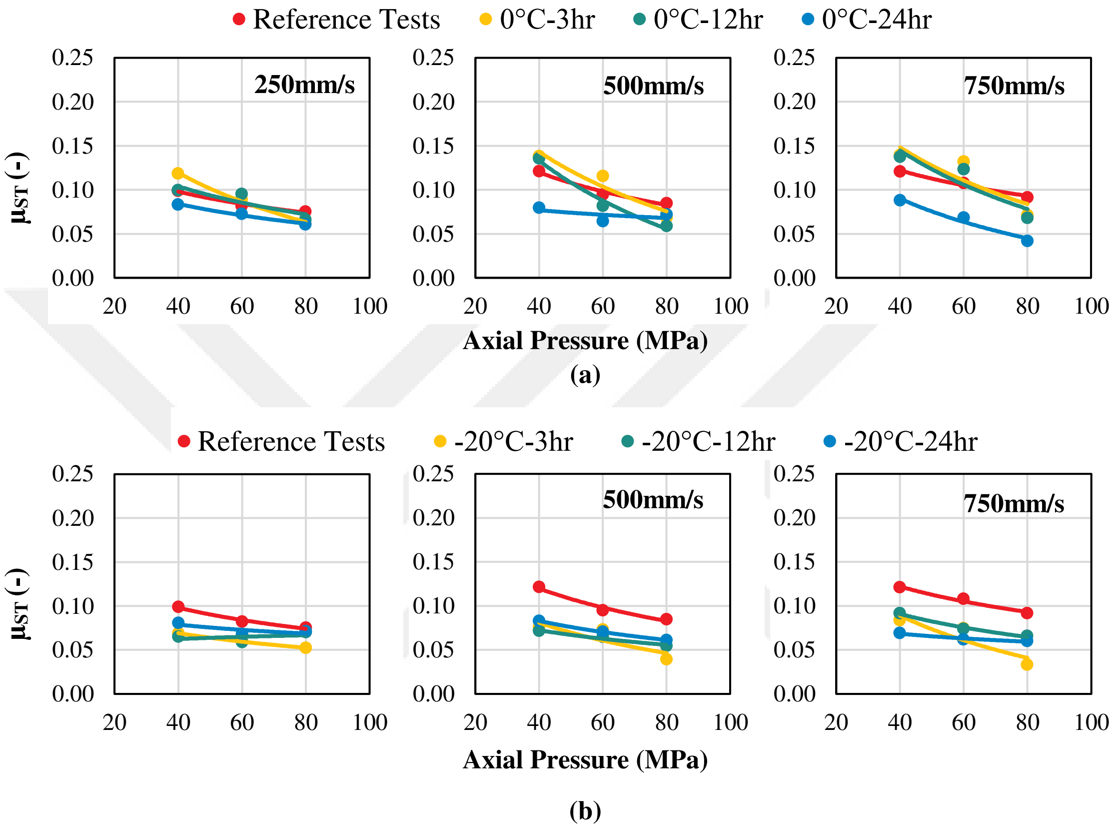

Figure 3.12. *Comparison of static friction coefficients with an emphasis on the effect of exposure time (a) for 0°C and (b) -20°C.*

As shown in the example in Fig. 3.8a, during the application of the vertical load before starting of horizontal motion the temperature of the sliding surface rose to about 4ºC, thawing the ice layer and restoring the dry friction regime. On the contrary, as in Fig. 3.13b, where the effect of exposure time on μ_{st} is presented for -20ºC, $(\mu_{st,-20\,^{\circ}C})/(\mu_{st,ref})$ ratios are always less than unity (generally between 0.5 and 0.8) without a clear dependence on the exposure time. During the stay at -20ºC a thick layer of ice forms, which is preserved during the installation of the specimen to the testing machine and the application of the loading cycles, allowing the mechanism of friction on the ice to develop.

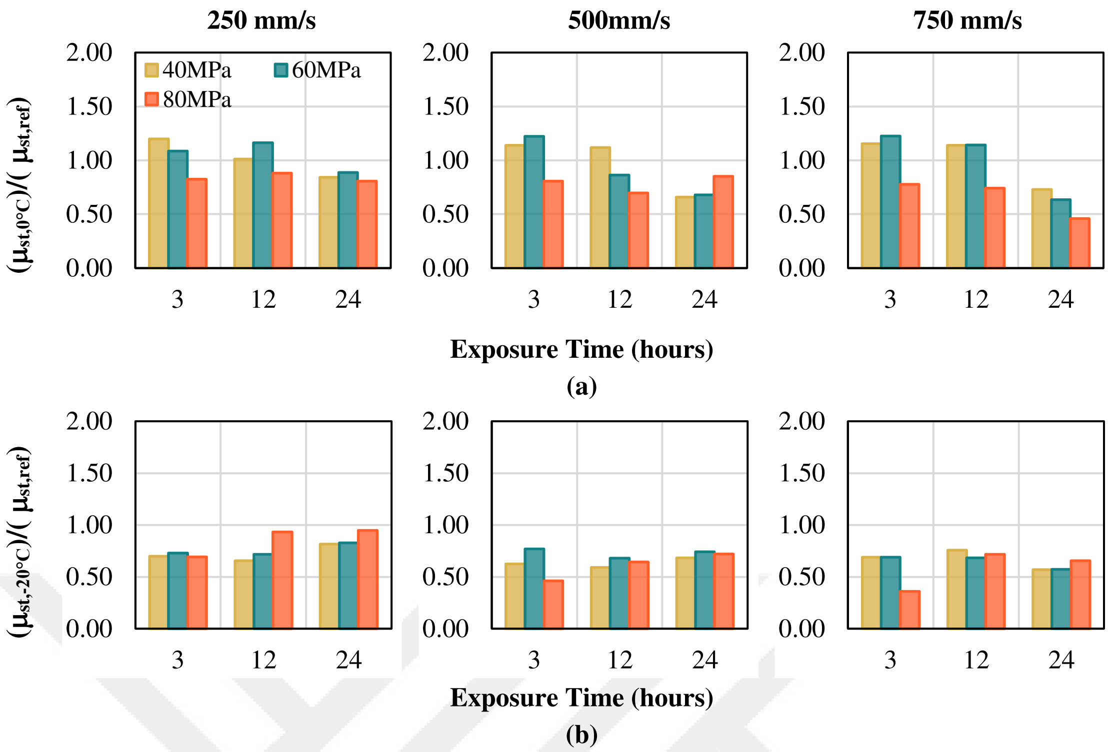

Figure 3.13. *Comparison of normalized static friction coefficients for (a) 0ºC and (b) -20ºC.*

Fig. 3.14 presents the test data from a different perspective to determine the effect of temperature on static friction coefficient when the exposure times are identical. Figs. 3.14a, b report μ_{st} values computed for different loading conditions and for exposure times of 3 and 12 hrs, respectively. As already commented with reference to Fig. 3.13, regardless of the exposure time, $\mu_{st,-20^{\circ}C}$ is always lower than $\mu_{st,ref}$ and, considering experimental uncertainties, almost independent of the actual duration of exposure. On the other hand, considering the tests after conditioning at 0ºC, for exposure time of 3 hrs $\mu_{st,0^{\circ}C}$ is close to $\mu_{st,ref}$. This result has been explained as a consequence of the heating up of the sliding surface during the installation of the specimen on the test set-up. Owing to the short exposure time, the ice layer formed on the sliding surface is very thin and it completely melts after few minutes at ambient temperature. Eventually, solid-solid contact without lubrication (the water formed from the melting of ice is squeezed out) occurs at the sliding interface, which justifies the friction coefficient similar to the one evaluated in the reference tests. As the exposure time at 0ºC increases, a thicker ice layer forms on the sliding surfaces, which will take longer to melt. After an exposure of 24 hrs, the coefficient of friction after conditioning at 0ºC practically overlap the value recorded for the same loading conditions after conditioning at -20ºC.

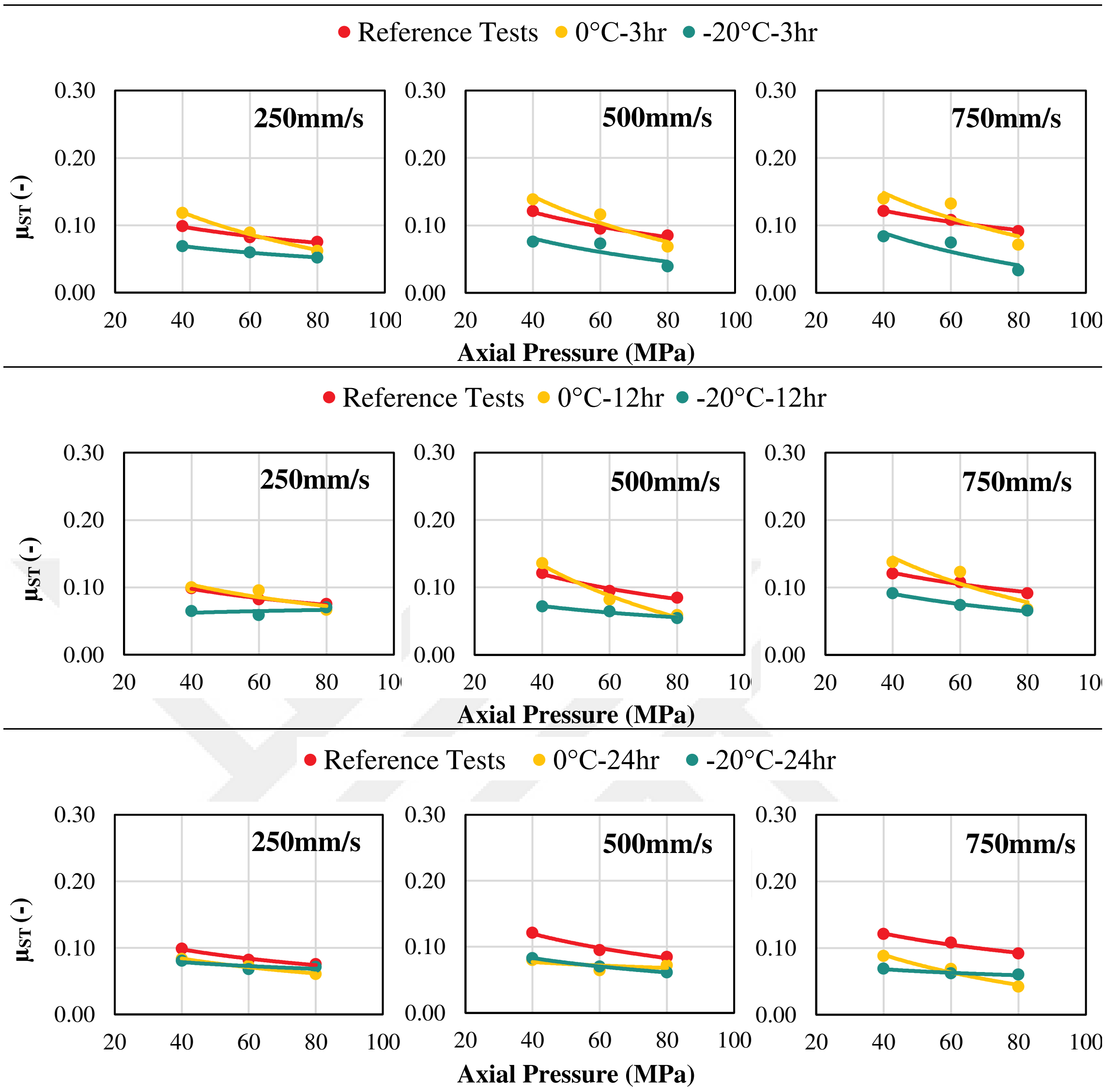

Figure 3.14. *Comparison of static friction coefficients with an emphasis on the effect of temperature for exposure times of (a) 3 hrs, (b) 12 hrs and (c) 24 hrs.*

3.5. Discussion

As described in the Introduction, static friction is an effect of the chemical bonds that form between mating surfaces when they are in the sticking phase; therefore the maximum friction resistance is expected to be triggered at the breakaway while friction decays during sliding. Further increases of friction (though at a less extent than at the breakaway) are noticed at motion reversals in a back-and-forth movement, where momentary stops occur. Recalling the results of the reference tests shown in Figs. 3.10 and 3.11, the maximum friction coefficient is observed at the very first movement of the slider. However, in the tests at low temperatures, the maximum friction coefficient was triggered not at the breakaway, but at isolator displacements in the range of 25–60 mm.

This different behavior is highlighted in Fig. 3.15, which shows the force and displacement histories recorded during the first cycle of two tests performed with the sliding surfaces at 20ºC (Fig. 3.15a) and -20ºC (Fig. 3.15b), respectively. Fig. 3.15a shows a clear transition from the sticking phase to the slipping phase at the initiation of motion. On the contrary, for the test at low temperature, there is not such a sharp transition between the two friction regimes, but friction continues to increase till a maximum value is eventually achieved, and then regular sliding starts. By examining more in detail, the initial branch of the friction force vs. horizontal displacement plot, the motion appears to be not smooth, but irregular, with short phases of sliding (slips) interrupted by stops (sticks). Initially there is relatively little movement and the force rises until it reaches some critical value. Once this force is exceeded movement starts at a much lower load which is determined by the dynamic friction coefficient, but the slider soon gets stuck, with local rises in the force before it starts to move again. Such stick-slip behavior depends on many phenomena (Berman et al. 1996). In the present case, it is proposed that a certain area of the ice layer between the sliding surfaces may undergo transitions from a solid-like state to a liquid-like state as a consequence of frictional heating developed as sliding starts, causing the drop in friction. However, once sliding starts, the friction coefficient drops from the static to the (smaller) dynamic value, causing a decrease in the heat flux. And, due to the low temperature of the sliding plate around the area crossed by the slider, the liquid-like layer freezes, reducing its thickness and promoting an increase in the frictional resistance according to the boundary friction regime shown in Fig. 3.2. This causes a new temporary stop, until the driving force exceeds the static friction resistance, and sliding starts again. Therefore, the stick-slip phenomenon is a consequence of the continuous change in the heat flux due to the transition from the sticking to the sliding condition.

That proposal is in line with the data provided in Fig. 3.8.b where the change in temperatures of both the sliding interface and the surface of the stainless-steel plate are presented. The graph shown in Fig. 3.8.b is for an exposure time of 24 hrs at -20ºC which is the case discussed in Fig. 3.15.b. Fig. 3.8.b shows that the temperature of the sliding interface between the slider pad and the stainless-steel plate started to increase with the application of vertical force while the surface temperature of the stainless-steel plate was almost constant throughout the test. Thus, the ice between the slider pad and stainless-steel plate has melted due to combined effects of both pressure melting and frictional heating. However, since the temperature of the DCSS (-15ºC and -17ºC at the sliding interface and the surface of stainless-steel plate, respectively) is still lower than the freezing temperature of water, the corresponding liquid-like layer is most likely to be in the form of a noncontinuous film due to local melting of ice. Hence, until the formation of a continuous liquid-like layer at the sliding interface, the corresponding slip and stick behavior illustrated in Fig. 3.15.b was recorded. A similar and more detailed discussion related to physics of ice friction can be found in the study of Kietzig et al. (2010). Such stick-slip behavior continues until the frictional heating is sufficient to promote the melting of a sufficiently wide area of ice on the sliding surface, and the formation of a stable liquid-like layer. From this time on, the frictional behavior is governed by the dynamic friction coefficient, which is discussed in the next chapter.

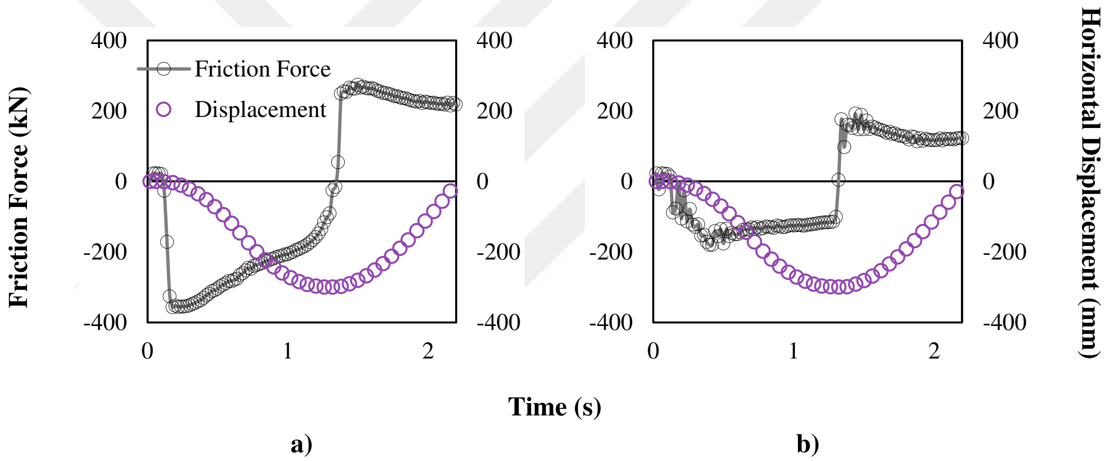

Figure 3.15. *Time histories of friction force and horizontal displacement of the DCSS during the first half-cycle of motion: (a) test at 20°C; (b) test at -20°C and exposure time 24 hrs. Test conditions: axial pressure 80 MPa, maximum loading velocity 500 mm/s.*

In this study, the friction coefficient was investigated at two temperatures of the sliding surface (T = 0ºC and T = -20ºC) and three exposure times (3 hrs, 12 hrs, 24 hrs). T = 0ºC is taken as representative of moderately low temperatures, and T = -20ºC as representative of low temperatures. The results of the tests show that:

- at moderately low temperatures, short exposure times (e.g. some hours, typically overnight) are not sufficient to promote the formation of a sufficiently thick ice layer; the formed thin layer melts after just few minutes at temperature above 0ºC, or during sliding as a consequence of frictional heating, and the friction coefficient is similar to that observed at regular temperature (20ºC);

- in case of longer exposure times (e.g. for at least 24 hrs) the ice film is sufficiently thick and stable, resulting in a substantial decrease in friction with respect to regular temperature under the same loading conditions;
- at low temperatures, only few hours of exposure (e.g., overnight exposure) are sufficient to promote the creation of a thick and stable ice layer, and the low-temperature friction coefficient is always lower that its counterpart at regular temperature;
- in case the ice layer formed on the sliding surface is sufficiently thick not to melt in full (which can be achieved either by exposure at moderately low temperature for long time, or by exposure to low temperature even for short time, e.g., hours), similar friction coefficients were observed at 0ºC and -20ºC, i.e., the influence of the subzero temperature is negligible.

It is also worth noting that the test results of the present study are in apparent contradiction with property modification factors, or lambda factors, recommended in the codes. Both the European and the North American codes and standards (CEN 1998; CEN 2009; AASHTO 2014), recommend for unlubricated PTFE/steel interfaces, a 10% increase in the coefficient of friction at 0ºC, a 20% increase at -10ºC and a 50% increase at -30ºC, while the findings of the present study point out that friction on ice provides a substantial decrease in the static friction coefficient. This is due to the fact that the codes focused on the effect of low temperature on the sliding material only and disregarded the effects of icing on the surfaces of sliding isolators. The results of the present study should therefore be taken into account for a proper consideration of the coefficient of friction of sliding isolators operating in cold regions.

3.6. Conclusion

The study investigates, by means of tests performed on a full-scale isolator, the friction coefficient of Curved Surface Sliders in icing conditions, i.e., when an ice layer forms at the sliding interfaces due to permanence at ambient temperatures below 0ºC. This situation, which can occur during the service life of isolators installed outdoor in cold regions, has been disregarded by past research on sliding materials for sliding bearings and sliding isolators. In fact, in such research, the attention was focused on the dry coefficient of friction of the sliding material at low temperature. Another novelty of the study lies in the fact that for the first time, to the best Authors' knowledge, the effect of low temperature was investigated on a full-scale sliding isolator, instead of small samples of sliding material.

The main results of the study can be summarized in the following points:

(a) at temperatures below 0ºC, a liquid-like layer of melted ice forms on the iced sliding surface; such layer performs like a lubricant layer avoiding the solid-solid contact between the mating sliding surfaces and producing a (substantial) decrease in the static friction coefficient with respect to the relevant value measured at regular temperature (20ºC), where friction is governed by solid-solid contact between the asperities of the mating surfaces;

(b) pressure and sliding velocity contribute to determine the thickness of the liquid-like layer and therefore the resulting friction coefficient;

(c) at moderately low temperature, in case of short exposure time (on the order of few hours in the experiments), the thickness of the ice layer is small and the layer quickly melts in case the ambient temperature is raised above 0ºC; the liquid-like layer is lost and the friction coefficient is similar to the reference value measured on a specimen previously not exposed to low temperature;

(d) at low temperature, a stable and thick ice layer forms on the sliding surfaces even for short exposure times (on the order of few hours), and the friction coefficient is significantly lower than the value at the reference temperature (20ºC);

(e) the static coefficient of friction in icing conditions is not affected by the exposure temperature, provided that the duration of exposure is sufficient to promote the formation of a thick and thermally stable ice layer.

The results of the study can be considered as preliminary, because restricted to a single isolator and a single sliding material but can serve as the basis for future investigations on this topic.

4. DYNAMIC FRICTION COEFFICIENT OF SLIDING ISOLATORS AT DIFFERENT LOW TEMPERATURES AND EXPOSURE TIMES

4.1 Introduction

According to Eurocode (CEN 1998; CEN 2005), the value of the λ factor changes depending on whether the material is lubricated or not and suggests an increase of the friction coefficient at -30°C, in comparison to the value assessed at 20°C, up to 150% for unlubricated PTFE and 300% for lubricated PTFE. However, such λ factors were defined on an empirical basis, essentially based on laboratory tests conducted on small-scale specimens avoiding the formation of ice on the mating steel surface as the regular practice. However, it is questionable whether the laboratory conditions under which the friction coefficient was assessed realistically represent the real case experienced by the isolators. Sliding isolators are commonly provided with cover seals and skirts all around the outer bearing to prevent exposure and contamination of the sliding surfaces. However, cracked seals and standing water on the sliding surfaces have been sometimes reported from inspections of in-service devices (Alvarado and Ryan 2023). In cold regions, an even bigger concern is the fact that entrapped water or air humidity will freeze during the winter months, affecting in an unpredictable sliding behavior of the isolators (Alvarado and Ryan 2023). According to the Authors' knowledge, the effect of water and ice contamination on the coefficient of friction of sliding surfaces is missing in prior literature. This situation is plausible when considering countries like Italy and Türkiye, which are prone to severe earthquakes and at the same time experience low temperatures in winter. In this regard, the European seismicity map is shown in Figure 4.1, correlated with a map of the average minimum surface air temperature of the two countries observed in the coldest months, from December to February, during the period 1991-2020, sourced from the website climateknowledgeportal.worldbank.org. Several high seismic risk areas, characterized by Peak Ground Acceleration (PGA) values exceeding 0.2g, experience average temperatures below 0°C for several days over the year. As an example, by referring to the Friuli-Venezia Giulia region in Italy and the Erzurum region in Türkiye (tagged in Figure 4.1), average minimum temperatures of about -2°C and -11°C in the winter seasons are expected, respectively.

In literature, there are no studies examining the effect of ice on the dynamic friction coefficient, which is the main parameter of interest for the design of the isolated structure. Therefore, the objective of this research is to investigate the influence of ice on the dynamic friction coefficient of CSSs. The structure of the paper will follow this scheme: details on the analyzed CSS and on the adopted testing protocol are provided in Section 4.2. The experimental results are provided and discussed in Section 4.3, considering the practical implications associated with the behavior of sliding isolators in icing conditions. Finally, in Section 4.4 the conclusions are reported.

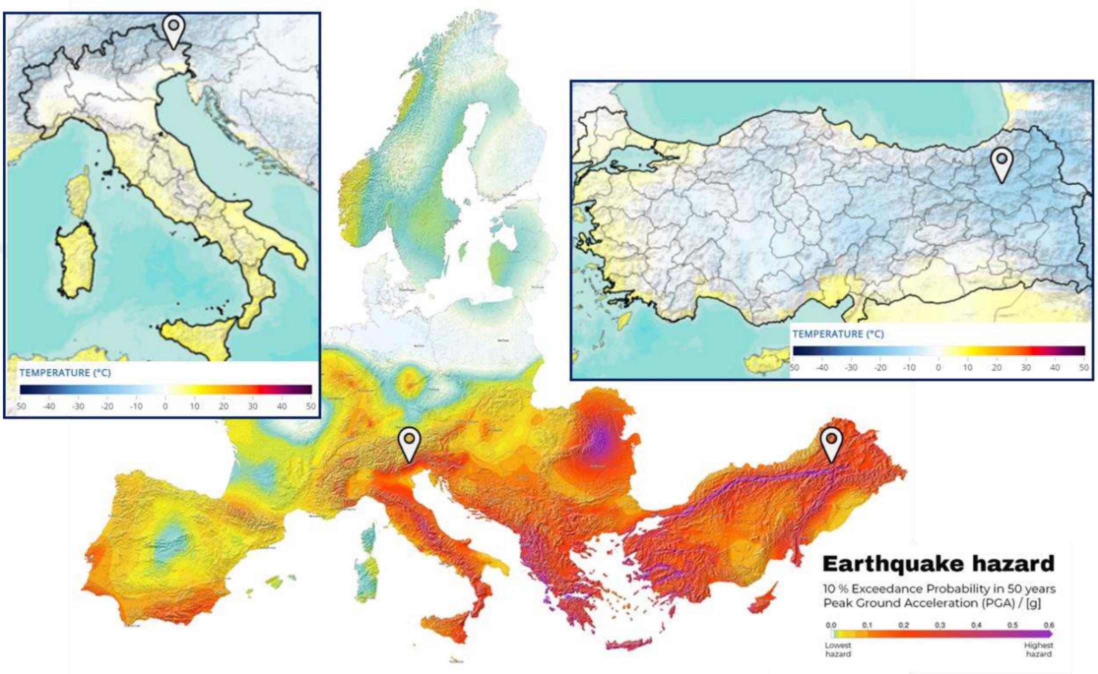

Figure 4.1. *Seismic map of Europe (Danciu et al. 2021) with indication of the average minimum surface air temperature observed in the cold months (December – February) of the period 1991 – 2020 in Italy and Türkiye (source: climateknowledgeportal.worldbank.org)*

4.2. Materials and Methods

4.2.1. Description of the specimen

The seismic isolator used in this experimental program is identical to the one described in Section 3, with its geometric characteristics illustrated in Figure 3.3.

4.2.2. Experimental program

In the literature, most of the studies have focused on the effects of low temperatures on the hysteretic properties of rubber bearings, typically examining a temperature range of 0 to -30ºC, as in (Constantinou et al. 2007) and (Hasegawa et al. 1997; Yakut and Yura 2002a; Yakut and Yura 2002b; Fuller et al. 2004; Cho et al. 2008; Cardone and Gesualdi 2012; Park et al. 2012; Mendez-Galindo et al. 2017; Zhang and Li 2020; Cavdar et al. 2022; Yaşar et al. 2023a; Yasar et al. 2023b). While, regarding the choice of the exposure times, there is a significant difference among the various works, passing from cases in which the isolators are exposed just for a few minutes (Nakano et al. 1993) to others that considered several days of exposure, e.g., (Yakut and Yura 2002a; Yakut and Yura 2002b; Mendez-Galindo et al. 2017). However, all these studies remarked that the exposure time to low temperature is one of the key parameters affecting the isolator response. Therefore, with the goal of having realistic loading scenarios, an initial statistical study was conducted to determine the minimum temperature and the longest exposure time to consider in this work. In particular, it was assumed that the DCSS of Figure 3.3 was used in the base isolation system of a bridge located in Erzurum, one of the coldest cities in Türkiye with high seismic risk, (as shown in Figure 4.1), and the related temperature records were obtained from Turkish State Meteorological Service. Figure 4.2 shows the frequency in Erzurum of having low temperatures under 0, -5, -10, -15 and -20ºC referring to the years 2016, 2017 and 2018. In particular, the indicated frequency is the ratio of the number of temperature readings below these target values to the number of all temperature readings. For instance, in Figure 4.2(a), the frequency of having -20ºC (blue column) for 24 consecutive hours is almost zero. This means that it is unlikely to have temperatures less than or equal to -20ºC for a period longer than 24 hours.

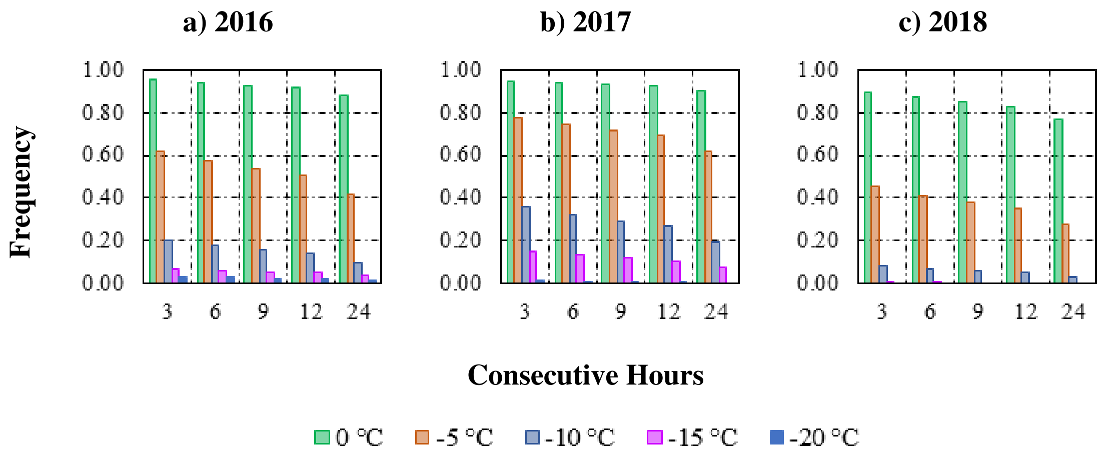

Figure 4.2. *The number of consecutive hours of low temperatures recorded in Erzurum in 2016-2017-2018*

Based on the results of this analysis, the temperatures considered in the experimental program were -20, 0 and 20ºC, while the exposure times were 3, 12 and 24 hours. Moreover, to further investigate the effects of both normal stresses acting on the sliding pads and the loading velocity on the dynamic friction of the tested DCSS, tests were performed considering normal stresses of 40, 60 and 80 MPa and maximum loading velocities of 50, 250, 500 and 750 mm/s. Table 4.1 summarizes the loading protocol followed in the experimental program.

Table 4.1. *Loading protocol implemented in full-scale DCSS experiments*

Temperature (°C)	-20, 0, 20			
Exposure Time (hours)	3, 12, 24			
Axial Pressure (MPa)	40-60-80			
Maximum Loading Velocity (mm/s)	50	250	500	750

4.2.3. Experimental set-up

Tests were performed at Seismic Isolator Test Laboratory of Eskişehir Technical University, using the test set-up shown in Figure 2.6. The DCSS were tested under displacement-controlled uni-directional sinusoidal cyclic motions in the horizontal direction, with amplitude, D_{iso}, of 300 mm. The maximum loading velocities, namely, 50, 250, 500 and 750 mm/s, listed in Table 4.1, correspond to loading frequencies of 0.0266, 0.133, 0.265 and 0.398 Hz, respectively. Figure 4.3 shows the displacement histories considered in the experimental program and characterized by three loading cycles in accordance with the requirements of the codes (CEN 2009; ASCE 2017; TBEC 2018).

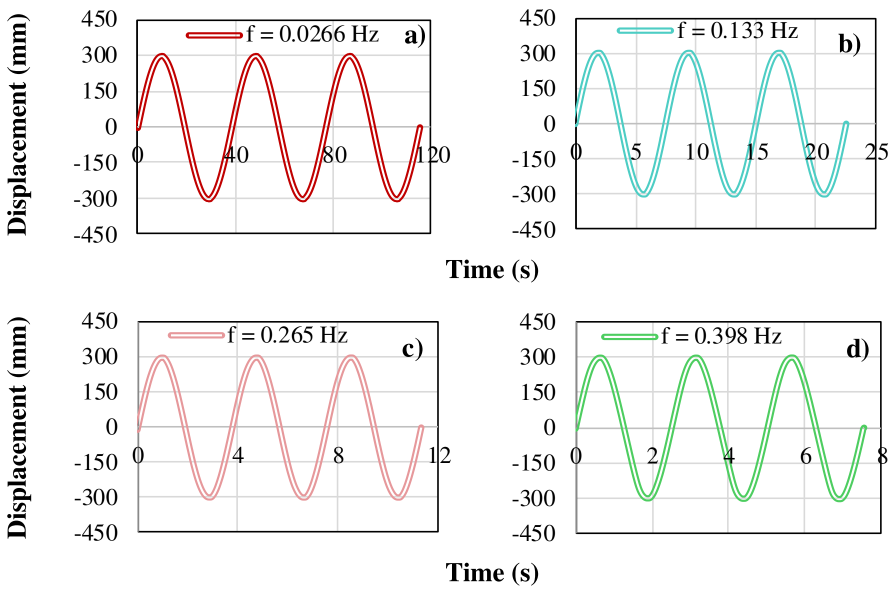

Figure 4.3. *Sinusoidal displacement histories with frequencies of (a) 0.0266 Hz, (b) 0.133 Hz, (c) 0.265 Hz, (d) 0.398 Hz.*

4.2.4. Conditioning procedure

The DCSS was conditioned prior to each test in the environmental chamber of Seismic Isolator Test Laboratory shown in Figure 3.7(a). This system has dimensions of 3x3x3 m, and its maximum and minimum temperature capacities are +50 ºC and -40 ºC, respectively. The controller of the chamber shown in Figure 3.7(b) allows to control the temperature within a tolerance of ±1 ºC for the desired exposure duration.

In order to track the temperature of the specimen prior to and during the tests, ten K-type thermocouples were used, as shown in Figure 3.5. Eight of them (labeled as t_1-t_8 on Figure 3.5) were embedded in holes drilled on the top plate of the specimen. Probes of the thermocouples embedded into these holes were in contact with the back surface of the concave stainless-steel sheets. In this way, it was possible to monitor the instantaneous temperature of the sliding interface during the test. Moreover, two additional thermocouples (t_9 and t_{10} on Figure 3.5) were used to track the surface temperature of the concave stainless-steel at points outside the area crossed by the slider. In addition to that, t_9 and t_{10} were also used to check whether the temperature of the sliding surface of DCSS fit the target temperatures considered in the experimental campaign. The connectors of the thermocouples were positioned through channels shown in Figure 3.5 and plugged in the data acquisition system (see Figure 3.6) employed to record the temperature data.

Once the DCSS was conditioned at the selected temperature and exposure time, it was removed from the environmental chamber (Figure 4.4(a)) and directly transferred to the mounting table and attached to the test set-up, as shown in Figure 4.4(b). Since the tests were conducted at laboratory conditions (20 ± 1°C), this operation was performed in the shortest possible time, in order to limit the rise in temperature of the specimen after its removal from the environmental chamber. Figure 4.5 shows the variation in temperature of the DCSS starting at its removal from the environmental chamber to the beginning of the test for two representative cases, namely test after conditioning at -20ºC for 24 hours (Figure 4.5(a)) and test after conditioning at 0ºC for 24 hours (Figure 4.5(b)). Green and blue lines in Figure 4.5 represent the averages of temperatures recorded by thermocouples embedded into the top plate (t_1-t_8) and in contact with the surface of the stainless-steel plate (t_9-t_{10}), respectively. Both Figure 4.5(a) and (b) indicate that the temperature of the DCSS increases by only 2 - 3ºC before the start of the test. Figure 4.6(a) shows the physical condition of the DCSS after being conditioned at -20ºC at 24 hours. It is clear that both the slider and the sliding surfaces were covered with ice. Figure 4.6(b) presents a scene of the DCSS taken during the cyclic motion.

Figure 4.4. *(a) The removal of the DCSS from the environmental chamber, (b) mounting of the DCSS to the test set-up*

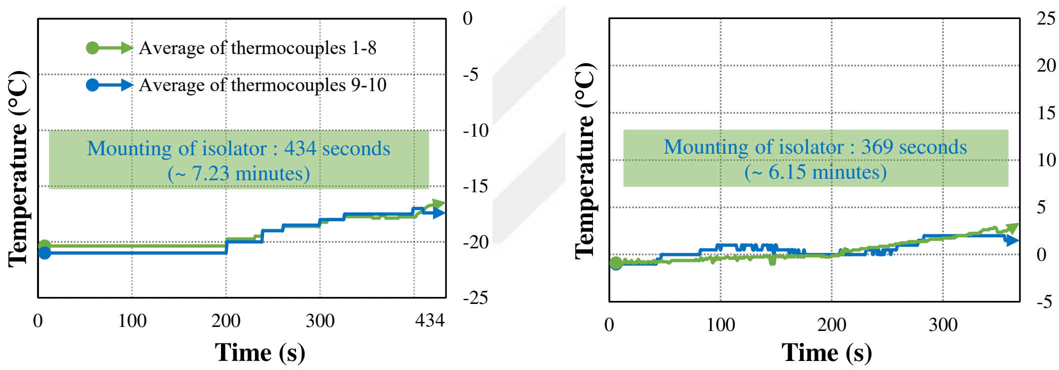

(a) (b)

Figure 4.5. *Change in average temperatures for the time period between the removal of the isolator and start of the test after conditioning of the DCSS at (a) -20°C for 24 hours and (b) 0°C for 24 hours*

(a) (b)

Figure 4.6. *(a) The physical condition of both the slider and the stainless-steel plate, (b) a scene of the tested DCSS taken during the cyclic motion*

4.3. Results and Discussions

In this study, tests were conducted on the same DCSS considering different combinations of temperature, exposure time, stress and velocity levels indicated in Table 4.1, for a total of 84 tests. More specifically, 36 tests were conducted for each temperature (either 0 or -20ºC), by considering 3 exposure times, 3 normal stress levels and 4 maximum loading velocities; while 12 tests were conducted at the room temperature (20 ± 1ºC), referring to 3 normal stress levels and 4 maximum loading velocities. To ensure that the sliding properties of the DCSS were unaffected by low temperature exposure and possible wear of the sliding material during repeated cycles, benchmark tests at 40 MPa and 250 mm/s were conducted at room temperature at the beginning of the experimental campaign and after the low temperature test sequences at 0°C and at -20°C. Force-displacement plots from benchmark tests are compared in Figure 4.7, showing only minimal changes despite the multiple loading cycles and exposure periods to low temperature. These differences are quantitatively assessed in Table 4.2 by comparing the friction coefficients of each loading cycle. The friction coefficients for each cycle are calculated using Eq. (2.2), as defined in Section 2.

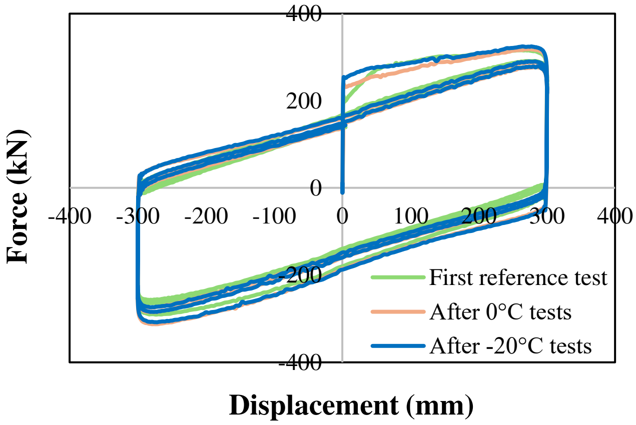

Figure 4.7. *Comparison of force-displacement curves recorded in benchmark tests performed at different stages of experimental campaign*

Table 4.2. *Comparison of friction coefficients calculated for each cycles of benchmark tests*

	μ_1	μ_2	μ_3
First Ref. Test	0.086	0.072	0.067
After 0°C Tests	0.089	0.075	0.070
After -20°C Tests	0.091	0.076	0.071

Figure 4.8 shows the force-displacement loops of the isolator tested at 20 ± 1 °C, highlighting the effects of both increasing normal stress (from 40 to 80 MPa) at constant sliding velocity of 50 mm/s in Figure 4.8(a), and rising loading velocities (from 50 mm/s to 750 mm/s) at constant normal stress of 40 MPa in Figure 4.8(b). In the tests, DCSS was subjected to three cycles of displacement controlled motions and corresponding dynamic friction coefficients were computed for each cycle by means of Eq. (2.2). The average dynamic friction coefficient, μ_{ave}, was calculated by means of Eq. (4.1), in order to estimate the representative friction coefficient and reported in Figure 4.9 for different loading velocities and normal stresses.

$$\mu_{ave} = \frac{\mu_1 + \mu_2 + \mu_3}{3} \tag{4.1}$$

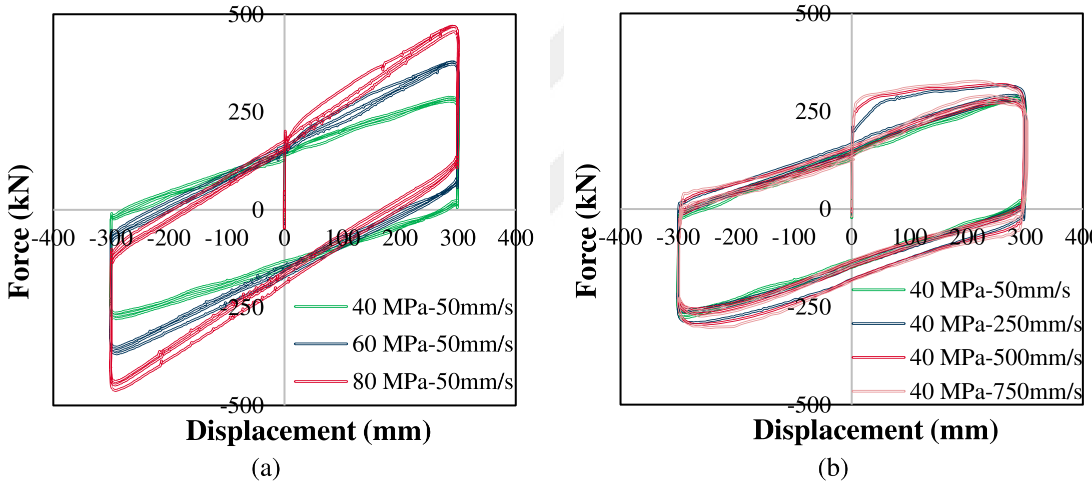

Figure 4.8. *Comparison of force-displacement relations of the tested DCSS to highlight the effect of (a) normal stress while the maximum loading velocity is constant and equals to 50 mm/s, (b) maximum loading velocity while the normal stress is constant and equals to 40 MPa.*

In accordance with other studies in the literature (Tyler 1977; Constantinou et al. 1987; Mokha et al. 1990; Tsopelas et al. 1996; Dolce et al. 2005; Quaglini et al. 2012a; Lomiento et al. 2013; Barone et al. 2019, Cavdar et al. 2022), Figure 4.9(a) shows that the friction coefficient decreases as the normal stress increases, regardless of the loading velocity. Moreover, as shown in Figure 4.9(b), the friction coefficient tends to increase with an increase in loading velocity from 50 mm/s to 250 mm/s and then settles at an asymptotic value regardless of a further increase in the loading velocity.

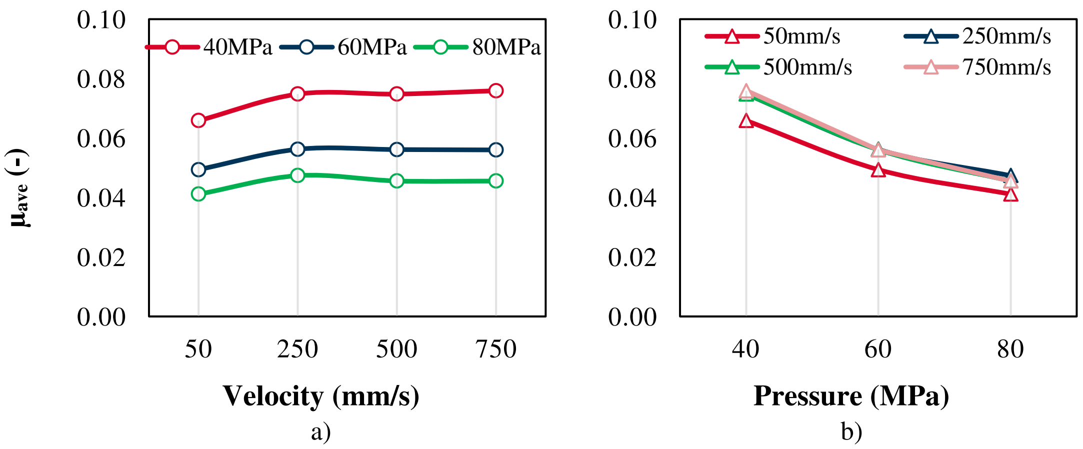

Figure 4.9. *Change in average friction coefficient, μ_{ave}, as a function of (a) normal stress and (b) loading velocity*

Figure 4.10 compares the hysteretic loops recorded at 1st, 2nd and 3rd cycles of the DCSS conditioned at -20ºC for different exposure times and tested at normal stress of 40 MPa and loading velocity of 250 mm/s. Hysteretic cycles obtained from the tests at ambient temperature are also reported in Figure 4.10 as a reference. In the 1st cycle, all the isolator forces recorded at -20ºC are significantly less than the ones recorded at ambient temperature, while in the 2nd cycle and mostly in the 3rd cycle, the isolator forces recorded for all exposure times get closer to the reference ones. The reason of having smaller isolator forces (in other words, smaller friction coefficients) at each loading cycles of -20˚C can be explained referring to physics of friction on ice. In seismic isolation applications exposed to low temperatures (i.e., seismically isolated bridges constructed in cold regions), the temperature below the freezing point causes the formation of an ice layer on the sliding surface of the stainless-steel plate, which behaves like a lubricant. Therefore, the friction coefficient on ice is typically less than its counterpart assessed in dry condition (Petrenko and Whitworth 1999; Rosenber 2005; Kietzig et al. 2010).

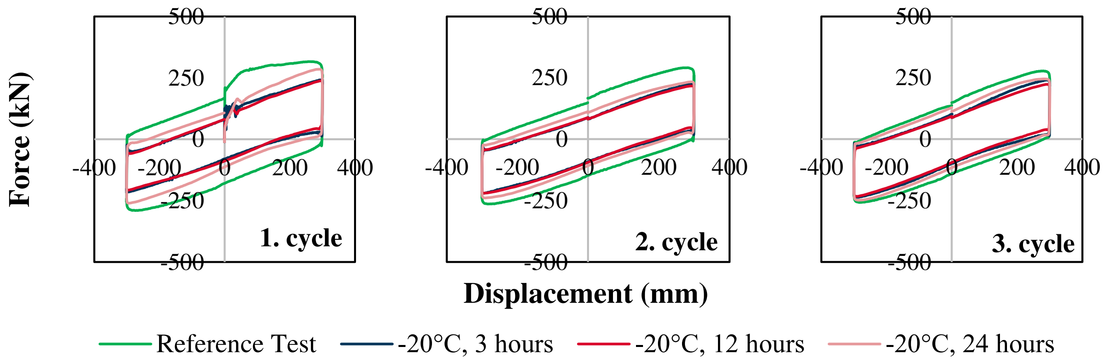

Figure 4.10. *Comparison of the reference force-displacement relation of the tested DCSS recorded at (a) 1st, (b) 2nd and (c) 3rd cycles with the ones recorded after conditioning at -20°C for 3, 12 and 24 hours (normal stress=40MPa, maximum loading velocity=250mm/s)*

On the other hand, the gradual reduction in the isolator force from cycle to cycle at 20ºC is due to the temperature rise, ΔT, at the sliding interface as shown in Figure 4.11(a). where the temperature rises recorded by thermocouples t_1-t_8 (see Figure 3.6) are presented for three cycles of motion. Such a response modification in hysteretic behavior of the isolator is alleged to the change in the friction coefficient at the sliding interface during the cyclic motion. The dissipation of energy through friction promotes a temperature rise on the sliding interface. The larger friction coefficient observed at 20ºC causes a larger dissipation of energy, and consequently, a larger temperature rise (53ºC in average at the end of 3rd cycle) in the sliding interface. Such a temperature rise in turn results in reduced friction coefficient. Thus, the isolator forces recorded at the 1st cycle are larger than the ones recorded at the 2nd and 3rd cycles. But, for the cases at -20ºC, the averages of maximum temperature rises recorded by the thermocouples are less than 20ºC (16, 9 and 18ºC for 3, 12 and 24 hrs of exposure times, respectively) at the end of the second cycle of the motion, which means that the absolute temperatures of the sliding interfaces are still less than 0ºC. Since the temperature of the sliding interface is below the freezing point, the ice formed at the sliding interface during the low temperature exposure preserves its existence throughout the motion. Thus, the friction coefficients are reduced and the corresponding temperature rises are limited. This is why the amounts of change in isolator forces from cycle to cycle at -20ºC are also limited.

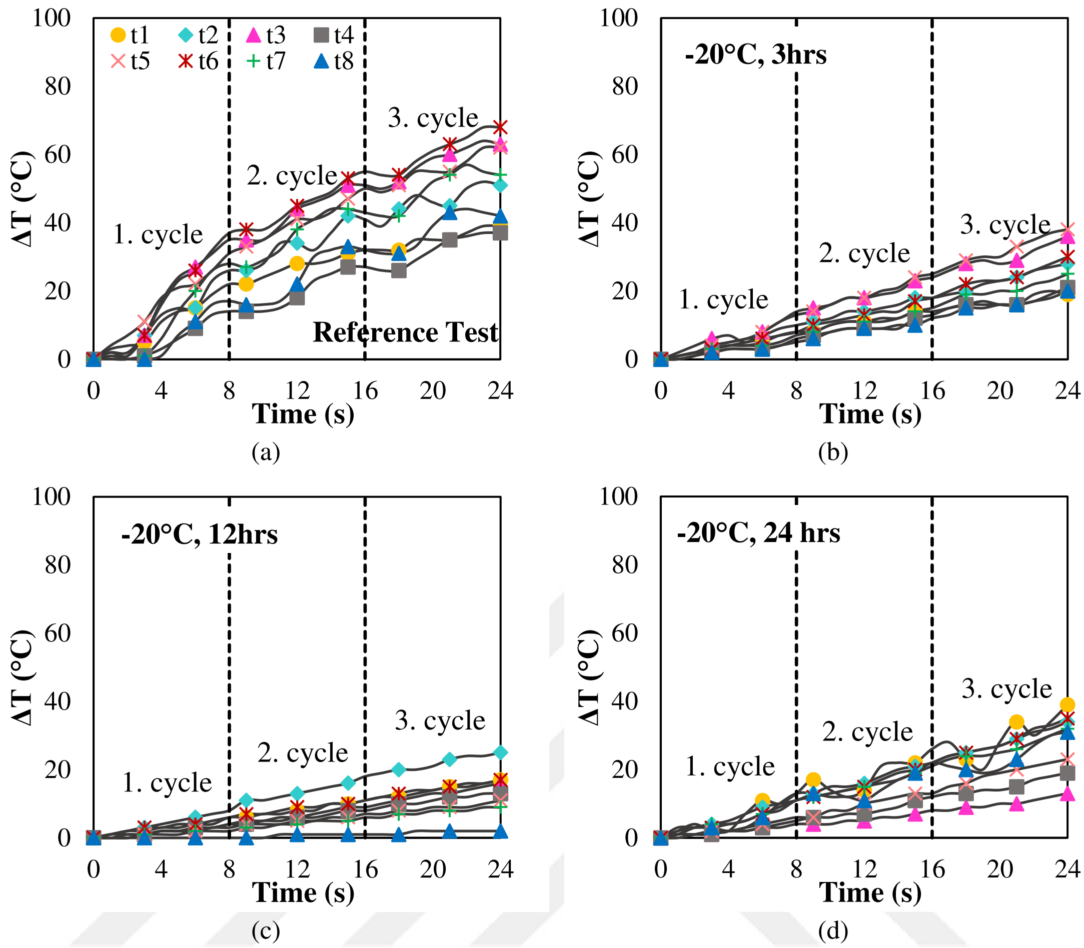

Figure 4.11. *Temperature changes recorded by thermocouples t1-t8 during the (a) reference test, and tests performed after conditioning (b) 3 hours, (c) 12 hours, (d) 24 hours at -20 °C (normal stress=40MPa, maximum loading velocity=250mm/s)*

Figure 4.12 shows the trend of the average dynamic friction coefficients μ_{ave} calculated by means of Eq. (4.1) for all the loading cases given in Table 4.1. It is apparent that, regardless of the normal stress and loading velocity, the minimum value of μ_{ave} is always obtained for low temperature exposures at -20ºC. On the other hand, for exposures at 0°C, μ_{ave} may be either lower or higher compared to the value obtained in the reference test conducted at room temperature depending on the loading conditions (stress and velocity). As an example, μ_{ave} assessed in tests after exposure at 0ºC for 24 hrs, is consistently lower than μ_{ave} from the reference test; while, for exposures of 3 or 12 hrs at 0°C, μ_{ave} is greater than the reference value at 40 and 60 MPa, and lower at 80 MPa. The result seems counterintuitive, as one expects that increasing the normal stress would correspondingly increase the mechanical work, leading to higher dissipated energy and temperature rise.

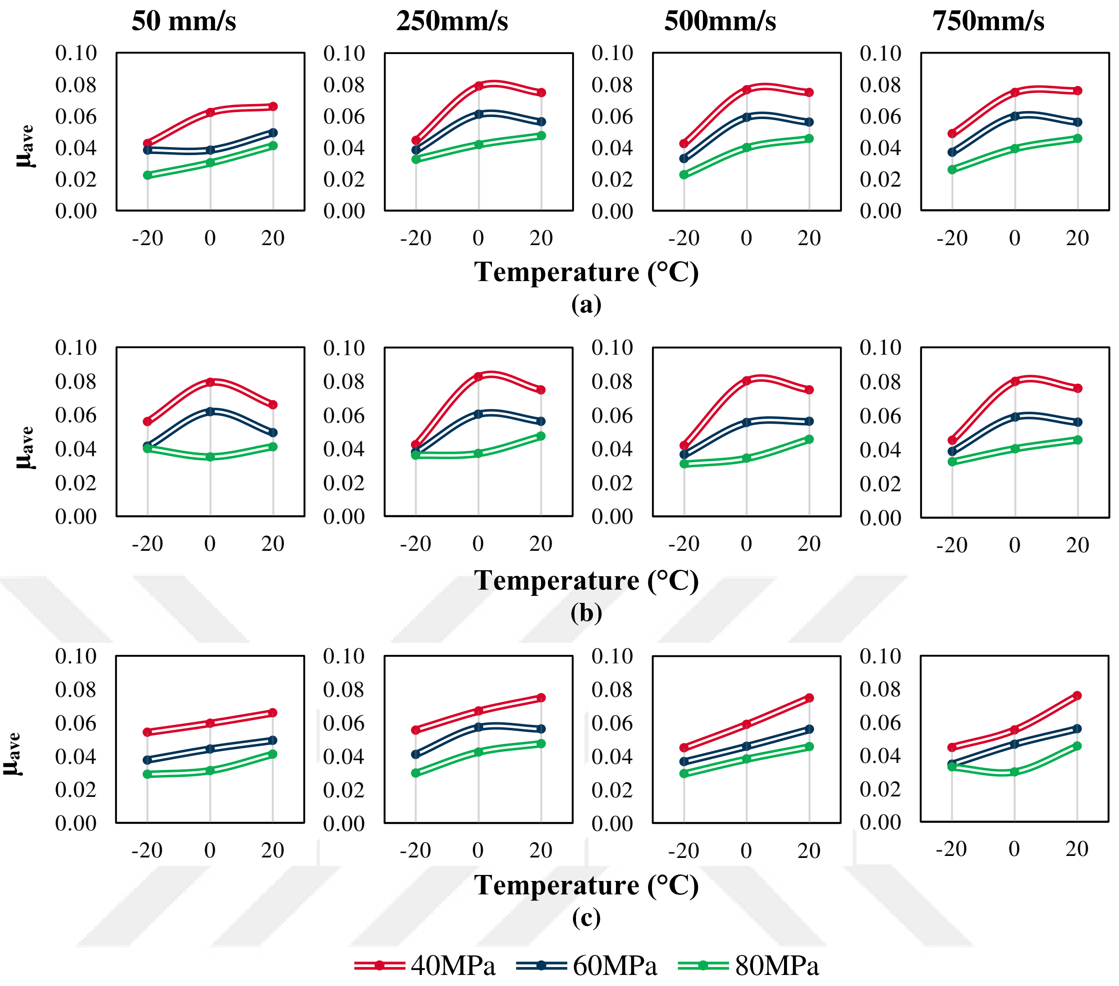

Figure 4.12. *Temperature versus μ_{ave} values as a function of normal stress for exposure times of (a) 3 hours, (b) 12 hours and (c) 24 hours.*

However, the increase in normal stress also triggers a decrease in the friction coefficient, as evident from Figure 4.9(a); consequently, there is an overall decrease in energy dissipation. In addition to these considerations, it should also be noted that after exposure at -20°C, ice formation always occured regardless of the exposure time. For this reason, the coefficient of friction in tests at – 20°C is systematically lower than the other cases. However, in the case of exposure at 0°C, ice formation is strongly influenced by the duration of exposure. After 24 hours of exposure, μ_{ave} is usually observed to be lower than in the reference test at 20°C, indicating ice formation. In contrast, for exposures of 3 and 12 hrs, the values of μ_{ave} reveal that perhaps the exposure time is not sufficient for the formation of the ice layer on the sliding surfaces. This latter consideration is confirmed also by the results shown in Figure 4.13, which indeed focuses on the effect of exposure time at low temperatures on the variation of μ_{ave}. It turns out that for normal stress of 40 and 60 MPa, μ_{ave} values at -20ºC are almost the same regardless of the exposure time

(Figure 4.13(a) and (b)). Similar results are obtained also for normal stress of 80 MPa and temperatures of 0°C and -20°C, as shown in Figure 4.13(c). On the other hand, at 0°C, μ_{ave} assessed for 24 hrs of exposure time is always lower than for 3 and 12 hrs of exposure time. As previously mentioned, this can be ascribed to the fact that short exposure times at 0°C are not sufficient to cool down the whole mass of the isolator, and therefore it is likely that the bulk of the steel plates will remain above 0°C preventing the formation of a stable ice layer.

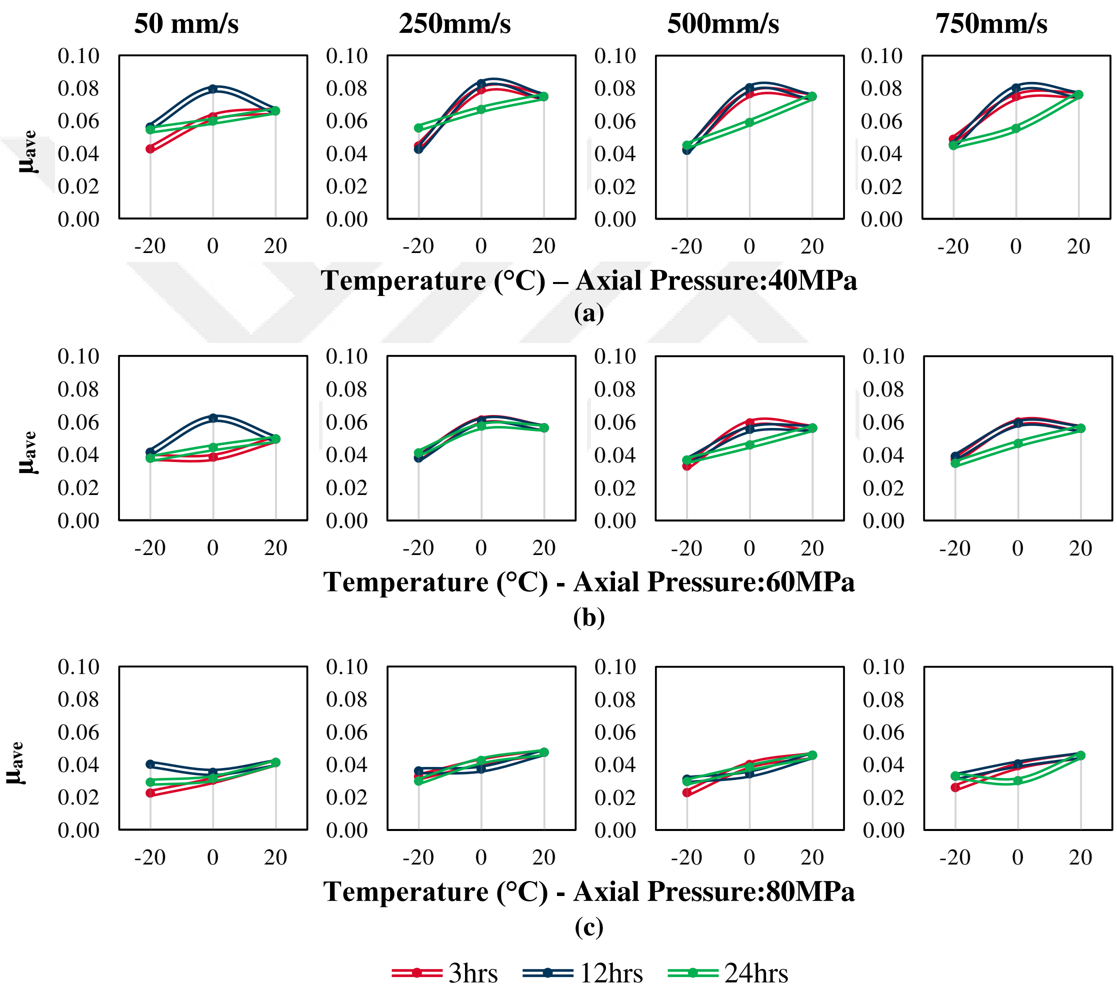

Figure 4.13. *Temperature versus μ_{ave} values as a function of exposure time for normal stresses of (a) 40 MPa, (b) 60 MPa and (c) 80 MPa*

Finally, Figure 4.14 reports the variation in percentage of μ_{ave} values at low temperatures with respect to the reference ones at 20°C: blue bars represent decrease whereas red bars stand for increase. The findings reveal that low-temperature exposure can lead to reductions in friction coefficient of up to 50%, which is the case of DCSS tested at an axial pressure of 80 MPa and sliding velocity of 500 mm/s after an exposure at -20°C for 3 consecutive hrs. As discussed earlier, low temperature exposure mostly results in reduced dynamic friction coefficients which is contrary to design approach called as bounding analyses. In bounding analyses, both lower- and upper-bound properties (assumed to be representative of probable variations in isolator properties due to several parameters) of seismic isolators are considered in the analyses. The lower-bound properties of seismic isolators are used to estimate the maximum isolator displacement while the upper-bound properties are employed to estimate superstructure response. In accordance with code provisions (CEN 2009; ASCE 2016; TBEC 2018) these properties are determined by multiplying the friction coefficients (obtained from tests performed at room temperature) with response modification factors, λ. The λ factors suggested for lower-bound analysis are generally less than 1.0 while they are greater than 1.0 for upper-bound analysis. And as listed in Table 4.3, the code suggestion to consider the effect of low temperature exposure is to increase the friction coefficient by having λ factors greater than 1.0 for temperatures ≥ 0ºC. Such a design philosophy assumes that the friction coefficient of a CSS increases with low temperature exposure. However, the data presented in this study reveals mostly the opposite. The reason of such a contradiction between the presented test data and the suggested λ factors is due to the procedures followed in the test programs they are obtained. Suggested λ factors are essentially based on small-scale tests conducted by avoiding the formation of ice on the sliding interface as the regular practice. On the other hand, in this study, a full-scale CSS was tested and formation of ice on the sliding interface was observed (see Figure 4.6). It is clear that there is a need to define a test procedure for determination of friction coefficient of CSSs exposed to low temperature.

Table 4.3. *Property modification factor for temperature variation of CSSs (CEN 1998)*

Temperature [°C]	Unlubricated PTFE	Lubricated PTFE
20	1.0	1.0
0	1.1	1.3
-10	1.2	1.5
-30	1.5	3.0

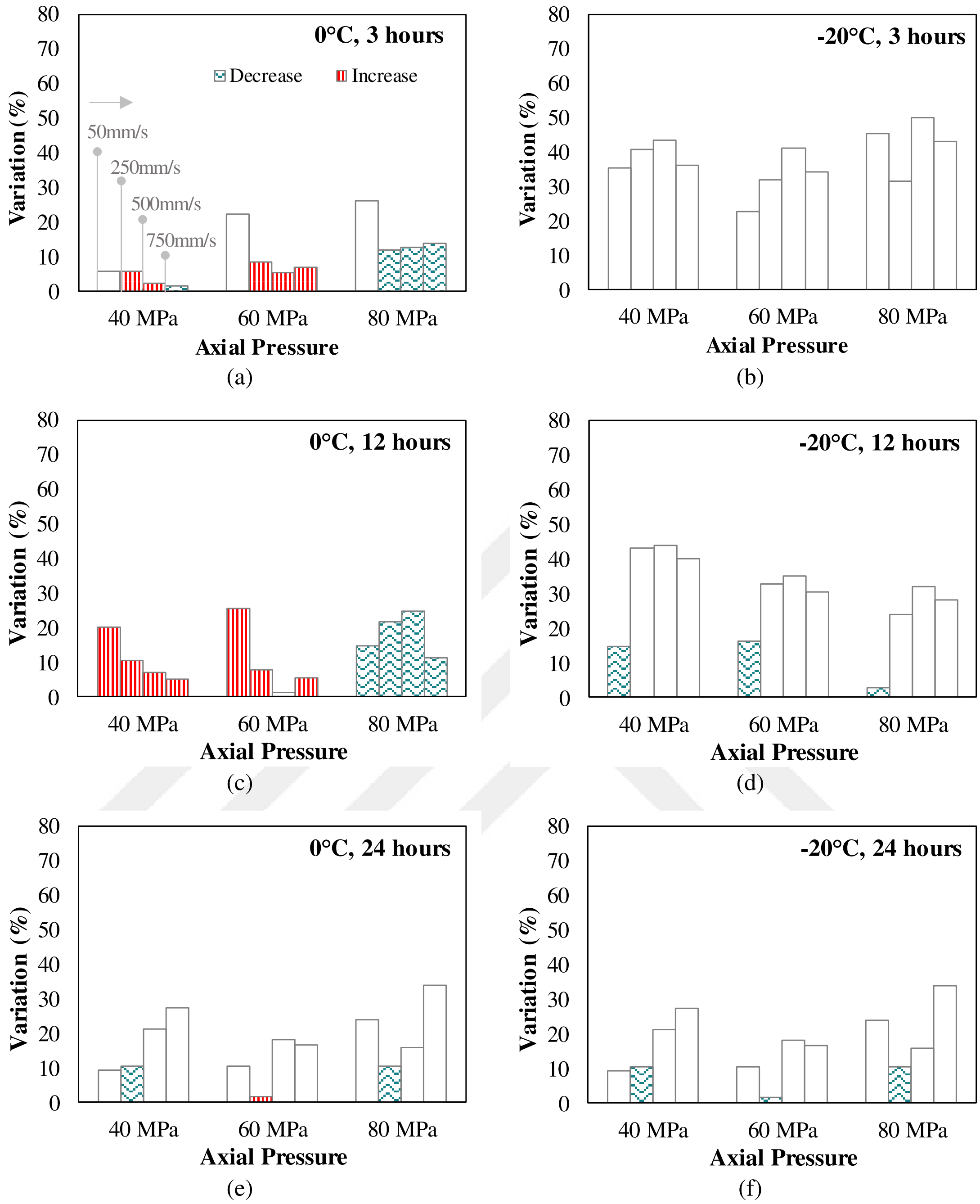

Figure 4.14. *Variation in μ_{ave} values obtained from different loading cases with respect to reference one (a) 0°C 3 hours, (b) -20°C 3 hours, (c) 0°C 12 hours, (d) -20°C 12 hours, (e) 0°C 24 hours (f) -20°C 24 hours*

4.4. Conclusions

In this study, to the best of Authors' knowledge, the effect of exposure time to low temperatures on dynamic friction coefficient of a full-scale Curved Surface Slider (CSS) was investigated for the first time in literature. In the experimental program conducted within the scope of this study, a double CSS was subjected to different levels of normal stresses and loading velocities after being conditioned at varying low temperatures and exposure times. In the tests, a CSS was subjected to displacement controlled cyclic motions and corresponding dynamic friction coefficients were presented in a comparative manner. Results of this study reveal the followings:

- Although the literature related to small-scale test results indicate that the dynamic friction coefficient increases with decreasing temperature, this study reveals an opposite behavior. The dynamic friction coefficient of the tested full-scale CSS decreases with decreasing temperature. The reason of the reduction in friction coefficient is the formation of ice layer at the sliding interface which is avoided in small-scale tests. The ice layer observed in full-scale tests behaves like a lubricant at the sliding interface and results in reduced friction coefficients.
- When the temperature is -20ºC, the effect of exposure time on friction coefficient becomes insignificant. This observation is valid for all of the normal stresses and loading velocities considered in the test protocol. Because, in all the loading combinations performed after the CSS was conditioned at -20ºC, there was always formation of ice layer at the sliding interface. However, in case of 0°C, minimum value of μ_{ave} is obtained only for the longest duration of exposure. This indicates that for 0ºC, the friction coefficient decreases with increasing exposure time. Such a response modification this can be ascribed to the fact that short exposure times at 0 °C may not be sufficient to cool down the whole mass of the isolator, and therefore it is likely that the bulk of the steel plates will remain above 0°C preventing the formation of a stable ice layer.
- The comparison between the results of the conducted tests and the property modification factors, λ_s, recommended in CEN 1998 and in CEN 2009 in order to consider the effect of low temperature on friction coefficient, shows that the current form of λ_s is not representative of what occurs in practical situation, as they disregard the effect of ice. Thus, there is a need to define a more realistic test protocol to assess the effect of low temperature on friction coefficient of CSSs.
- In the presence of ice at the sliding interface, low temperature does not affect the upper bound value of friction coefficient as suggested by the codes. On the contrary, it turns out to be a phenomenon that should be considered as a parameter affecting the lower bound value of friction coefficient. This affects the design of the seismic isolation units. Because, if the actual friction coefficient is lower than

the design value, the corresponding maximum isolator displacements will be greater than the ones computed by using the lower bound values.

It is to be noted that the discussions and conclusions presented in this study are only preliminary and need to be further developed. Future efforts to understand effects of both low temperature and exposure time should be directed to (i) small-scale tests with and without ice formation at the sliding interface; (ii) further full-scale isolator tests having different geometrical properties.

5. ESTIMATING THE FRICTION COEFFICIENT OF SLIDING ISOLATORS BY MEANS OF SMALL-SCALE TESTS

5.1. Introduction

Current standards such as CEN EN 15129 (2009), AASHTO (2014), and ASCE/SEI 7 (2016) specify protocols for testing full-scale prototypes to characterize the properties of isolation systems, including the effective friction coefficient μ_{eff}. These tests are mandatory for both qualification and acceptance, ensuring that the performance of production devices meets the design targets. In order to avoid the possible bias of size effects on the determination of the isolator's properties, CEN EN 15129 (2009) allows only small variations between the size of production devices and the tested prototypes, specifically, a maximum ±20% difference in vertical load and/or displacement capacity. On the other hand, CEN EN 15129 (2009) permits reduced-scale tests to assess the wear endurance of the sliding materials and the effect of wear on the coefficient of friction in non-seismic conditions.

Small-scale tests based on simplified models are commonly used for the characterization of sliding materials in research and development due to their proven reliability (Quaglini et al. 2012a; Quaglini 2012b; Quaglini et al. 2022) and their suitability to reduce experimental costs or accommodate equipment limitations. This is particularly advantageous in applications such as shake table tests on base-isolated structural mock-ups (Becker and Mahin 2012; Sarlis et al. 2013; Ponzo et al. 2017; Wen et al. 2019). However, due to the simplifications introduced in the physical model, the extrapolation of small-scale results to the real scale is generally not straightforward and should be evaluated case by case (Quaglini et al. 2009; Quaglini et al. 2012a; Quaglini et al. 2022).

The aim of this chapter is to explore the use of small-scale tests for the assessment of the friction coefficient, by investigating the relationship between the effective coefficient of friction μ_{eff} of a full-scale CSS and the coefficient of friction of the thermoplastic sliding material determined in small-scale tests. The goal is to validate a procedure for characterizing the coefficient of friction of CSSs by means of small-scale tests that can be used at the research and development stages of new devices or new materials, reserving large-scale prototype tests, as required by standards, solely for the final validation of the device, thereby optimizing the design process and reducing overall costs. A second goal is to formulate a unified model of the coefficient of friction of sliding material and develop a procedure for calibrating the relevant parameters by means of small-scale tests.

The structure of the chapter will follow this scheme: Section 5.2 presents the experimental campaign conducted on small-scale specimens to identify the main factors influencing the frictional behavior of the sliding material consisting of filled PTFE. In Section 5.3, a unified model to describe the friction coefficient at the material level (μ_M) is proposed. Then, to verify the suitability of small-scale tests in predicting the isolator's performance, the estimated values for small-scale material are compared with the effective friction coefficient (μ_{eff}) of full-scale isolator incorporating the above material (Section 5.4). Finally, in Section 5.5 the conclusions are reported.

5.2. Small-Scale Experiments at Room Temperature

5.2.1. Test set-up

The small-scale tests are performed on specimens of sliding material consisting of flat circular pads with a diameter of 75 mm and a thickness of 8 mm (Figure 5.1). The specimens are recessed by 5 mm into a steel backing plate, leaving a 3 mm sliding gap, and mate a flat stainless steel partner surface.

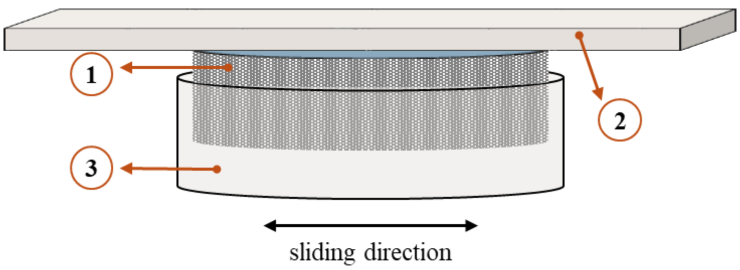

Figure 5.1. *Sketch of the small-scale specimen arrangement: (1) sliding material pad, (2) mating surface, (3) steel backing plate*

In the present study, the tested specimens are made of a proprietary sliding material consisting of filled PTFE (Figure 5.2.a and 5.2.b) and are tested in combination with mating stainless-steel plates (Figure 5.2c) mirror finished to $R_a \leq 0.2$ µm and $R_z \leq 1$ µm roughness.

(a) (b) (c)

Figure 5.2. *Small-scale PTFE specimen (a); connection apparatus (b) and stainless-steel mating plate (c)*

The experimental campaign is conducted using a custom testing machine at the Material Testing Laboratory of Politecnico di Milano (Figure 5.3.a) that allows two specimens to be tested in a double shear configuration. The two specimens are connected to the lower base plate of the testing machine and to the vertical jack (shows in 5.3.b as "bottom specimen" and "top specimen", respectively), while the mating stainless-steel surfaces are fitted to a horizontal moving plate, driven by a horizontal jack. The vertical jack, with 500 kN capacity, applies a compressive force to the specimens, ensuring the target contact pressure at the sliding interface. The horizontal jack, rated at 75 kN, drives the moving plate with a maximum velocity of approximately 300 mm/s. Load cells and inductive displacement transducers are employed to measure the loads and the displacements applied to the specimens. Both jacks operate under closed-loop control via servovalves, allowing accurate control of load and velocity. Test set-up also enables the monitoring of the temperature at the sliding interface during cyclic motions by means of thermocouples shown in Figure 5.3.c.

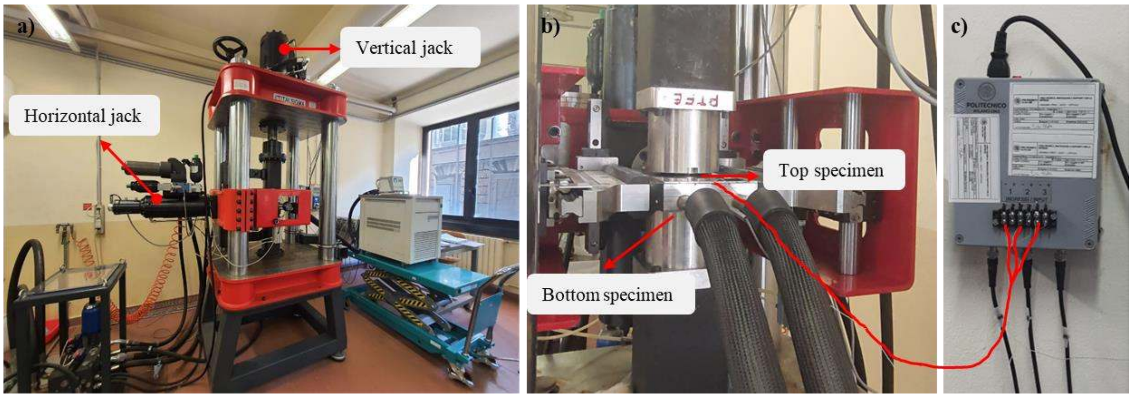

Figure 5.3. *(a) Testing machine; (b) top and bottom specimens and relevant mating surfaces; c) thermocouple design*

5.2.2. Testing procedure

The pair of specimens is subjected to a combined compressive load, providing the rated contact pressure, and horizontal motion at constant velocity. The displacement amplitude of the horizontal motion is set to d_{max} = 50 mm. The detailed loading protocol is reported in Table 5.1 and is performed at the room temperature of 20 °C. The tests are carried out at three pressure levels: 20 MPa, 40 MPa, and 60 MPa. At each pressure, cycles of motion are performed at various speeds between 1 and 250 mm/s. Each test consists of 10 fully reversed cycles, corresponding to a total distance of 2000 mm, plus an introductory cycle used to accommodate inertial effects and allow self-tuning of the testing machine control system. This initial cycle is disregarded for the evaluation of the dynamic coefficient of fiction. Only in the test at very low velocity (1 mm/s) a single cycle is performed.

Table 5.1. *Small-scale loading protocol*

Contact Pressure p (MPa)	20, 40, 60					
Velocity v (mm/s)	1	25	50	100	200	250
Amplitude d_{max} (mm)	50	50	50	50	50	50
N° of Cycles (-)	1	10	10	10	10	10
Sliding Distance per test D (mm)	200	2000	2000	2000	2000	2000

Two quantities are determined from the tests: (1) the breakaway friction coefficient μ_B, evaluated in the step at 1 mm/s as the ratio between the maximum horizontal resisting force at the breakaway and the vertical compressive load; (2) the dynamic friction coefficient $\mu_{dyn(k)}$, which is evaluated as the average dynamic friction coefficient from the 1st to the *k-th* cycle according to Eq.(5.1)

$$\mu_{dyn(k)} = \frac{1}{k}\sum_{i=1}^{k}\frac{EDC_i}{4 \cdot p \cdot d_{\max}} \tag{5.1}$$

The definition of the average coefficient of friction is introduced in order to allow direct comparison between the friction coefficients evaluated in small-scale and in large-scale tests which usually employ cycles of different amplitudes. In Eq. (5.1) EDC_i is the energy dissipated in the *i-th* cycle, and p and d_{max} are the correspondent applied contact pressure and maximum displacement.

5.2.3. Small-scale test results and discussions

Small-scale tests performed to identify the friction characteristics of the sliding material (made of filled PTFE) were conducted for 3 different contact pressures and 6 loading velocities (see Table 5.1). Accordingly, 18 different loading combinations were considered in the small-scale tests and at each test, the number of cycles were 10 (with the exception of tests conducted at a loading velocity of 1 mm/s). To better illustrate the variation in friction characteristics of the sliding material as a function of contact pressure, loading velocity and number of cycle, horizontal force divided by vertical force (F_h/F_v) vs displacement graphs are presented in Figure 5.4.

The data given in Figure 5.4.a belongs to tests performed at both 1 mm/s and 250 mm/s when the pressure is 40 MPa. Figure 5.4.a clearly indicates that low (at 1 mm/s) and high (at 250 mm/s) velocity responses of the tested sliding material are considerably different from each other. As the loading velocity increases, the F_h/F_v ratio increases indicating that the friction coefficient increases. A similar comparison in terms of F_h/F_v ratio is given in Figure 5.4.b for loading velocities of 50 mm/s and 250 mm/s. Opposite to phenomena shown in Figure 5.4.a, increasing the loading velocity from 50 mm/s to 250 mm/s do not change the friction characteristic of the sliding material. This observation is parallel to the literature (Dolce et al. 2005) indicating that increasing the loading velocity beyond a threshold value does not affect the friction coefficient. To observe the effect of pressure on F_h/F_v ratio, Figure 5.4.c is presented for 40 and 60 MPa when the loading velocity is 250 mm/s. In Figure 5.4.c it is seen that friction coefficient decreases as a result of increasing pressure. Finally, Figure 5.4.d illustrates the effect of number of loading cycles on F_h/F_v ratio. It is clear that friction coefficient degrades when the number of cycles increases from 1 to 10.

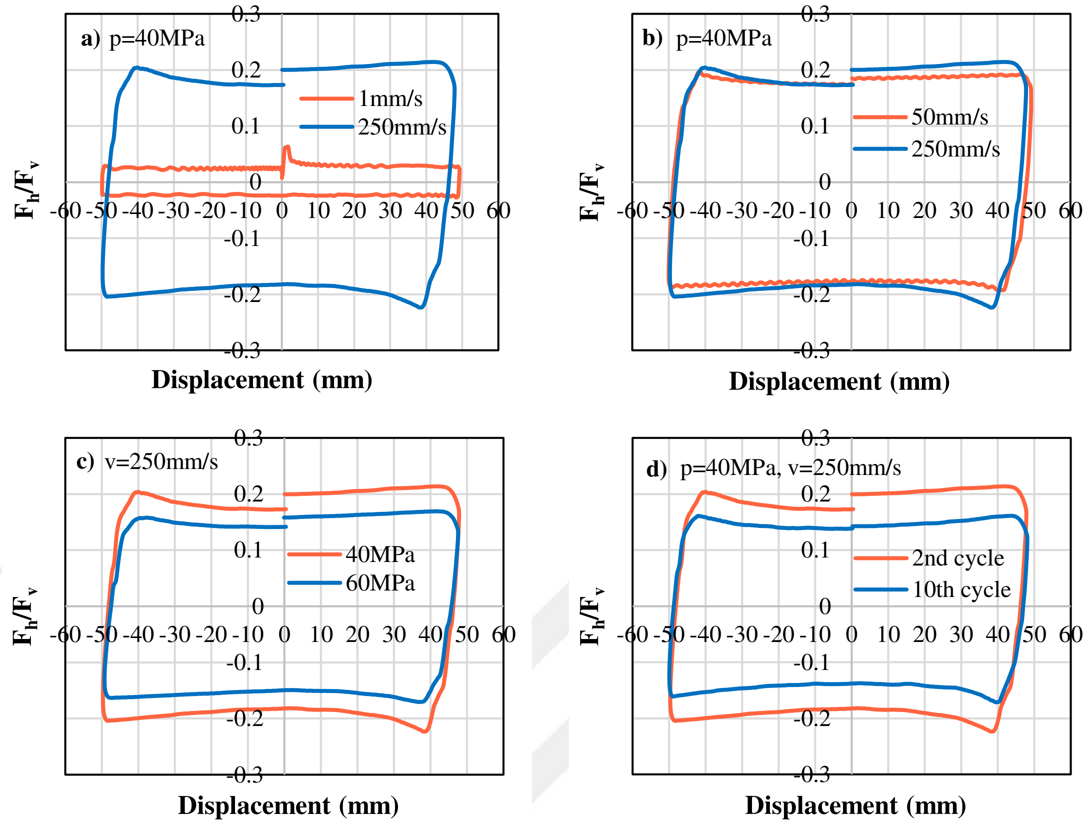

Figure 5.4. *Effects of (a) and (b) loading velocity, (c) pressure, (d) number of cycle on friction characteristics of tested sliding material.*

Figure 5.4 is presented to discuss the effects of pressure, loading velocity and number of cycles on friction characteristics of the sliding material considering only individual loading cases. To illustrate the general trends observed in the experimental program, Figure 5.5 presents the variation of dynamic friction coefficient μ_{dyn} (computed by means of Eqn. (5.1)) for all of the loading combinations. Figure 5.5 also displays the effect of number of cycles on the variation of dynamic friction coefficient by presenting μ_{dyn} values assessed at the 1st, 3rd, 7th and 10th cycles, corresponding to sliding distances of 200, 600, 1400 and 2000 mm. Figure 5.5 highlights the combined effects of pressure (p), velocity (v), and sliding distance (number of cycles) on $\mu_{dyn(k)}$, showcasing three primary behaviors:

1. $\mu_{dyn(k)}$ decreases with increasing pressure, which is attributed to the elasto-plastic behavior of the sliding material (Bowden and Tabor 1964; Gandelli et al. 2019);

2. initially, $\mu_{dyn(k)}$ rises with increasing velocity due to the viscous behavior of the polymer (Constantinou et al 1990). However, beyond a certain velocity this increase stops, and the coefficient of friction tends to settle at a constant value,
3. at constant pressure and velocity, $\mu_{dyn(k)}$ shows a declining trend with increased travel distance.

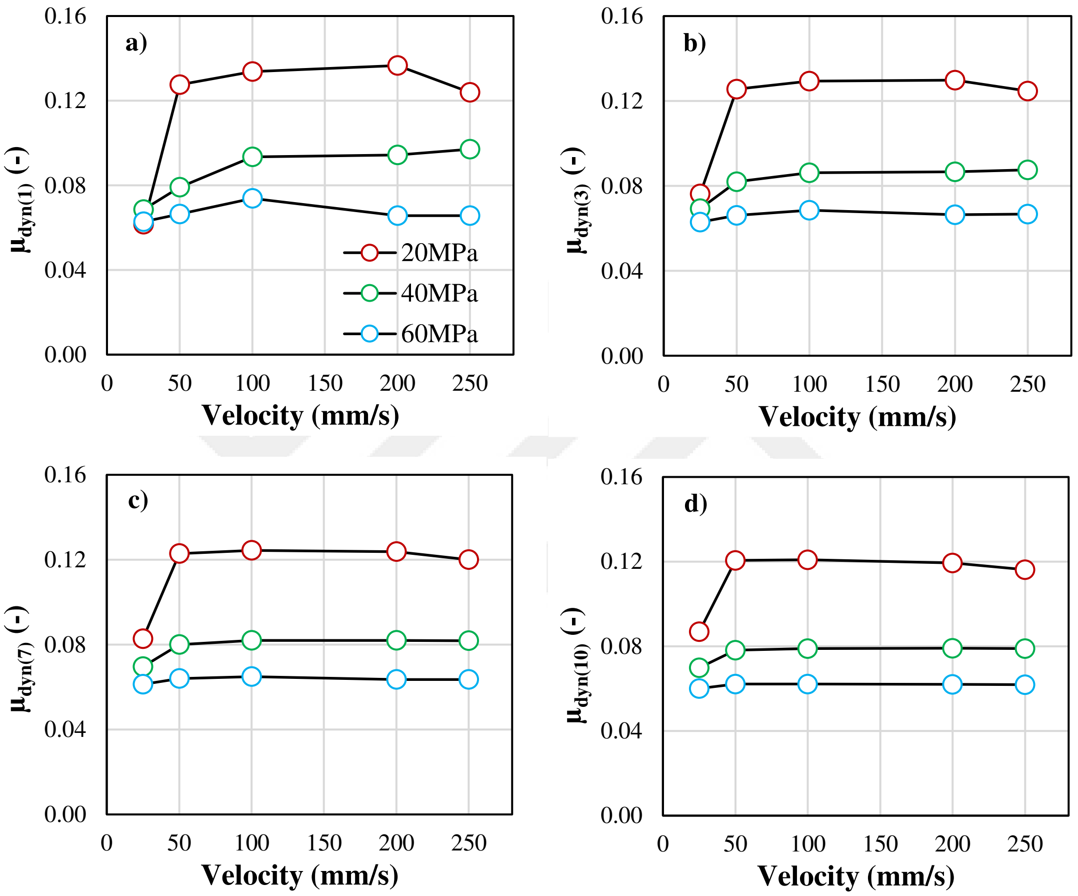

Figure 5.5. *Variation of dynamic friction coefficient due to change in normal stress and maximum loading velocity at (a) 1st cycle, (b) 3rd cycle, (c) 7th cycle, and (d) 10th cycle*

5.3 Estimation of Small-Scale Test Results

As discussed in the previous section, stabilization of the friction coefficient at high loading velocities and its reduction with increasing sliding distance (increasing number of cycles) are two effects of the mechanism of frictional heating (Quaglini et al. 2009): the energy dissipated by friction is converted into heat, causing local melting of the sliding material at the sliding surface; this melted polymer behaves as a lubricant, reducing friction (Quaglini et al. 2014). The energy dissipated per unit time increases with velocity, while the total amount of dissipated energy increases with the distance.

These behaviors are widely noted (Gandelli et al 2019), and in literature, several formulations for analyzing and interpreting the experimental results have been proposed. Lomiento et al. (2013) formulated an integrated model that captures the variation in friction as a function of three mechanical factors, namely pressure, velocity, and heating. In this model, pressure and velocity are considered as independent variables, and the effect of heating is represented by means of a function that depends on the histories of axial load and velocity. Alternatively, Kumar et al. (2015) proposed a three-function model in which the reference friction coefficient, μ_{ref}, evaluated under reference conditions of axial bearing pressure p_0, temperature T_0 and high velocity v_0, is modified using three adjustment factors, k_p, k_T and k_v, which account for variations at the sliding surface in pressure, temperature and velocity, respectively. Quaglini et al. (2014) developed a comprehensive friction model that accounts for the influences of axial load, velocity, and heating, while also introducing novel aspects, including the static coefficient of friction at the breakaway.

In this section, a comprehensive and unified model capable of describing the coefficient of friction of the sliding material μ_M as a function of contact pressure (p), velocity (v) and energy dissipated (ED) is proposed in Eq.(5.2).

$$\mu_M(p, v, ED) = \mu_{pv}(p, v) \cdot c(ED) \tag{5.2}$$

According to the model, μ_M is expressed as the product of two functions, decoupling the effects of pressure and velocity from the degradation of the friction coefficient caused by the dissipated energy. This approach, based on variable separation, aligns with previous formulations (Lomiento et al. 2013; Quaglini et al. 2014; Kumar et al. 2015; Gandelli et al 2019). In particular, the first function $\mu_{pv}(p, v)$ includes the influence of the instantaneous values of axial pressure p and velocity v, while the second function $c(ED)$ includes the effect of the cumulative heat generated at the sliding surface from energy dissipation, which depends on past histories of pressure and velocity, as well as on the travelled distance (ΣD) and the coefficient of friction. The expression of the first function $\mu_{pv}(p, v)$, provided in Eq.(5.3), is developed upon the formulation proposed by Quaglini et al. (2014) as the sum of two contributions.

$$\mu_{pv}(p,v) = \mu_{dyn}(p,v) + \mu_{Static}(p,v) \quad (5.3)$$

The first contribution corresponds to the dynamic or kinetic coefficient of friction μ_{dyn} activated during sliding, and is described by the standard formulation proposed by Mokha et al. (1988) and Constantinou et al. (1990) recalled in Eq.(5.4).

$$\mu_{dyn} = \mu_{HV}(p) - [\mu_{HV}(p) - \mu_{LV}(p)] \cdot e^{-\beta_1|v|} \quad (5.4)$$

where the parameters μ_{LV} and μ_{HV} represent the friction coefficients at low velocity and high velocity respectively, and $\beta_1 > 0$ is a transition rate parameter relating the transition between the low velocity and the high velocity regimes.

This contribution is then combined with a second term, reported in Eq.(5.5).

$$\mu_{Static} = (\mu_B(p) - \mu_{LV}(p)) \cdot e^{-\beta_2|v|} \cdot \left(\frac{|sgn(v) - sgn(d)|}{2}\right) \quad (5.5)$$

here the parameter μ_B represents the coefficient of friction at breakaway, which governs the sticking phase preceding the triggering of the sliding motion, and $\beta_2 > 0$ is a second transition rate parameter governing the rate of change of coefficient of friction from the static to the dynamic regime. By referring to the test protocol presented in Table 5.1, the parameters of the friction function $\mu_{pv}(p,v)$ are estimated based on the experimental values determined in the 1st cycle of tests at the relevant pressures and velocities, since the temperature rise in the 1st cycle is assumed to be small, and insufficient to produce a substantial change of the coefficient of friction.

The degradation function $c(ED)$ applies to the reference friction coefficient $\mu_{pv}(p,v)$ as a reduction factor. Assuming that all the energy dissipated by friction is entirely converted into heat (Quaglini et al. 2014) the degradation function $c(ED)$ is formulated as a negative power function of the cumulative dissipated energy *ED*, according to Eq.(5.6)

$$c(ED) = C \cdot ED^{-\gamma} \quad (5.6)$$

where $\gamma > 0$ is a parameter that controls the rate of degradation of the coefficient of friction (e.g., smaller values of γ results in a slower decrease for a given *ED*), while C is a multiplicative factor introduced to enhance the fit with experimental data at small *ED* values, where theoretically $C = 1$. The parameters of the degradation function will be estimated by fitting the relative change of the friction coefficient over the sequences of cycles performed at different pressures and velocities, corresponding to different values of *ED*.

The following paragraphs show how the experimental data obtained from the experimental campaign on small-scale specimens are used to calibrate the parameters of the unified model.

5.3.1. Dependency of coefficient of friction on pressure

The effects of pressure on the coefficient of friction have been extensively researched in literature and show that the sliding friction coefficient reduces while increasing pressure with a rate of reduction proportional to $p^{-\alpha}$, with $\alpha > 0$, and quite insensitive to sliding velocity, as shown in Lomiento et al. (2013) and Dolce et al. (2005). Bowden et al. (1964) proposed the first model, Eq.(5.7), relating the applied pressure p to the friction coefficient

$$\mu(p) = A \cdot p^{-\alpha} \tag{5.7}$$

where A and α are positive constants to be determined in tests.

Since the proposed formulation is defined in terms of μ_B, μ_{LV} and μ_{HV}, the dependence of friction coefficients at breakaway μ_B, low velocity μ_{LV}, and high velocity μ_{HV} are evaluated as functions of the applied pressure. For each pressure, the breakaway friction coefficient μ_B is evaluated in the test at 1 mm/s, while dynamic friction coefficients $\mu_{dyn(1)}$ measured at the 1st cycle of the test at velocities of 1 mm/s and of 250 mm/s are assumed as the low velocity μ_{LV} and the high velocity μ_{HV} friction coefficients, respectively (see Table 5.2).

Table 5.2. *Summary of experimental values used for the calibration of the friction coefficients*

Friction parameters	Experimental values for calibration
μ_B	μ_B at 1 mm/s
μ_{LV}	$\mu_{dyn(1)}$ at 1 mm/s
μ_{HV}	$\mu_{dyn(1)}$ at 250 mm/s

Figure 5.6 presents the experimental results at pressures of 20, 40 and 60 MPa and the fitting according to Eq.(5.8) to Eq.(5.10).

$$\mu_B(p) = A_1 \cdot p^{-\alpha_1} = 1.1753 \cdot p^{-0.982} \tag{5.8}$$

$$\mu_{LV}(p) = A_2 \cdot p^{-\alpha_2} = 0.0257 \cdot p^{-0.194} \tag{5.9}$$

$$\mu_{HV}(p) = A_3 \cdot p^{-\alpha_3} = 0.6605 \cdot p^{-0.532} \tag{5.10}$$

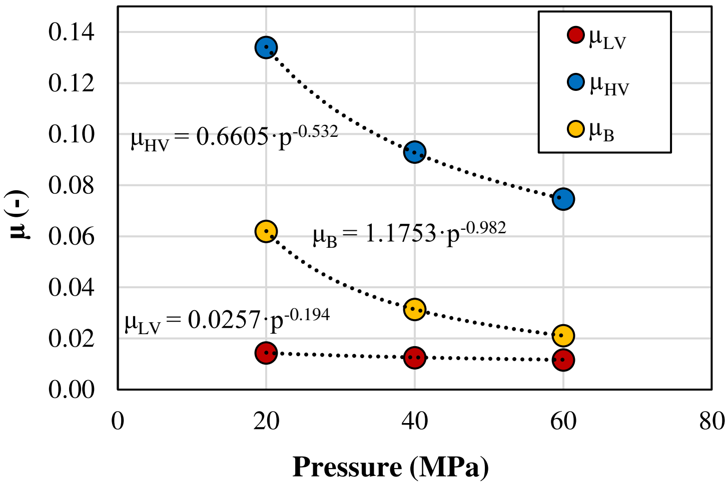

Figure 5.6. *Variation of μ_B, μ_{LV}, and μ_{HV} on the contact pressure*

5.3.2. Dependency of coefficient of friction on velocity

During the motion of the CSS, the friction coefficient usually increases from a minimum value μ_{LV}, in the low-velocity regime, to a steady value μ_{HV}, in the high-velocity range. The most widely recognized model describing the increase in the friction coefficient as the sliding velocity (v) rises for a constat pressure was developed by Constantinou et al. (1990) and is defined by Eq.(5.4). However, this model does not consider the contribution of static friction. But, experiments showed that a rapid drop of the friction force occurs whenever the sliding is triggered, e.g., at the breakaway and at any reversals of motion during unidirectional trajectories (Mokha et al.1988), due to the transition from the static to the kinetic regime. Therefore, in order to properly reproduce the actual response of CSSs during both the breakaway (pre-sliding) and the sliding phases, the numerical formulation should include also μ_B, as defind in Eq.(5.5) proposed by Quaglini et al. (2014).

To quantify the success of Eqns. (5.4) and (5.5) to estimate the experimental data (corresponds to 1st cycle of motion) obtained in this study, Figure 5.7 is presented by considering the original β_1 (0.015) and β_2 (0.25) values proposed by Quaglini et al. (2014). Although these constants were proposed for a different sliding material, as shown in Figure 5.7 they are still effective to estimate friction coefficient at 250 mm/s. However, for smaller velocities, Figure 5.7 indicates that proposal of Quaglini et al. (2014) is not capable of representing the experimental data with its original β_1 and β_2 values. This is why parameters β_1 and β_2 of Eqns. (5.4) and (5.5) are calibrated by fitting the experimental data, while the values of breakaway, low velocity and high velocity friction coefficients μ_B, μ_{LV} and μ_{HV} are those determined by Eqns. (5.8)-(5.10) of Section 5.3.1.

Figure 5.8. shows that the model with parameters β_1= 0.057 s/mm and β_2= 3 s/mm provides a good match of the experimental data over the whole range of velocities up to 250 mm/s, where experimental data from the small-scale tests (corresponds to 1st cycle of motion) are represented by the red circles, and the model output by the purple ones. The largest deviation between model and experimental data is on the order of 40% and observed for the loading combination where pressure is 20 MPa and loading velocity is 25 mm/s. For all of the loading combinations where the loading velocity is larger than or equal to 50 mm/s, the difference between the model and the experimental data is less than 1%, in an average sense.

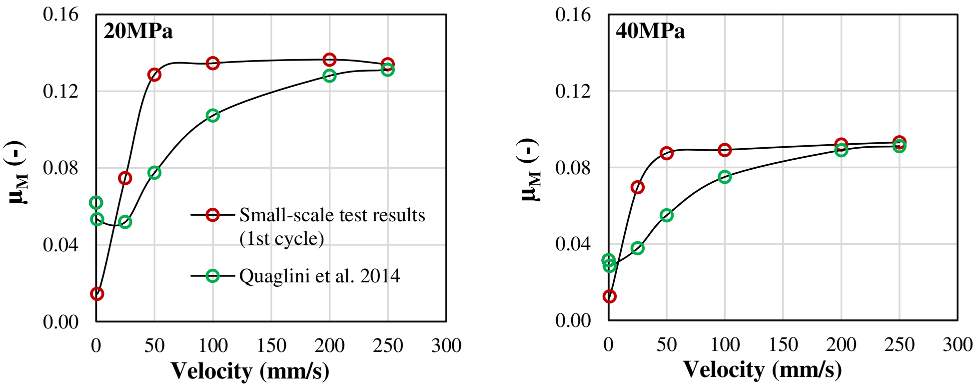

Figure 5.7. *Comparison of small-scale test data obtained from the 1st cycle of motion with the proposed formula of Quaglini et al. (2014) by using the original values of β_1 and β_2.*

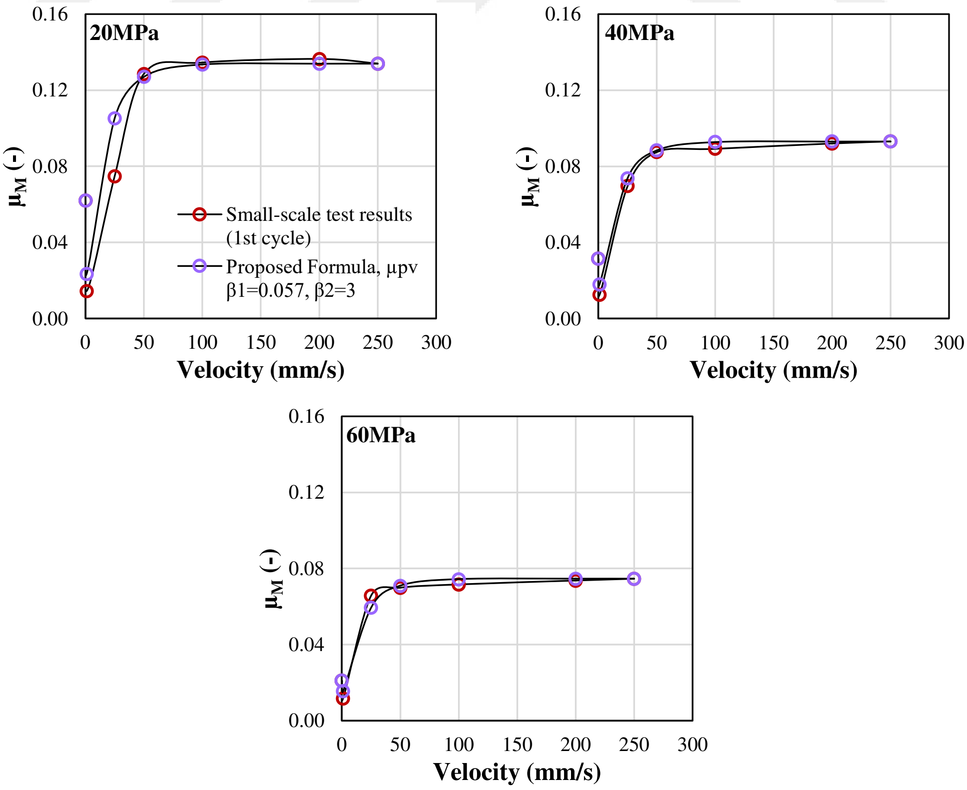

Figure 5.8. *Comparison of small-scale test data obtained from the 1st cycle of motion with the proposed formula considering the updated values of β_1 and β_2.*

5.3.3. Dependency of coefficient of friction on dissipated energy

Previous research demonstrated that the effective friction coefficient of full-scale sliding isolators decreases during sustained motion, a phenomenon attributed to the heating of the sliding surface due to energy dissipation (Sextro 2002; Dolce et al. 2005; Constantinou et al. 2007; Lomiento et al. 2013). As the temperature increases, the softening of the thermoplastic liner material is considered to activate a thin, soft layer on the slider surface, which acts as a solid lubricant, thereby reducing the coefficient of friction. Thus, increasing the number of cycles of motion (or increasing the cumulative sliding distance) leads to gradual degradation of friction coefficient from cycle to cycle. Accordingly, any model that aims to estimate the variation in friction coefficient of a sliding material during cyclic motion shall consider such a degradation. Figure 5.9 is addressed to illustrate what happens if the effect of heating on the friction coefficient is not considered in the formulations used to estimate cyclic response of the sliding material. In Figure 5.9, comparison of the friction coefficients obtained from the 10^{th} cycle of small-scale tests and estimated by means of Eqn. (5.3) when only the effects of pressure and loading velocity are taken into account (see Sections 5.3.1 and 5.3.2). Figure 5.9 shows that predictions of Eqn. (5.3) overestimate the friction coefficients at the 10^{th} cycle regardless of the pressure and loading velocity. However, Figure 5.8 has already illustrated that the estimations of Eqn. (5.3) is highly accurate for the 1^{st} cycle of motion. The reason of such transition in the success of Eqn. (5.3) in estimating the friction coefficients from 1^{st} to 10^{th} cycles is that its current form does not consider the heating effects. But, as shown in Figure 5.10, the temperature at the sliding interface increases as the number of cycle increases.

To consider the heating effects in estimation of friction coefficient, μ_{pv} is transformed to μ_M by being multiplied by the term $c(ED)$ as defined in Eqn. (5.2). For the calibration of the parameters C and γ of the degradation function $c(ED)$ of Eq.(5.6), the dynamic friction coefficient $\mu_{dyn(k)}$ is determined according to Eq.(5.1) at the 1^{st}, 3^{rd}, 7^{th} and 10^{th} cycles of each experimental test performed for a given combination of pressure and velocity (see Table 5.1).

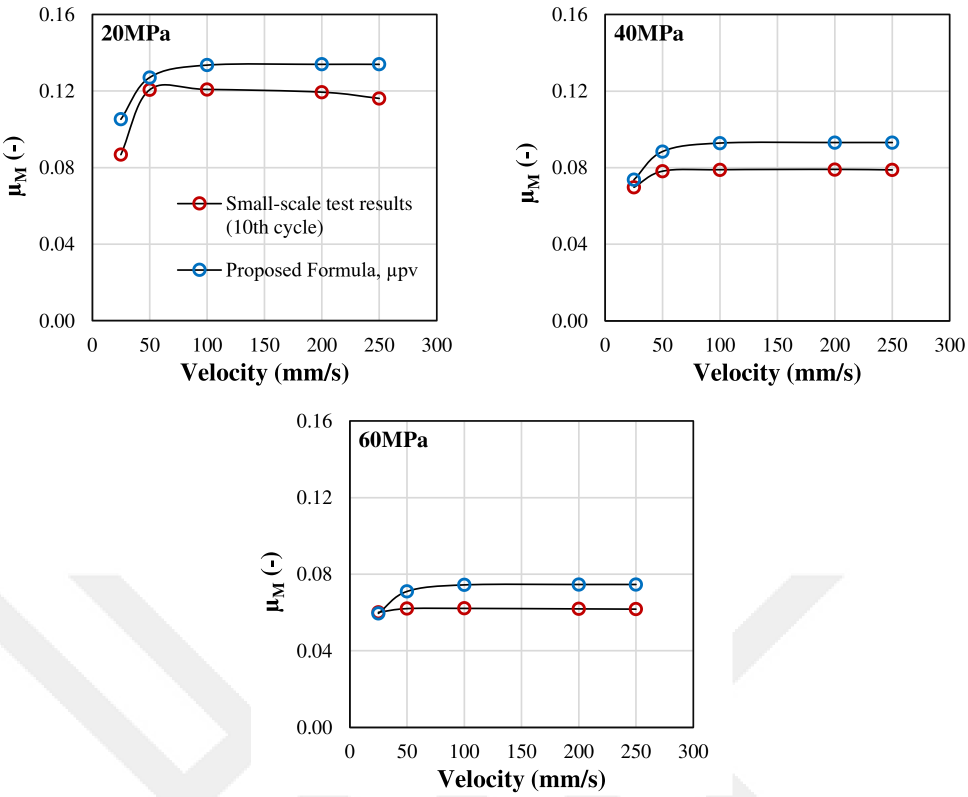

Figure 5.9. *Comparison of small-scale test data obtained from the 10th cycle of motion with the proposed formula considering the updated values of β_1 and β_2.*

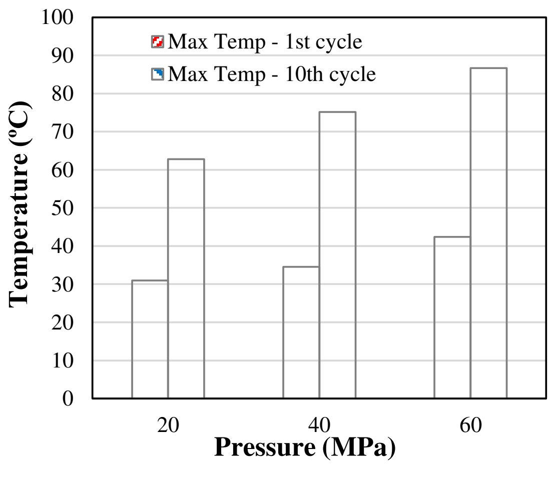

Figure 5.10. *Comparison of maximum temperatures recorded at the sliding interface for 1st and 10th cycles of motion loading velocity is 100 mm/s.*

The values of $\mu_{dyn(k)}$ for each test are then normalized with respect to the value at the 1st cycle, where the temperature rise is minimal and insufficient to significantly alter the coefficient of friction. The corresponding $\mu_{dyn(k)}/\mu_{dyn(1)}$ values are then given in Figure 5.11 as a function of the cumulative dissipated energy *ED* (shown as blue circles), and fitted with the exponential function of Eq.(5.6), where the values of C and γ are taken as

1.211 W^{γ} and 0.048 respectively. It is to be noted that these parameters were calibrated based on the experimental campaign summarized in Table 5.1, the values of C and γ are valid for *ED* greater than 50 W.

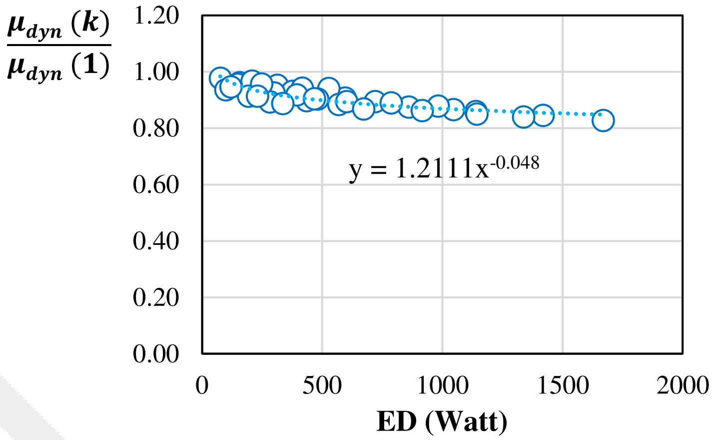

Figure 5.11. *Variation of the friction coefficient on the dissipated energy*

$$c(ED) = 1.2111 \cdot ED^{-0.048} \tag{5.11}$$

Incorporating Eqns. (5.11) into Eqn. (5.2) results in the formulation proposed to estimate the friction coefficient of the tested sliding material when the heating effects are taken into account. Figure 5.12 is presented to show the efficiency of Eqn. (5.2) in estimation of dynamic friction coefficient obtained from the 10th cycle of small-scale tests performed for different pressures and loading velocities. Figure 5.12 clearly indicates that the proposed formulation is very successful in estimation of the experimental data.

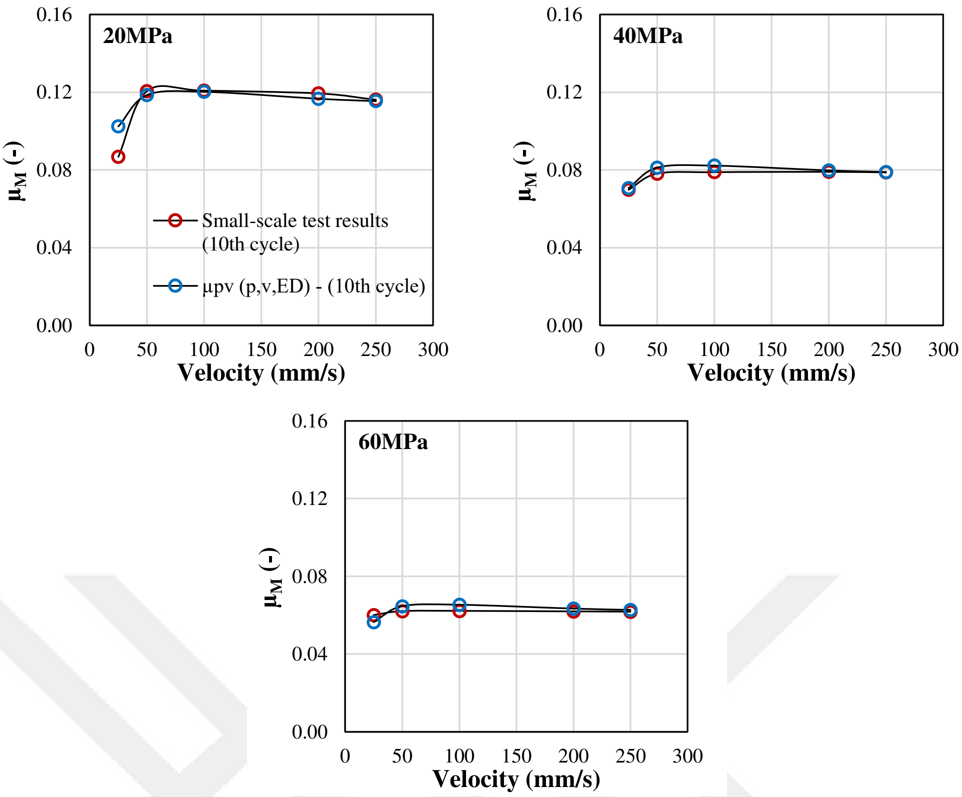

Figure 5.12 *Comparison of friction coefficients obtained from the 10^{th} cycle of small-scale tests with the ones estimated by Eqn. (5.2).*

5.4. Verification of Proposed Formula Using Full-Scale Test Results

This section is devoted to discussing whether the formulation proposed to estimate the friction coefficients obtained from small-scale tests can also be used to predict the friction coefficients assessed from full-scale test results. The following sections introduce both the tested full-scale seismic isolator and the corresponding test campaign.

5.4.1. Materials and methods

The seismic isolator considered in the study to validate the small-scale procedure is a full-scale double CSS, shown in Figure 3.3, which uses the same filled PTFE investigated in the small-scale tests as sliding material. The top and bottom concave plates have the same radii of curvature $R_1 = R_2 = 2500$ mm and are lined with a stainless-steel sheet with a surface roughness of $R_z \leq 1$ μm. The isolator is manufactured by Technological Isolation Systems (TIS) and the relevant geometric properties are reported in Figure 3.3.b.

To enable a direct comparison between the results obtained in small- and large-scale tests, the testing protocol adopted for the experimental campaign on the double CSS

(Table 5.3) is designed considering the behavior of the sliding pad during the test. As shown in Figure 5.13, when the double CSS accommodates the total displacement d_D through sliding on both surfaces, the displacement of the single pad (in contact with the top or bottom plate) d_P corresponds to 50% of d_D. Given the period of oscillation of the device, the velocity of sliding of each pad v_P is half of the velocity v_D of the isolator. Accordingly, Table 5.3 reports the loading conditions for the isolation device and their correspondence for the single sliding pad. Apart from the small-scale tests (where three different levels of pressure were considered), the full-scale tests were conducted under four levels of pressures, namely, 20, 40, 60 and 80 MPa. The reason of considering an additional level of pressure (80 MPa) in full-scale tests is to see the ability of the proposed formulation to estimate a data set which is not covered during the proposal of the formulation. A similar approach was followed also in maximum loading velocities (50, 250, 500 and 750 mm/s) applied to isolation device. The maximum loading velocity considered in the full-scale tests was 750 mm/s, (375 mm/s for the single sliding pad) and it is beyond the maximum loading velocity (250 mm/s) considered in small-scale tests.

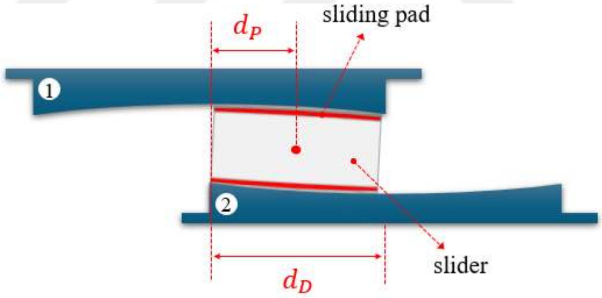

Figure 5.13. *Displacement at the device level (d_D) and displacement at the pad level (d_P) in the full-scale isolator*

In the full-scale tests, isolation device was subjected horizontally to sinusoidal displacement histories with an amplitude of 300 mm. Figure 5.14 presents a representative displacement versus time graph for a loading velocity of 250 mm/s, including both entrance and exit half-cycles. Excluding these two half-cycles, the total sliding distance d_D travelled by the device in a test is 3600 mm, which corresponds to a distance d_P = 1800 mm for the single sliding pad. In this way, the friction coefficients of the sliding pad extrapolated from the full-scale tests can be compared to the friction coefficients of the small-scale tests evaluated over 9 cycles (1800 mm / 200 mm (the travelled distance at each cycle of small-scale tests)).

Table 5.3. *Loading protocol for the full-scale tests*

	For the isolation device				For single sliding pad			
Contact Pressure p (MPa)	20, 40, 60, 80				20, 40, 60, 80			
Peak Velocity $v_{max,D}$ (mm/s)	50	250	500	750	25	125	250	375
Total Sliding Distance D_D (mm)	3600				1800			
N° of Cycles (-)	3				3			

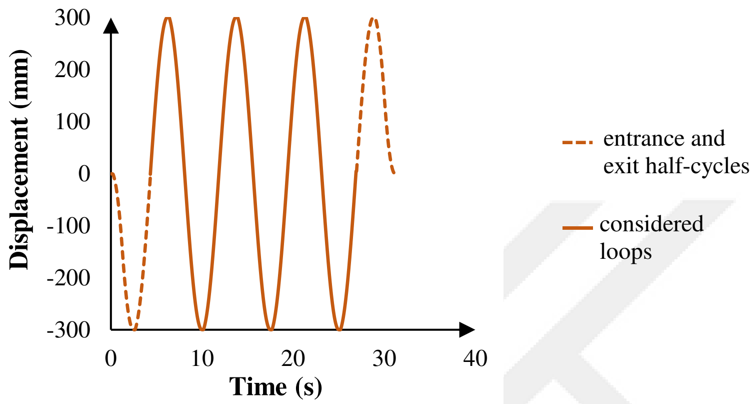

Figure 5.14. *Representative displacement histories for loading velocity 250 mm/s*

5.4.2. Results and discussion

In the full-scale tests, force-displacement relations were recorded for each loading condition and the corresponding effective friction coefficients μ_{eff} of the isolation device were computed by means of Eqn. (5.1). A representative force-displacement curve obtained from full-scale tests is presented in Figure 5.15 for a loading combination where pressure is 40 MPa and maximum loading velocity is 250 mm/s.

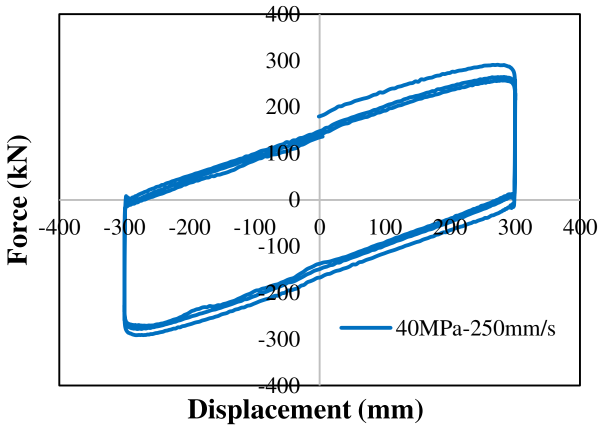

Figure 5.15. *Force-displacement curve recorded at full-scale tests when pressure is 40 MPa and maximum loading velocity is 250 mm/s.*

The suitability of the friction coefficients estimated by Eqn. (5.2) which is proposed by considering the small-scale test results to predict the effective friction coefficient μ_{eff} of the full-scale isolator is assessed using the comparison graphs presented in Figure 5.16. Specifically, the values of μ_{eff} determined from the full-scale tests are compared with the ones calculated by the product of Eqn. (5.2) and Eqn. (5.12), where the friction coefficients at the individual sliding surfaces $\mu_1 = \mu_2$ correspond to friction coefficient determined from small-scale tests for the corresponding sliding distance travelled by the pad. For the tested double CSS, in Eqn. (5.12) the radii of curvature are $R_1 = R_2 = 2500$ mm and the thickness of the slider is $h = 73$ mm, while the friction coefficients $\mu_1 = \mu_2$ are obtained from the 3rd, 6th and 9th cycles of small-scale tests, corresponding to sliding distances of 600 mm, 1200 mm, and 1800 mm, respectively. These sliding distances also correspond to distances travelled by a single sliding pad of the double CSS at the ends of 1st, 2nd and 3rd cycles of sinusoidal motions with an amplitude of 300 mm. Considering the geometric properties of the tested isolator, Eqn. (5.12) leads to $\mu_{eff} = 1.015\mu_M$ where μ_M is the friction coefficient of the sliding material obtained from small-scale tests.

$$\mu_{eff} = \frac{\mu_1 R_1 + \mu_2 R_2}{R_1 + R_2 - h} \tag{5.12}$$

Figure 5.16 reveals that there is a fair agreement between the effective friction coefficients of the double CSS evaluated in the full-scale tests (represented by red circles) and the values estimated by the proposed formulation (represented by blue circles). The maximum amount of error between estimated and calculated friction coefficients is 20% with an average value of 12% when the data that corresponds to 20 MPa is not considered. It is to be noted that although 20 MPa pressure was included in the loading protocols, it is very unlikely to have such a low level of pressure in seismic isolation applications. Thus, it can be said that the proposed formulation provides satisfactory estimations for prediction of friction coefficients obtained from full-scale tests. Another key observation from Figure 5.16 is that the proposed formulation still provides good estimations for the loading cases with 80 MPa pressure or 750 mm/s (375 mm/s for single pad) loading velocity. This is important because these values are beyond the limits covered in small-scale tests.

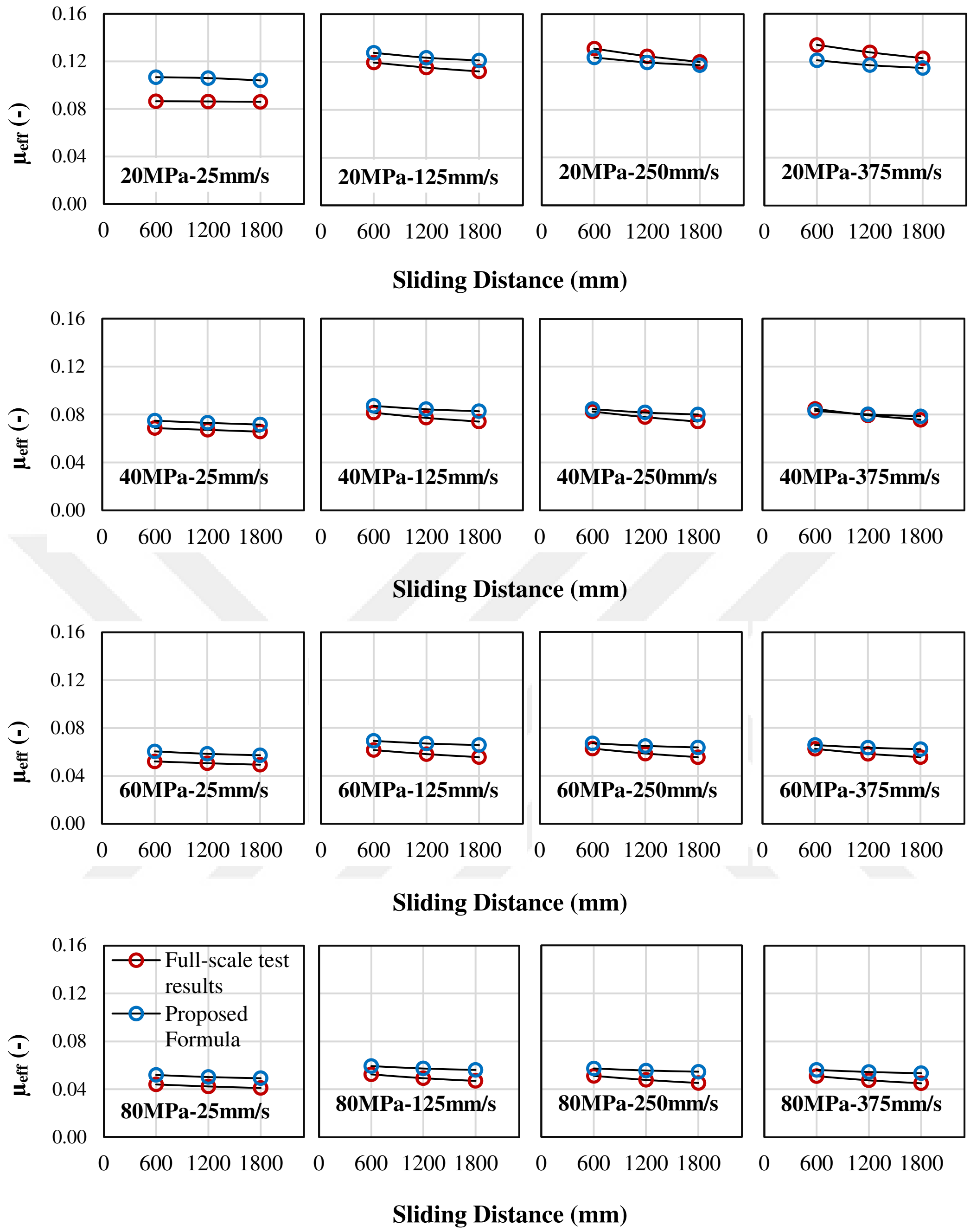

Figure 5.16. *Comparison of friction coefficients estimated by using small-scale test results with the ones obtained from full-scale test results.*

5.5. Conclusion

Code specifications related to seismic isolator tests require experimental campaigns performed with full-scale specimens. These experimental programs are used to conduct either prototype or quality control tests. Specifically for sliding isolation devices, these tests are performed to quantify the effective friction coefficient that dominates the design of both seismic isolation system and the superstructure. Although these characterization tests have to be performed with full-scale specimens, there is also a need to work with small specimens for research and development purposes. It is essential to be able to estimate the friction properties of full-scale specimens using the small-scale test results. Because, small-scale tests and required test set-ups are cheaper than their full-scale counterparts. This study provides a methodology to estimate effective friction coefficient of full-scale double CSS by means of small-scale test results. The proposed unified formulation considers the effects of pressure and loading velocity as well as the heating effects at the sliding interface during cyclic motion. The comparison of the estimated friction coefficients and full-scale test data revealed that the proposed formulation is highly accurate to predict the effective friction coefficient of full-scale specimens by using small-scale test data.

6. EFFECTIVENESS OF SMALL-SCALE TEST RESULTS IN ESTIMATION OF FULL-SCALE ISOLATOR BEHAVIOR AT LOW TEMPERATURES

6.1. Introduction

In the previous chapter, friction coefficients of the tested sliding material (made of filled PTFE) for different normal stresses ad loading velocities were obtained from small-scale test results performed at room temperature. Then, a comparison was presented with the friction coefficients obtained from full-scale tests performed at identical loading conditions. As a result, a model that considers the effect of frictional heating on coefficient of friction was proposed to estimate the friction coefficient of a DCSS obtained from full-scale tests. It is to be noted that the proposed model is valid only in case of room temperature. This chapter is devoted to discuss the effectiveness of small-scale test results in estimation of full-scale isolator tests performed at low temperatures.

Research studies that investigated the behavior of CSSs under cyclic loading revealed that normal stress, loading velocity, and ambient temperature are the key parameters influencing the isolator response (Tyler 1977; Constantinou et al. 1987; Mokha et al. 1990; Dolce et al. 2005; Lomiento et al. 2013; Barone et al. 2019; De Domenico et al. 2018; Keikha and Amiri 2019; Furinghetti et al. 2019; Gandelli et al. 2019; Pigouni et al. 2020). While extensive studies have been conducted on the effects of both normal stress and loading velocity, research efforts to determine the impact of ambient temperature—particularly the low temperatures—remain limited. And, none of the existing studies account the exposure time to low temperatures as a parameter in the experimental campaigns. Furthermore, prior research studies have primarily focused on the behavior of the sliding material rather than the full-scale isolation system itself. This is mainly due to the widespread availability and ease in use of small-scale test setups compared to full-scale seismic isolator test facilities. As defined in detail in previous chapters, a 75 mm diameter specimen made from the same material as the slider is subjected to loading conditions in small-scale tests. Results of these tests are used as an indicator of the full-scale behavior of CSSs. However, there is no established evidence in the literature confirming that small-scale test results accurately represent the behavior of full-scale isolation systems under low ambient temperature conditions.

This study aims to bridge this gap by conducting both small- and full-scale tests under various normal stress and loading velocity conditions, with a specific focus on response modifications due to low temperatures and exposure time. For the first time in the literature, the ability of small-scale test results to represent the full-scale response of isolation systems at low ambient temperatures will be systematically investigated.

To achieve the objectives of this study, small-scale tests were conducted using 75 mm diameter specimens made of the same slider material as the full-scale isolator, under identical loading conditions. The force-displacement curves recorded from each test were used to compute the friction coefficients, particularly for low temperatures and different exposure times. These values were then compared with the full-scale isolator test results (presented in Chapter 4) to evaluate the reliability of small-scale tests in representing full-scale system behavior. Such a comparison provides insights into the effectiveness of small-scale tests in predicting the performance of isolation systems under different low temperatures and exposure times.

The structure of this chapter is as follows: Section 6.2 presents the experimental campaign conducted on small-scale specimens under low temperatures to investigate the effects of temperature and exposure time on the friction coefficient of the sliding material composed of filled PTFE. Section 6.3 evaluates the suitability of small-scale tests in predicting the performance of the full-scale isolator under low temperatures. Finally, Section 6.4 provides the conclusions of the research.

6.2. Methodology for Small-Scale Tests

The test setup of Politecnico di Milano, introduced in previous chapters, was used to conduct tests on small-scale slider specimens. As discussed earlier, this setup is capable of applying both vertical and horizontal motions through servo-hydraulic jacks (see Figure 5.3.a). During horizontal motion, the temperature of the mating plate can be controlled to apply low temperature by means of a cooling system (see Figure 5.3.c). Figure 6.1.a shows the surface of the mating plate after the temperature was dropped to -20oC. Additionally, a climatic chamber at Politecnico di Milano (Figure 6.1.b) allows test specimens to be maintained at the desired temperatures for any desired time. The chamber is capable of applying temperatures ranging from -40°C to 90°C.

In accordance with code specifications (CEN EN 1337-2; CEN EN 15129), the small-scale slider specimens were tested with dimensions of 75 mm in diameter and 8 mm in thickness (see Figures 5.2.a and 5.2.b). Testing of the slider specimens was conducted following the loading protocol outlined in Table 6.1. In total, 48 tests were performed to assess the effects of low temperature, exposure time, normal stress, and loading velocity on the material's behavior.

Figure 6.1. *Small-scale test setup of Politecnico di Milano a) Temperature controlled steel plate, b) Climatic chamber*

Table 6.1. *Low temperature test protocol for small-scale sliding material*

Test Parameters				
Normal Stress (MPa)	20, 40, 60			
Velocity (mm/s)	50	100	200	250
Total Sliding Distance (mm)	2200	2200	2200	2200
# of Cycle	11	11	11	11
Frequency (Hz)	0.25	0.5	1	1.25
Temperature (ºC)	-20, 0			
Exposure Time (hrs)	3, 24			

In low temperature tests, first, the small-scale slider specimens were conditioned at the temperature of interest (-20ºC or 0ºC) in the climatic chamber shown in Figure 6.1.b for the desired period of time (3 hrs or 24 hrs). Then, they were removed from the climatic chamber and attached to the test set-up (see Figure 5.3.a). In the meantime, the cooling system of the test set-up was also set to the desired level of low temperature prior to loading. During the tests, the slider specimens were subjected to displacement-controlled cyclic motions where the amplitude of the motion was 50 mm and the number of cycles was 10. The temperature at the sliding interface was recorded by means of thermocouples placed at three different points throughout the tests (see Figure 5.3.b). As an example, Figure 6.2 presents the temperature readings taken from the mating stainless-steel plate prior to and during the test for a temperature of -20^{o}C and 3 hrs of exposure time. After each test, the corresponding force-displacement records were used to assess the dynamic friction coefficients for each cycle of the loading.

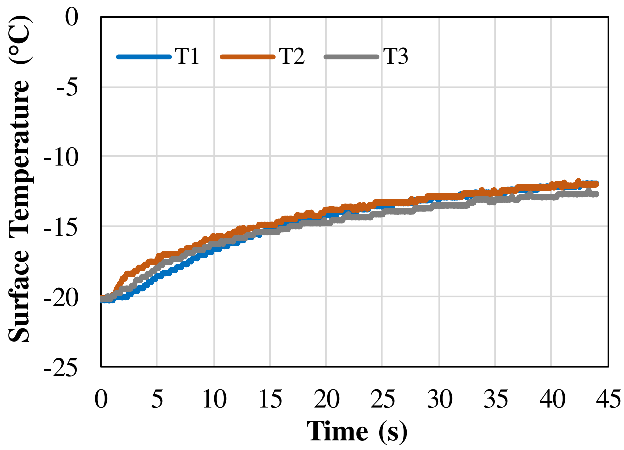

Figure 6.2. *Temperature readings taken from contact surface during the test 40MPa, 50mm/s.*

6.2.1. Small-scale test results at low temperature

In this section, friction coefficients obtained from small-scale tests are presented for different combinations of temperatures (-20oC, 0oC), exposure times (3 and 24 hrs), normal stresses (20, 40 and 60 MPa) and maximum loading velocities (50, 100, 200 and 250 mm/s).

To evaluate the impact of low ambient temperature and exposure time on the coefficient of friction, the graphs in Figure 6.3 were presented. These graphs illustrate the variation of friction coefficients when the slider was exposed to low temperatures for different time intervals. In Figure 6.3, assessed friction coefficients versus maximum loading velocities are presented for different temperatures, exposure times and normal stresses. Test results reveal a significant reduction in coefficient of friction under low-temperature conditions compared to the reference tests (Figure 5.5). Specifically, the reduction ranges from a minimum of 57% (-20°C, 3 hr, 20 MPa, 50 mm/s) to a maximum of 90% (-20°C, 3 hr, 60 MPa, 250 mm/s).

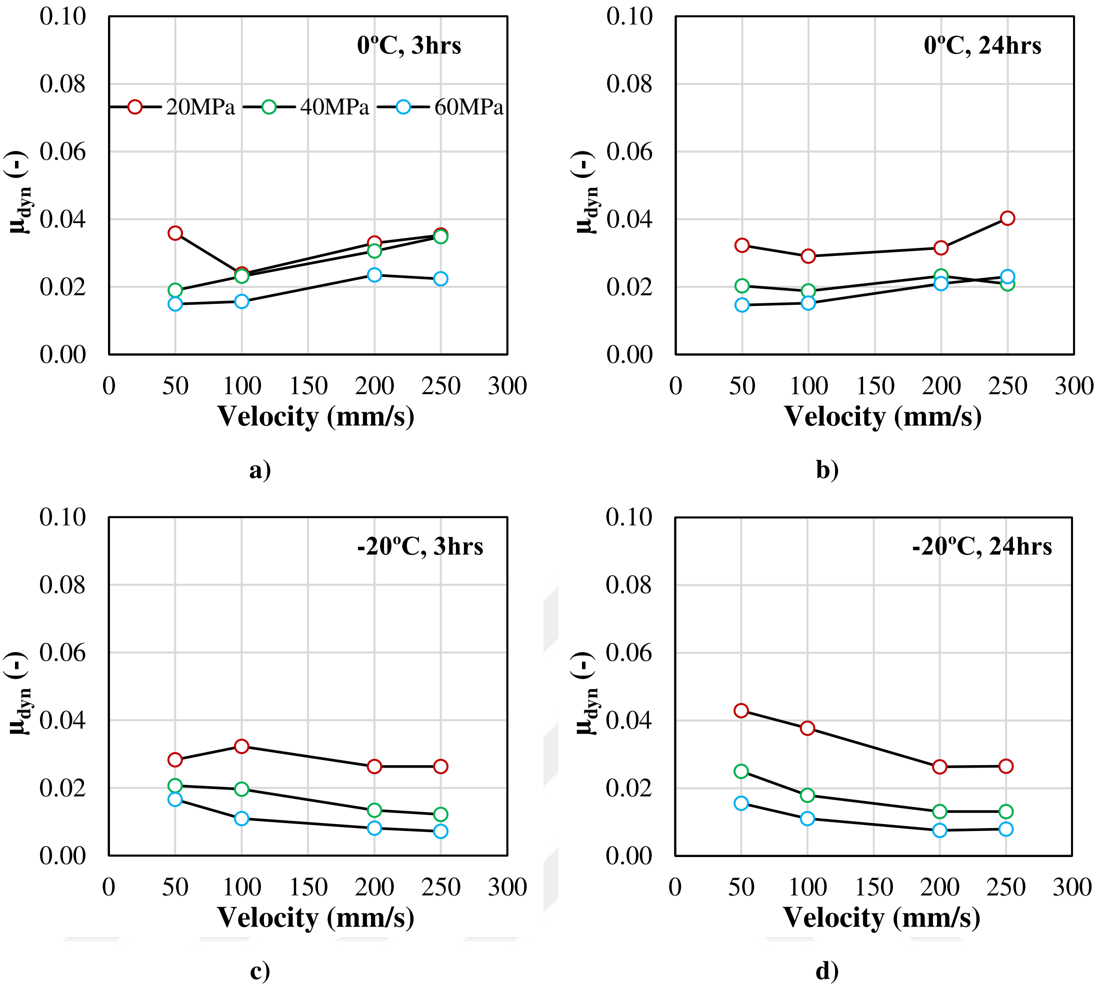

Figure 6.3. *Maximum loading velocity versus friction coefficients assessed at first cycles of the tests performed at a temperature of 0°C and -20°C with an exposure time of 3hrs and 24hrs.*

To better assess the effect of exposure time on the variation of the friction coefficient, the data presented in Figure 6.3 was reorganized and plotted in Figure 6.4 as a function of exposure time. The results indicate that the calculated friction coefficients for exposure times of 3 and 24 hours remain nearly identical for the temperatures, normal stresses, and maximum loading velocities considered in the experimental program. This suggests that within the examined conditions, an exposure time of 3 hours is sufficient for the formation of an ice layer at the sliding interface at both -20°C and 0°C. Therefore, based on the test results, exposure times longer than 3 hours do not need to be considered for small-scale specimens tested at low temperatures.

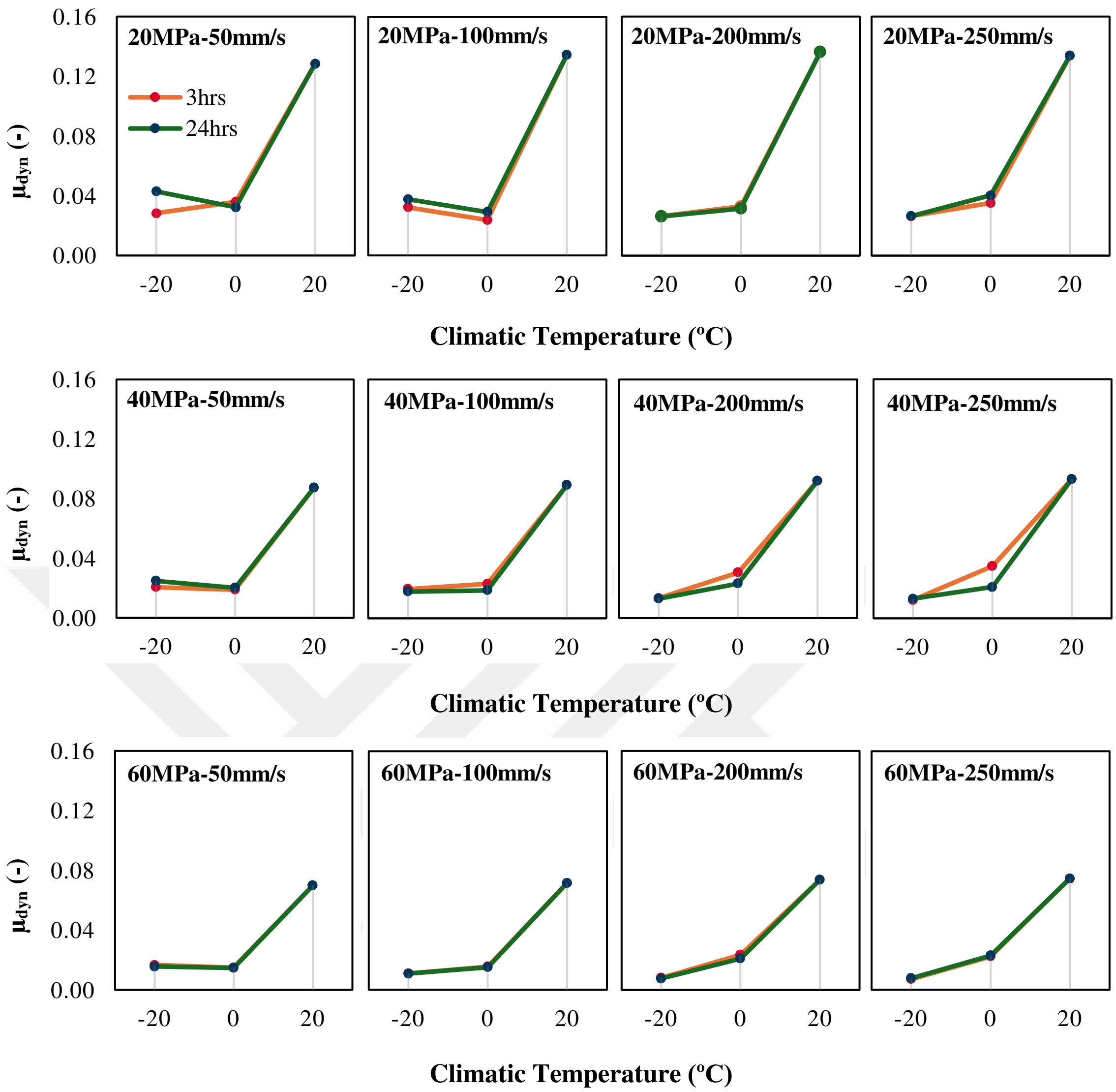

Figure 6.4. *Effect of temperature and exposure time on the friction coefficient of small-scale test specimen*

6.3. Comparison of small-scale and full-scale test results at low temperature

The isolator unit used in the full-scale tests was a double CSS, as shown in Figure 3.3. The loading protocol applied in the experimental program followed the same conditions as those used for the sliding material and is detailed in Table 3.1.

Following the completion of low-temperature tests on small-scale PTFE specimens, the next stage of the study focuses on evaluating the consistency between small-scale and full-scale test results. To ensure a reliable comparison of experimental outcomes, it is crucial to maintain the same sliding distance in small-scale tests with filled PTFE material. Details regarding this methodology are provided in Section 5.4.2.

The friction coefficients, obtained from small-scale tests at various normal stresses and loading velocities, were computed and compared with those from full-scale isolator tests conducted at normal stresses of 20 MPa, 40 MPa, and 60 MPa, with loading velocities of 250 mm/s and 500 mm/s. Based on the geometric properties of the tested isolator, Eqn. (5.13) yields an effective friction coefficient of $\mu eff = 1.015\mu M$ where μM represents the friction coefficient of the sliding material obtained from small-scale tests.

The diagrams given in Figure 6.5 compare the friction coefficient obtained from small-scale tests with that of full-scale tests conducted at 0°C with a 3-hour exposure time. To provide further insight into the observed differences, each graph is accompanied by the corresponding temperature profile for the related sliding distance. Figure 6.5 indicates that the friction coefficients from small- and full-scale tests are not in agreement for such loading conditions. This discrepancy arises due to the presence of an ice layer on the contact surface during low-temperature tests, which significantly influenced the outcomes. In full-scale isolator tests, the maximum recorded temperatures at the sliding interface were higher than those observed in small-scale tests. As a result, increasing the loading velocity and normal stress can mitigate the icing effect by generating additional heat at the sliding interface. However, in small-scale material tests, the heat generated was insufficient to counteract the formation of ice, preventing the PTFE-based sliding material from making direct contact with the steel plate.

The same trend is observed in other loading scenarios, including tests at 0°C for 24 hours, -20°C for 3 hours, and -20°C for 24 hours, as shown in Figures 6.6, 6.7, and 6.8. In all cases, the friction coefficient calculated for small-scale tests is lower than that of the full-scale isolator, primarily due to the lower temperature at the mating surface.

A closer examination of the temperature profiles for tests conducted at -20°C reveals that, throughout the sliding distance, the surface temperature in small-scale tests consistently remained below 0°C. This strongly indicates the continuous presence of ice at the interface, which significantly influenced frictional behavior by acting as a lubricant. In contrast, the surface temperatures in full-scale tests were always above 0°C, ensuring that the ice layer did not persist. The absence of ice allowed for a contact surface between the PTFE-based sliding material and the steel plate, leading to higher friction coefficients.

These findings highlight a fundamental difference between small- and full-scale test conditions, emphasizing the importance of considering thermal effects when extrapolating small-scale test results to real-world applications.

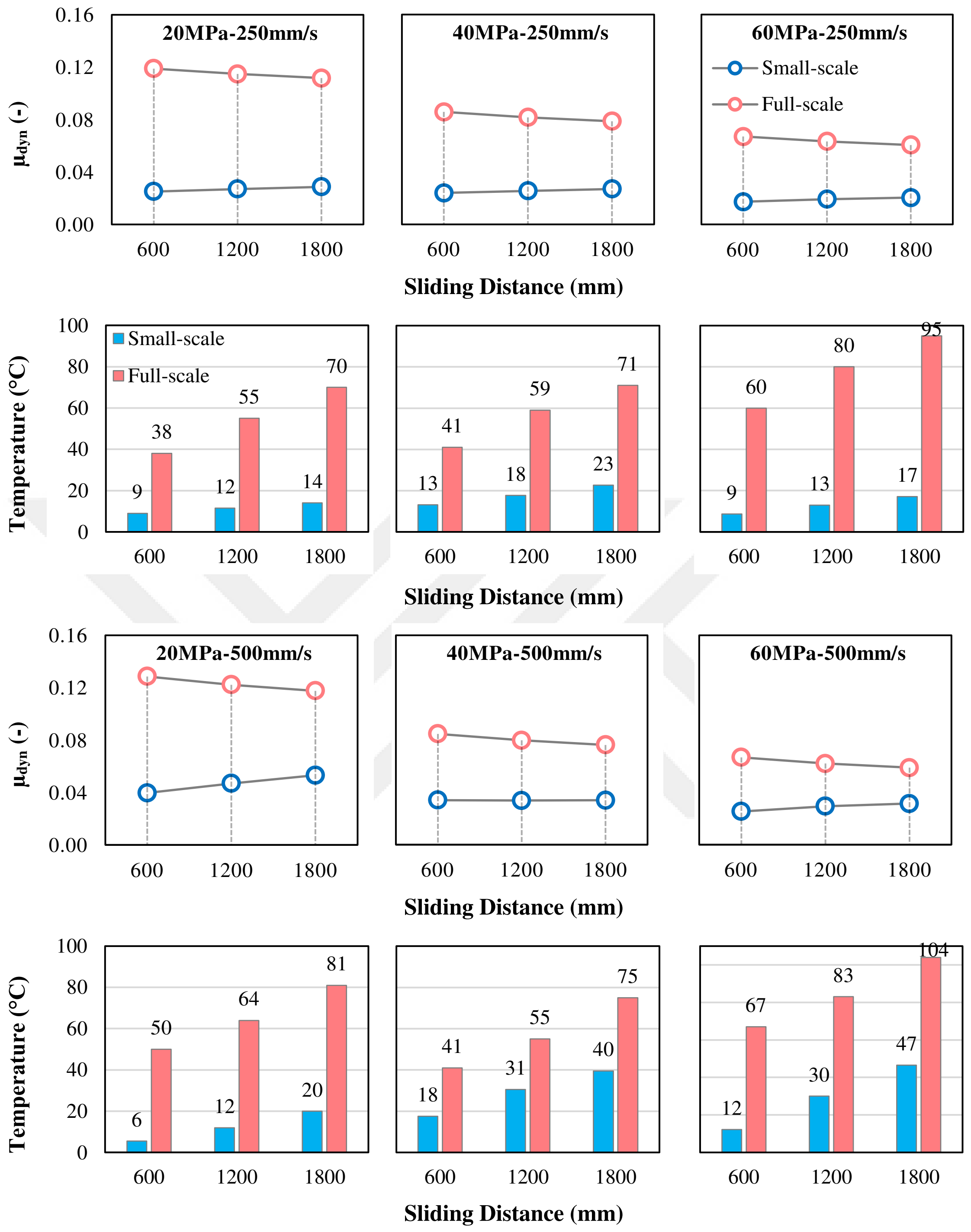

Figure 6.5. *Comparison of small- and full-scale test results in term of friction coefficient and mating surface temperature (T=0°C – 3hrs)*

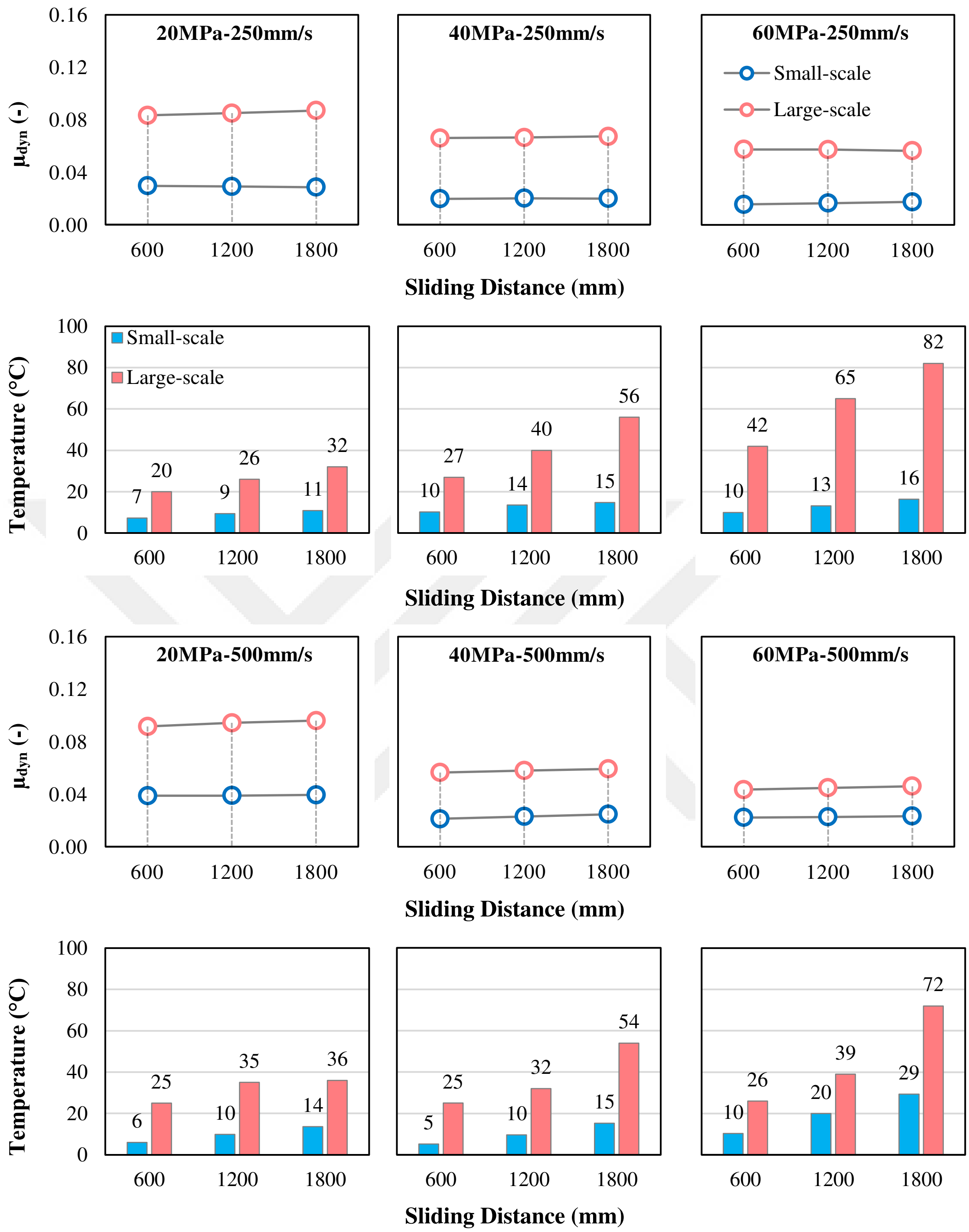

Figure 6.6. *Comparison of small- and full-scale test results in term of friction coefficient and mating surface temperature (T=0°C – 24hrs)*

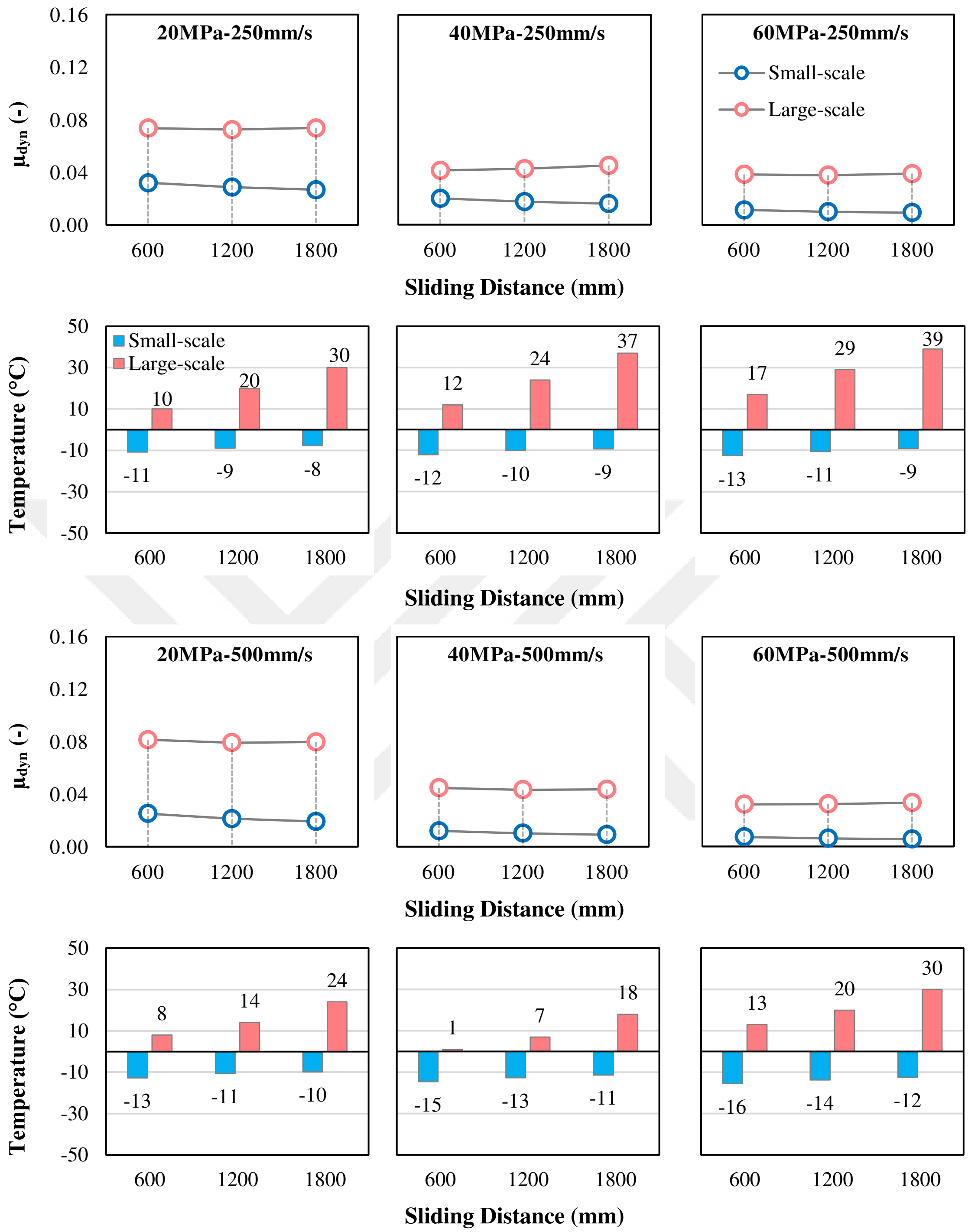

Figure 6.7. *Comparison of small- and full-scale test results in term of friction coefficient and mating surface temperature (T=-20°C – 3hrs)*

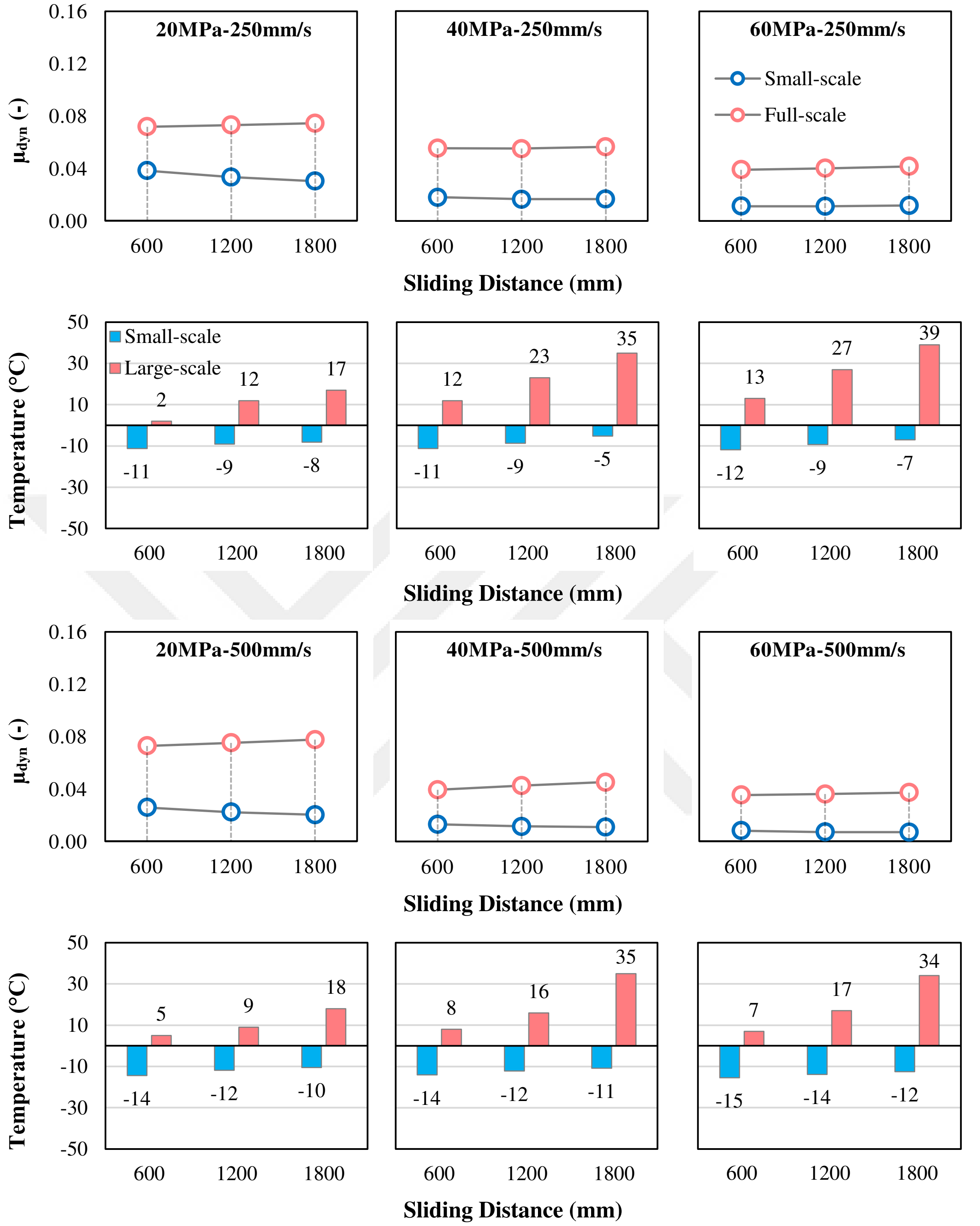

Figure 6.8. *Comparison of small- and full-scale test results in term of friction coefficient and mating surface temperature (T=-20°C – 24hrs)*

6.4. Conclusion

The experimental program performed in this chapter aimed to investigate the change in friction characteristics of a PTFE-based material used as the slider of a double CSS when exposed to low temperature. In this context, the slider material was first conditioned at low temperatures of 0 and -20oC for periods of 3 and 24 hrs. Then, subjected to cyclic motions with different normal stresses (20, 40 and 60 MPa) and maximum loading velocities (50, 100, 200 and 250 mm/s). Once the corresponding small-scale tests have been completed, their results were compared with the full-scale test results to evaluate the effectiveness of small-scale test results in representing the full-scale response.

Small-scale test results revealed that the friction coefficients of the sliding material computed at both 0 and -20oC are substantially less than the ones computed at room temperature. The formation of an ice layer at the sliding interface plays a significant role in reducing friction. In low-temperature tests, the ice layer at the interface acts as a lubricant, leading to a noticeable reduction in friction. Results also showed that friction coefficients for both exposure times (3 and 24 hrs) are almost identical. This indicates that there is no need to consider exposure times longer than 3 hrs in small-scale tests performed at low temperature.

Comparison between friction coefficients obtained from small- and full-scale tests shows that small-scale tests underestimate the friction coefficients of full-scale tests at low temperatures. Such an inconsistency is basically due to size effect. The larger specimen (slider of the double CSS) absorbs more energy, generating more heat during the cyclic motion, which in turn melts the ice layer. On the other hand, the heat generated in small-scale tests remain insufficient to eliminate the ice layer. As a result, using small-scale test results to mimic the full-scale isolator behavior at low temperatures is not as effective as the scenario for room temperature.

7. SUMMARY AND CONCLUSION

This study investigated the changes in the friction coefficient of a double curved surface slider (DCSS) under different loading conditions. The research questions addressed in this dissertation regarding the behavior of DCSS are as follows:

1. How does the accumulation of service movements over the lifetime of the isolator affect the frictional and hysteretic properties of a CSS, and can small-scale test results reliably predict the behavior of full-scale systems under different operational conditions? This question was investigated in Chapter 2.
2. What is the impact of ice formation on the static friction coefficient and sliding behavior of CSSs under icing conditions, and how do these findings contribute to the practical application of sliding isolators in cold regions? This phenomenon was addressed in Chapter 3.
3. How does ice formation affect the dynamic friction coefficient of CSSs, and what are the practical implications of these changes for the design and performance of sliding isolators in icing conditions? Chapter 4 was devoted the related investigations.
4. How can small-scale tests be used to accurately assess the friction coefficient of sliding materials, and how reliable are the estimated small-scale values in predicting the performance of full-scale CSSs? This question was investigated in Chapter 5.
5. How accurately do small-scale test results represent the full-scale performance of isolation systems at low temperatures, and what is the reliability of small-scale tests in predicting the frictional behavior of full-scale isolators under varying exposure times? Corresponding discussions were presented in Chapter 6.

A comprehensive experimental program was conducted to answer the above questions. Results obtained at each Chapter are given individually as follows:

<u>Findings from Chapter 2:</u>

Chapter 2 focused on the effect of accumulated service movements on the response modification of a CSS. Complementary examinations were carried out on both a small-scale sliding material and a double curved surface slider (DCSS) system, providing comprehensive insights into their characteristics. In the experimental campaign, specimens for both small-scale sliding material and full-scale DCSS were subjected to cyclic motions with a total sliding distance of 1000 m. The friction properties obtained from small- and full-scale tests are assessed and presented in a comparative manner to validate the use of results from small-scale tests in estimating the behavior of full-scale DCSS. Findings from this chapter indicate that:

- During the initial cycles of movement at low sliding velocity, the friction coefficient calculated from small-scale experiments is slightly lower than that observed in the full-scale DCSS. However, both small-scale and full-scale tests yield nearly identical friction coefficients after 1000 m of accumulated displacement. It is observed that using small-scale experiments to determine the friction coefficient of a full-scale sample is an effective, reliable, and practical approach, especially when considering low-velocity friction scenarios.
- The gradual reduction in friction coefficient of DCSS with increasing number of cycles is due to the frictional heating at the sliding interface. Test results showed that temporary stop of motion leads to cooling down of the sliding interface. Thus, the friction coefficient recovers to its initial value after this cooling interval. Accordingly, the seismic response of the DCSS do not change even after an accumulated sliding distance of 1000 m.

<u>Findings from Chapter 3:</u>

Chapter 3 investigates the change in static friction coefficient of CSSs under icing conditions, focusing on the hysteretic behavior of a full-scale DCSS subjected to low temperatures. The DCSS underwent cyclic tests with controlled displacement after being exposed to temperatures of 20°C, 0°C, and -20°C for durations of 3, 12, and 24 hours. Tests were conducted under various conditions, including normal stresses of 40, 60, and 80 MPa, and maximum sliding velocities of 250, 500, and 750 mm/s. Static friction coefficients were calculated by considering the force-displacement curves obtained from each test, providing insight into how ice formation affects the sliding interface. Results of this chapter reveal that:

- At sub-zero temperatures (below 0ºC), the iced sliding surface develops a liquid-like layer of melted ice. This layer functions as a lubricant, eliminating direct solid-solid contact between the interacting sliding surfaces. Consequently, there is a considerable decrease in the static friction coefficient compared to the value observed at the room temperature.

- The thickness of the liquid-like layer, and consequently the resulting friction coefficient, is influenced by both pressure and sliding velocity.
- When the temperature is moderately low and the exposure time is short, the thickness of the ice layer will be thin. This layer quickly dissolves if the surrounding temperature rises above 0ºC. As a result, the liquid-like layer disappears, and the friction coefficient becomes comparable to the reference value obtained from a sample that was not previously subjected to low temperatures.
- The exposure temperature does not influence the static friction coefficient under icing conditions, as long as the exposure time is long enough to allow for the development of a thick and thermally stable layer of ice.
- The decrease in friction due to the formation of an ice layer may result in amplified isolator displacements. Therefore, it would be critical to consider the formation of an ice layer on the sliding interface for seismic isolation applications in bridges located in cold climate regions.

Findings from Chapter 4:

Chapter 4 focuses on the effect of low temperature exposure on the dynamic friction coefficient of the tested full-scale DCSS. As part of the experimental program, a double CSS specimen was tested under various loading conditions. The specimen was subjected to different normal stress levels (40, 60, 80 MPa) and loading velocities (50, 250, 500, and 750 mm/s). Prior to testing, the DCSS was conditioned at low temperatures (20, 0, and -20°C) for varying durations (3, 12, and 24 hours). In the tests, the isolator undergoes displacement controlled cyclic motions, and the corresponding dynamic friction coefficients were obtained. Key findings of Chapter 4 are:

- As the temperature decreases, the dynamic friction coefficient of the full-scale DCSS decreases. This reduction can be attributed to the formation of an ice layer at the sliding interface. The presence of ice acts as a lubricant that reduces the friction at the sliding interface.
- At -20°C, the effect of exposure time on the friction coefficient is found to be negligible. Because, after conditioning the DCSS at -20°C an ice layer consistently formed at the sliding interface. However, at 0°C, the lowest

friction coefficient is observed only when the exposure time is maximized. Thus, in this case, exposure time becomes an important parameter.

- A comparison of the test results with the property modification factors (λ_s) proposed in CEN 1998 and CEN 2009 indicates that the current λ_s suggestion does not accurately represent the real-world conditions. This discrepancy stems from its failure to consider the impact of ice formation in practical applications. Therefore, a more refined testing protocol is needed to precisely assess the influence of low temperatures on the friction coefficient of CSSs.
- Contrary to building code recommendations, the presence of ice at the sliding interface does not increase the friction coefficient as suggested by the upper bound property modification at low temperatures. Instead, this phenomenon should be considered a factor influencing the lower bound value of the friction coefficient. If the actual friction coefficient is lower than the design value, the maximum isolator displacements will exceed those estimated using the lower bound values.

Findings from Chapter 5:

Chapter 5 investigates whether the frictional properties of a full-scale DCSS at room temperature can be accurately represented by small-scale test results. Initially, the frictional characteristics of the sliding material were evaluated through small-scale experiments conducted at room temperature. These tests were performed under various normal stresses (20, 40, and 60 MPa) and different sliding velocities (5, 25, 50, 100, 200, and 250 mm/s). Based on the experimental data, a comprehensive analytical model was developed to characterize the friction coefficient of the material. To determine the reliability of small-scale tests in predicting the isolator performance, the estimated friction values were compared with the effective friction coefficient of a full-scale isolator. This comparison provided insight into the use of small-scale test results for evaluating the full-scale isolator behavior. Results presented in this chapter show that:

- Small-scale experiments reveal that μ_{dyn} decreases as pressure increases, which is attributed to the elasto-plastic nature of the sliding material. Initially, μ_{dyn} increases with higher velocities due to the polymer's viscous properties. However, this increase ceases after a certain velocity, and the friction coefficient tends to stabilize at a constant value. That threshold was determined as 50 mm/s for the tested filled-PTFE.

- The proposed unified model takes into account the impact of pressure, loading velocity, and heating effects at the sliding interface during cyclical motion. A comparison between the estimated friction coefficients and data from full-scale tests demonstrated that the proposed formula accurately predicts the effective friction coefficient of full-scale specimens using small-scale test results.

Findings from Chapter 6:

Chapter 6 focuses on assessing the accuracy of small-scale tests in representing the friction characteristics of a full-size DCSS under low temperature conditions. To achieve this objective, the frictional properties of the sliding material were first examined through small-scale experiments conducted at low temperatures (0°C and -20°C) for durations of 3 and 24 hours. These tests were performed under various normal stresses (20, 40, and 60 MPa) and sliding speeds (50, 100, 200, and 250 mm/s). The friction coefficients obtained from small-scale experiments were then compared with those measured in full-scale tests to evaluate the reliability of small-scale testing in simulating full-scale performance. The results of this chapter highlight that:

- Small-scale sliding material exhibits behavior similar to that of full-scale isolator tests when subjected to low-temperature conditions. The formation of an ice layer at the interface acts as a lubricant, significantly reducing friction. However, studies indicate that in small-scale experiments, an exposure duration of just 3 hours is sufficient for this effect to become apparent regardless of the temperature.
- When small- and full-scale test results are compared, friction coefficients are observed to be higher in full-scale tests. This is because the full-scale isolator absorbs a greater amount of energy, generating more heat. The increased heat production leads to melting of the ice layer at the sliding interface. On the other hand, small-scale tests fail to produce sufficient heat to melt the ice layer.

It should be emphasized that the conclusions of this PhD thesis are constrained by the specific DCSS and the sliding material used at the sliding interface, and the particular low-temperature conditions considered. Future research could build upon this study by exploring various loading combinations and alternative sliding materials.

REFERENCES

AASHTO. (2014). *Guide specifications for seismic isolation design.* 4th ed. Washington, DC: American Association of State Highway and Transportation Officials.

Al-Hussaini, T. M., Constantinou, M. C., & Zayas, V. A. (1994). *Seismic isolation of multi-story frame structures using spherical sliding isolation systems (NCEER-94-0007).* New York: National Center for Earthquake Engineering Research.

Alvarado, R., & Ryan, K. (2023). *Testing and analysis of the effects of infiltrated water and ice on friction pendulum bearings.* Alaska: FHWA-AK-RD-4000(197);HFHWY00181.

Amontons, G. (1699). Me´moires de l'Acade´mie Royale A. 257-282.

Anita, P., & Kowalewski, P. (2018). The influence of reducing temperature on changing Young's Modulus and the coefficient of friction of selected sliding polymers. *Quarterly Tribologia, 279*, 107–111.

Apostoli, C., Giusti, G., Ciccoianni, J., Riva, G., Capozza, R., Woulaché, R. L., . . . et al. (2017). Velocity dependence of sliding friction on a crystalline surface. *Beilstein Journal of Nanotechnology, 8*(1), 2186-2199.

Archard, J. F. (1957). Elastic deformation and the laws of friction. *Proceedings of the Royal Society of London. Series A: Mathematical and Physical Sciences, 243*(1233), 190-205.

Archard, J. F. (1959). The temperature of rubbing surfaces. *Wear, 2*(6), 438–455.

ASCE/SEI 7. (2016). *Minimum design loads for buildings and other structures.* Reston, VA: American Society of Civil Engineers.

ASCE/SEI 7. (2022). *Minimum design loads for buildings and other structures.* Reston, VA: American Society of Civil Engineers.

Bai, L., Sun, J., Zhang, P., & Khan, Z. A. (2021). Friction behavior of a textured surface against several materials under dry and lubricated conditions. *Materials, 14*(18), 5228.

Bao, Y., Becker, T. C., & Hamaguchi, H. (2017). Failure of double friction pendulum bearings under pulse-type motions. *Earthquake Engineering and Structural Dynamics, 46*, 715–32.

Barone, S., Calvi, G. M., & Pavese, A. (2019). Experimental dynamic response of spherical friction-based isolation devices. *Journal of Earthquake Engineering, 23*(9), 1465-1484.

Barone, S., Calvi, G. M., & Pavese, A. (2019). Experimental dynamic response of spherical friction-based isolation devices. *Journal of Earthquake Engineering, 23*(9), 1465-1484.

Barucci, C. (1990). La casa antisismica [The antiseismic house]. Gangemi, Rome (In Italian).

Bechtold, J. (1907). Earthquake proof building. US patent 845046A.

Becker, T. C., & Mahin, S. A. (2012). Experimental and analytical study of the bi-directional behavior of the triple friction pendulum isolator. *Earthquake Engineering and Structural Dynamics, 41*, 355–73.

Becker, T. C., Bao, Y., & Mahin, S. A. (2017). Extreme behavior in a triple friction pendulum isolated frame. *Earthquake Engineering and Structural Dynamics, 46*, 2683–98.

Berman, A., Ducker, W., & Israelachvili, J. (1996). Origin and characterization of different stick-slip friction mechanisms. *Langmuir, 12*, 4559–63.

Berto, L., Favaretto, T., & Saetta, A. (2013). Seismic risk mitigation technique for art objects: experimental evaluation and numerical modelling of double concave curved surface sliders. *Bulletin of Earthquake Engineering, 11*, 1817-1840.

Bhushan, B. (1971). *Temperature and friction of sliding surfaces.* Doctoral dissertation, Massachusetts Institute of Technology.

Bhushan, B. (2013). *Introduction to tribology.* Hoboken, New Jersey: John Wiley & Sons, Ltd.

Białas, M., Maciejewski, J., & Kucharski, S. (2021). Friction coefficient of solid lubricating coating as a function of contact pressure: Experimental results and microscale. *Continuum Mechanics and Thermodynamics, 33*, 1733-1745.

Bijelić, I., Mor, N., Živković, M., Tubin, V., & Stožinić, T. (2017). The influence of the contact pressure on the value of the coefficient of friction. *Tribology in Industry, 39*(2), 255.

Blok, H. (1963). The flash temperature concept. *Wear, 6*(6), 483–494.

Bondonet, G., & Filiatrault, A. (1997). Frictional response of PTFE sliding bearings at high frequencies. *Journal of Bridge Engineering, 2*(4), 139-148.

Bowden, F. P., & Tabor, D. (1950). *The friction and lubrication of solids.* Oxford: Clarendon.

Bowden, F., & Tabor, D. (1964). *The Friction and Lubrication of Solids – Part II.* London, Great Britain: Oxford University Press.

Braun, C., & Butz, C. (2010). Static and dynamic friction in curved surface sliders. *IABSE Symposium: Large Structures and Infrastructures for Environmentally Constrained and Urbanised Areas*, (pp. 400-401). Venice, Italy.

Buckle, I., Constantinou, M., Dicleli, M., & Ghasemi, H. (2006). *Seismic isolation of highway bridges (MCEER REPORT_06-SP07).* Buffalo: Multidisciplinary Center for Earthquake Engineering Research.

Calvi, G. M., Calvi, P. M., & Moratti, M. (2017). Seismic isolation of buildings using devices based on sliding between surfaces with variable friction coefficient. *Innovative Infrastructure Solutions, 2*, 1-18.

Calvi, P. M., & Calvi, G. M. (2018). Historical development of friction-based seismic isolation systems. *Soil Dynamics and Earthquake Engineering, 106*, 14-30.

Campbell, T. I., Fatemi, M. J., & Manning, D. G. (1993). Friction in bridge bearings with contaminated tfe slide surface. *Journal of Structural Engineering, 119*, 3169–77.

Cardone, D., Gesualdi, G., & Brancato, P. (2015). Restoring capability of friction pendulum seismic isolation systems. *Bulletin of Earthquake Engineering, 13*(8), 2449–2480.

Cardone, D., Viggiani, L. R., Perrone, G., Telesca, A., Di Cesare, A., Ponzo, F. C., . . . al., e. (2022). Modelling and seismic response analysis of existing Italian residential RC buildings retrofitted by seismic isolation. *Journal of Earthquake Engineering, 27*(4), 1069–1093.

Carslaw, H. S., & Jaeger, J. C. (1959). *Conduction of Heat in Solids.* Londra: Oxford University Press.

Cavdar, E., & Ozdemir, G. (2021). Investigation on both experimental and analytical response of a double friction pendulum. *6th International Conference on Earthquake Engineering and Seismology (6ICEES).* Gebze, Türkiye.

Cavdar, E., Karuk, V., & Ozdemir, G. (2022). Modification in response of a bridge seismically isolated with lead rubber bearings exposed to low temperature. *Technical Journal of Turkish Chamber of Civil Engineers, 33*(5).

Cavdar, E., Ozdemir, G., & Ozcamur, U. (2022). Experimental investigation on hysteretic behavior of a double friction pendulum and frictional heating. *World Conference* *on Seismic Isolation* (pp. 229-239). Torino, Cham: Springer International Publishing.

CEN EN 1337-2. (2004). Structural Bearings - Part 2: Sliding Elements. *European Committee for Standardization (CEN).*

CEN EN 15129. (2009). *Anti-seismic devices.* Brussels, Belgium: European Committee for Standardization.

CEN EN 1998-2. (2005). *Design of structures for earthquake resistance – Part 2: Bridges.* Brussels, Belgium: Eurocode 8.

Chang, K. C., Hwang, J. S., & Lee, G. C. (1990). Analytical model for sliding behavior of Teflon-stainless steel interfaces. *Journal of Engineering Mechanics*, 2749-2763.

Cho, C., Kwahk, I., & Kim, Y. (2008). An experimental study for the shear property and the temperature dependency of seismic isolation bearings. *Journal of the Earthquake Engineering Society of Korea, 12*(1), 67-77.

Colbeck, S. C. (1994). A review of the friction of snow skis. *Journal of Sports Sciences, 12*, 285–95.

Colbeck, S. C. (1995). Pressure melting and ice skating. *American Journal of Physics, 63*, 888–90.

Constantinou, M. C. (1994). Seismic isolation systems: Introduction and overwiew. In *Passive and Active Structural Vibration Control in Civil Engineering* (pp. 81-96). Vienna: Springer.

Constantinou, M. C., Tsopelas, P., Kasalanati, A., & Wolff, E. D. (1999). *Property modification factors for seismic isolation bearings (MCEER-99-0012).* Buffalo: Multidisciplinary Center for Earthquake Engineering Research.

Constantinou, M. C., Whittaker, A. S., Kalpakidis, Y., Fenz, D. M., & Warn, G. P. (2007). *Performance of seismic isolation hardware under service and seismic loading (MCEER-07-0012).* University at Buffalo, State University of New York.

Constantinou, M., Cacceset, J., & Harris, H. (1987). Frictional characteristics of Teflon-steel interfaces under dynamic conditions. *Earthquake Engineering and Structural Dynamics, 15*(6), 751–759.

Constantinou, M., Mokha, A., & Reinhorn, A. (1990). Teflon bearings in base isolation II: Modeling. *Journal of Structural Engineering, 116*(2), 455-474.

Danciu, L., Nandan, S., Reyes, C., Basili, R., Weatherill, G., Beauval, C., . . . al., e. (2021). *The 2020 update of the european seismic hazard model: Model overview.* Zurich.

De Domenico, D., Cardone , D., & Croatto, F. (2005). Frictional behavior of steel-PTFE interfaces for seismic isolation. *Bulletin of Earthquake Engineering, 3*, 75-99.

De Domenico, D., Ricciardi, G., & Benzoni, G. (2018). Analytical and finite element investigation on the thermo-mechanical coupled response of friction isolators under bidirectional excitation. *Soil Dynamics and Earthquake Engineering, 106*, 131-147.

De Domenico, D., Ricciardi, G., Infanti, S., & Benzoni, G. (2019). Frictional heating in double curved surface sliders and its effects on the hysteretic behavior: an experimental study. *Frontiers in Built Environment, 5*, 74.

De Koning, J. J., Houdijk, H., de Groot, G., & Bobbert, M. F. (2000). From biomechanical theory to application in top sports: the Klapskate story. *Journal of Biomechanics, 33*, 1225–9.

Dolce, M., Cardone, D., & Croatto, F. (2005). Frictional behavior of steel-PTFE interfaces for seismic isolation. *Bulletin of Earthquake Engineering, 3*, 75-99.

Dolce, M., Cardone, D., & Palermo, G. (2007). Seismic isolation of bridges using isolation systems based on flat sliding bearings. *Bulletin of Earthquake Engineering, 5*, 491-509.

Dowson, D. (1979). *History of Tribology.* London: Longman.

Ettles, C. M. (1986). Polymer and elastomer friction in the thermal control regime. *ASLE Transactions, 108*, 98–104.

Evans, D. C., & Senior, G. S. (1982). Self-lubricating materials for plain bearings. *Tribology International, 15*(5), 243-248.

Fagà, E., Ceresa, P., Nascimbene, R., Moratti, M., & Pavese, A. (2015). Modelling curved surface sliding bearings with bilinear constitutive law: effects on the response of seismically isolated buildings. *Materials and Structures, 49*(6), 2179-96.

Fenz, D. M., & Constantinou, M. C. (2006). Behaviour of the double concave friction pendulum bearing. *Earthquake Engineering and Structural Dynamics, 35*(11), 1403-1424.

Fenz, D. M., & Constantinou, M. C. (2008). Spherical sliding isolation bearings with adaptive behavior: Theory. *Earthquake Engineering and Structural Dynamics, 37*(2), 163-183.

Fowler, A. J., & Bejan, A. (1993). Contact melting during sliding on ice. *International Journal of Heat and Mass Transfer, 36*, 1171–9.

Fuller, K., Gough, J., & Thomas, A. (2004). The effect of low-temperature crystallization on the mechanical behavior of rubber. *Journal of Polymer Science, Part B: Polymer Physics, 42*(11), 2181-2190.

Furinghetti , M., Pavese, A., Quaglini, V., & Dubini, P. (2019). Experimental investigation of the cyclic response of double curved surface sliders subjected to radial and bidirectional sliding motions. *Soil Dynamics and Earthquake Engineering, 117*, 190–202.

Furinghetti, M., Yang, T., Calvi, P. M., & Pavese, A. (2021). Experimental evaluation of extra-stroke displacement capacity for curved surface slider devices. *Soil Dynamics and Earthquake Engineering, 146*, 106752.

Gandelli, E., & Quaglini, V. (2018). Effect of the static coefficient of friction of curved surface sliders on the response of an isolated building. *Journal of Earthquake Engineering, 24*, 1361-1389.

Gandelli, E., De Domenico, D., Dubini, P., Besio, M., Bruschi, E., & Quaglini, V. (2020). Influence of the breakaway friction on the seismic response of buildings isolated with curved surface sliders: Parametric study and design recommendations. *Structures, 27*, 788-812.

Gandelli, E., Lomiento, G., Quaglini, V. S., Terzo, M., & Tordela, C. (2021). Estimation of the instantaneous friction coefficients of sliding isolators subjected to bi-directional orbits through a nonlinear state observer. *Engineering Structures, 249*, 113374.

Gandelli, E., Penati, M., Quaglini, V., Lomiento, G., Miglio, E., & Benzoni, G. M. (2019). A novel OpenSees element for single curved surface sliding isolators. *Soil Dynamics and Earthquake Engineering, 119*, 433-453.

Gao, J., Luedtke, W. D., Gourdon, D., Ruths, M., Israelachvili, J. N., & Landman, U. (2004). Frictional forces and Amontons' law: from the molecular to the macroscopic scale. *The Journal of Physical Chemistry B, 108*(11), 3410-3425.

Guaii, T., Liu, Y., Shou, H., & Li, F. (2021). Effects of load and rotational speed on the friction and wear properties of PTFE composites. *IOP Conference Series: Materials Science and Engineering. Vol. 1043, No. 5*, p. 052055. IOP Publishing.

Hasegawa, O., Shimoda, I., & Ikenaga, M. (1997). *Characteristic of lead–rubber bearing by temperature.* Tokyo, Japan.

Hornbogen, E. (1986). Friction and wear of materials with heterogeneous microstructures. In *Composite Materials Series* (Vol. 1, pp. 61-88). Elsevier.

Hutchings, I., & Shipway, P. (2017). *Tribology: friction and wear of engineering materials.* Butterworth-heinemann.

Hyakuda, T., Saito , K., Matsushita , T., Matsushita , T., Yoneki , S., & et al. (2001). The structural design and earthquake observation of a seismic isolation building using Friction Pendulum system. *7th international seminar on seismic isolation, passive energy dissipation and active control of vibrations of structures.* Italy: Assisi.

Jaeger, J. C. (1942). Moving Sources of Heat aand Temperature at Sliding Contacts. *Proceedings of the Royal Society of New South Wales, 76*, 203–224.

John, M., & Menezes, P. L. (2021). Self-lubricating materials for extreme condition applications. *Materials, 14*(19), 5588.

Joly, J. (1899). The phenomena of skating and Prof. J. Thomson's thermodynamic relation. *Nature, 59*, 485–6.

Kaiser, W. (223). *Kunststoffchemie für Ingenieure: von der Synthese bis zur Anwendung.* Munich : Carl Hanser Verlag GmbH Co KG.

Kang, B. M., & Park, Y. W. (2010). A study on phase separation of PA-PDMS composites dependent on molecular weight. *Polymer-Plastics Technology and Engineering, 49*(3), 223-227.

Kasar, A. K., Jose, S. A., D'Souza, B., & Menezes, P. L. (2024). Fabrication and tribological performance of self-lubricating porous materials and composites: A review. *Materials, 17*(14), 3448.

Keikha, H., & Ghodrati Amiri, G. (2019). Seismic performance assessment of quintuple friction pendulum isolator with a focus on frictional behavior impressionability from velocity and temperature. *Journal of Earthquake Engineering, 25*(7), 1256-1286.

Keikha, H., & Ghodrati Amiri, G. (2021). Numerical development and assessment of 3D quintuple friction pendulum isolator element based on its analytical and mathematical models. *Journal of Earthquake Engineering, 25*(13), 2718-2757.

Kietzig, A. M., Hatzikiriakos, S. G., & Englezos, P. (2010). Physics of ice friction. *Journal of Applied Physics, 107*, 081101.

Kikuchi, M., & Ishii, K. (2018). Thermal-mechanical coupled behavior of sliding bearings for seismic isolation. In *Proceedings of the 1st International Conference on Numerical Modelling in Engineering: Volume 1 Numerical Modelling in Civil Engineering* (pp. 30-43). NME 2018, 28-29 August 2018, Ghent University, Belgium: Springer Singapore.

Kumar, M., Whittaker, A. S., & Constantinou, M. C. (2015). Characterizing friction in sliding isolation bearings. *Earthquake Engineering and Structural Dynamics, 44*(9), 1409-1425.

Kurtz, S. M. (2015). *UHMWPE Biomaterials Handbook. Ultra-High Molecular Weight Polyethylene in Total Joint Replacement and Medical Devices.* Elsevier.

Lin, S. C., Han, J. Q., & Zhao, H. T. (2020). Experimental and theoretical studies of bidirectional variable curvature friction pendulum bearing. *KSCE Journal of Civil Engineering, 24*, 1568-1580.

Lomiento, G., Bonessio, N., & Benzoni, G. (2013). Friction model for sliding bearings under seismic excitation. *Journal of Earthquake Engineering, 17*(8), 1162-1191.

Makinson, K. R., & Tabor, D. (1964). The friction and transfer of polytetrafluoroethylene. *Proceedings of the Royal Society of London. Series A. Mathematical and Physical Sciences, 281*(1384), 49-61.

McConica, H. (1950). *Sliding on ice and snow.* Office of the Quartermaster General U.S. Army, American Ski Company.

McCook, N. L., Burris, D. L., Dickrell, P. L., & Sawyer, W. G. (2005). Cryogenic friction behavior of PTFE based solid lubricant composites. *Tribology Letters, 20*, 109–113.

Mendez-Galindo, C., Moor, G., & Rassy, S. (2017). Lead rubber bearings for seismic isolation of structures in cold climates - New developments. *IABSE Conference, Vancouver 2017: Engineering the Future - Report*, *109.*

Menezes, P. L., Rohatgi, P. K., & Omrani, E. (2018). *Self-Lubricating Composites.* Berlin: Springer.

Messina, A., & Miranda, E. (2022). Frictional behavior of low-cost steel-polymer interfaces for seismic isolation. *Journal of Structural Engineering, 148*(1), 04021239.

Messina, A., & Miranda, E. (2024). A novel friction model for steel-polymer interfaces in sliding seismic isolation bearings. *Earthquake Engineering and Structural Dynamics, 53*(8), 2592-2606.

Mirzaev, I., Sagdiev, K., & Yuvmitov, A. (2024). Experimental determination of dynamic coefficient of Amonton-Coulomb dry friction. *Facta Universitatis, Series: Mechanical Engineering*.

Mokha, A., Constantinou, M. C., & Reinhorn, A. M. (1991a). Further results on frictional properties of Teflon bearings. *Journal of Structural Engineering, 117*(2), 622-626.

Mokha, A., Constantinou, M. C., Reinhorn, A. M., & Zayas, V. A. (1991b). Experimental study of friction-pendulum isolation system. *Journal of Structural Engineering, 117*(4), 1201-1217.

Mokha, A., Constantinou, M., & Reinhorn, A. (1988). *Teflon Bearings in Aseismic Base Isolation: Experimental Studies and Mathematical Modeling, NCEER-88-0038.* Buffalo, NY: National Center for Earthquake Engineering Research (NCEER).

Mokha, A., Constantinou, M., & Reinhorn, A. (1990). Teflon bearings in base isolation. I: Testing. *Journal of Structural Engineering, 116*(2), 438-454.

Mosqueda, G., Whittaker, A. S., & Fenves, G. L. (2004). Characterization and modeling of friction pendulum bearings subjected to multiple components of excitation. *Journal of Structural Engineering, 130*(3), 433-442.

Naeim, F., & Kelly, J. M. (1999). *Design of seismic isolated structures: From theory to practice.* New York: John Wiley & Sons.

Nakahara, T. A. (2005). Model of seizure based on Burwell and Strang's concept of wear mode transition. *Proceedings of the 31st Leeds–Lyon Symposium on Life Cycle Tribology*, (pp. 547–553). Amsterdam, Hollanda.

Nakano, O., Nishi, H., Shirono, T., & Kumagai, K. (1993). Temperature-dependence of base-isolation bearings. *Proceedings of 2nd U.S.-Japan Workshop on Earthquake Protective Systems for Bridges.* Tsukuba Science City, Japonya: Public Works Research Institute.

Narisawa, I. (1993). High-speed tribology of polymer composites. In *Composite Materials Series* (Vol. 8, pp. 559-582). Elsevier.

Niven, C. D. (1959). A proposed mechanism for ice friction. *Canadian Journal of Physics, 37*, 247–55.

O'Reilly, G. J., Yasumoto, H., Suzuki, Y., Calvi, G. M., & Nakashima, M. (2022). Risk-based seismic design of base-isolated structures with single surface friction sliders. *Earthquake Engineering and Structural Dynamics, 51*(10), 2378–2398.

Opałka, M., Kowalewski, P., & Ptak, A. (2020). Numerical Analysis of the Influence of Temperature on the Friction Resistance of a Metal-Polymer Sliding Pair. *Tribologia*.

Otsuki, M., & Matsukawa, H. (2013). Systematic breakdown of Amontons' law of friction for an elastic object locally obeying Amontons' law. *Scientific Reports, 3*(1), 1586.

Ozdemir, G., & Constantinou, M. C. (2010). Evaluation of equivalent lateral force procedure in estimating seismic isolator displacements. *Soil Dynamics and Earthquake Engineering, 30*(10), 1036-1042.

Ozdemir, I., Bulbul, B., Kiracbedel, U., Grund, T., & Lampke, T. (2024). Wear Performance Evaluation of Polymer Overlays on Engine Bearings. *Materials, 17*(15), 3802.

Palmer , R. J. (2000). *Polyamides, plastics.* Kirk-Othmer Encyclopedia of Chemical Technology.

Park, J., Jang, K., Lee, H., Lee, Y., & Kim, H. (2012). Experimental study on the temperature dependency of full scale low hardness lead rubber bearing. *Journal of the Computational Structural Engineering Institute of Korea, 25*(6).

Pavese, A., Furinghetti, M., & Casarotti, C. (2019). Experimental assessment of the cyclic response of friction-based isolators under bidirectional motions. *Soil Dynamics and Earthquake Engineering, 114*, 1-11.

Petrenko, V. F., & Whitworth, R. W. (1999). *Physics of ice.* Oxford: Oxford University Press.

Pigouni, A. E., Castellano, M. G., Infanti, S., & Colato, G. P. (2020). Full-scale dynamic testing of pendulum isolators (Curved surface sliders). *Soil Dynamics and Earthquake Engineering, 130*, 105983.

Ponzo, F. C., Di Cesare, A., Leccese, G., & Nigro, D. (2017). Shake table testing on restoring capability of double concave friction pendulum seismic isolation systems. *Earthquake Engineering and Structural Dynamics, 46*(14), 2337-2353.

Ponzo, F. C., Di Cesare, A., Telesca, A., Pavese, A., & Furinghetti, M. (2021). Advanced modelling and risk analysis of RC buildings with sliding isolation systems designed by the Italian Seismic Code. *Applied Sciences, 11*(4), 1938.

Pounder, E. R. (1965). *The physics of ice.* Oxford: Pergamon.

Pranesh, M., & Sinha, R. (2000). VFPI: an isolation device for aseismic design. *Earthquake Engineering and Structural Dynamics, 29*, 603–27.

Quaglini, V. (2012b). High damping curved surface sliding isolators for bridges. *Bridge Maintenance, Safety, Management, Resilience and Sustainability: Proceedings of the Sixth International IABMAS Conference.* Stresa, Italy.

Quaglini, V., & Dubini, P. (2011). Friction of polymers sliding on smooth surfaces. *Advances in Tribology, 1*, 178943.

Quaglini, V., Bocciarelli, M., Gandelli, E., & Dubini, P. (2014). Numerical assessment of frictional heating in sliding bearings for seismic isolation. *Earthquake Engineering, 18*, 1198–216.

Quaglini, V., Dubini, P., & Poggi, C. (2012a). Experimental assessment of sliding materials for seismic isolation systems. *Bulletin of Earthquake Engineering, 10*(2), 717–40.

Quaglini, V., Dubini, P., Ferroni, D., & Poggi , C. (2009). Influence of counterface roughness on friction properties of engineering plastics for bearing applications. *Materials and Design, 30*, 1650–8.

Quaglini, V., Dubini, P., Furinghetti , M., & Pavese, A. (2022). Assessment of scale effects in the experimental evaluation of the coefficient of friction of sliding isolators. *Journal of Earthquake Engineering, 26*(1), 525-545.

Quaglini, V., Gandelli , E., & Dubini, P. (2019). Numerical investigation of curved surface sliders under bidirectional orbits. *Ingegneria Sismica, 36*(2), 118-136.

Quaglini, V., Gandelli, E., & Dubini, P. (2017b). Experimental investigation of the re-centring capability of curved surface sliders. *Structural Control and Health Monitoring, 24*, e1870.

Quaglini, V., Gandelli, E., Dubini, P., & Limongelli, M. P. (2017a). Total displacement of curved surface sliders under nonseismic and seismic actions: A parametric study. *Structural Control and Health Monitoring, 24*(12), e2031.

Rabinowicz, E. (1995). *Friction and Wear of Materials.* New York, ABD: John Wiley & Sons Inc.

Rosenberg, R. (2005). Why is ice slippery? *Physics Today, 58*, 50-4.

Sakurai, T., Okabe, H., & Sethuramiah, A. (1971). Surface temperatures in dry friction and boundary lubrication. *Bulletin of The Japan Petroleum Institute, 13*(1), 89-96.

Samyn, P., De Baets, P., Schoukens, G., & Van Peteghem, A. P. (2006). Large-scale tests on friction and wear of engineering polymers for material selection in highly loaded sliding systems. *Materials and Design, 27*(7), 535–555.

Sarlis, A. A., Constantinou, M. C., & Reinhorn, A. M. (2013). Shake table testing of triple friction pendulum isolators under extreme conditions. Technical Report MCEER-13–0011.

Sextro, W. (2002). *Dynamical Contact Problems with Friction.* Berlin: Springer.

Shakib, H., & Fuladgar, A. (2003). Effect of vertical component of earthquake on the response of pure-friction base-isolated asymmetric buildings. *Engineering Structures, 25*, 1841–50.

Skinner, R. I., Robinson, W. H., & McVerry, G. H. (1993). *An introduction to seismic isolation.* New York: Wiley.

Smith, F. W. (1962). The effect of temperature in concentrated contact lubrication. *Asle Transactions, 5*(1), 142-148.

Stachowiak, G. W., & Batchelor, A. W. (2005). *Engineering Tribology.* Dordrecht, Hollanda: Elsevier, Butterworth-Heinemann.

Steijn, R. P. (1968). Sliding experiments with polytetrafluoroethylene. *Asle Transactions, 11*(3), 235-247.

TBEC (Turkish Building Earthquake Code). (2018). *Specifications for Building Design.* Ankara, Türkiye.

Tiwari, A., Miyashita, N., Espallargas, N., & Persson, B. N. (2018). Rubber friction: The contribution from the area of real contact. *The Journal of Chemical Physics, 148*(22).

Touaillon, J. (1870). Improvement in buildings. US patent 99973.

Touris, A., Turcios, A., Mintz, E., Pulugurtha, S. R., Thor, P., Jolly, Ö., & Jalgaonkar, U. (2020). Effect of molecular weight and hydration on the tensile properties of polyamide 12. *Results in Materials,, 8*, 100149.

Trovato, D. (2013). *Degradation of dissipative characteristics of friction pendulum isolators due to thermal effect.* Doctoral dissertation, Ph. D. Dissertation, Politecnico di Torino.

Tsai, C. S., Chen, W. S., Chiang, T. C., & Chen, B. J. (2006). Component and shaking table tests for full-scale multiple friction pendulum system. *Earthquake Engineering and Structural Dynamics, 35*, 1653–75.

Tsai, C. S., Chen, W. S., Chiang, T. C., & Chen, B. J. (2006). Component and shaking table tests for full-scale multiple friction pendulum system. *Earthquake Engineering and Structural Dynamics, 35*(13), 1653-1675.

Tsai, C. S., Chiang, T. C., & Chen , B. J. (2003). Shaking table tests of a full scale steel structure isolated with MFPS. *ASME Pressure Vessels and Piping Conference*, (pp. 41-47). Ohio, USA.

Tsopelas, P., Constantinou, M., Kim, Y., & Okamoto, S. (1996). Experimental study of FPS system in bridge seismic isolation. *Earthquake Engineering and Structural Dynamics, 25*(1).

Tyler, A. G. (1977). Dynamic tests on PTFE sliding layers under earthquake condition. *Bulletin of the New Zealand National Society for Earthquake Engineering, 10*(3), 129-138.

Wen, J., Han, Q., & Du, X. (2019). Shaking table tests of bridge model with friction sliding bearings under bi-directional earthquake excitations. *Structure and Infrastructure Engineering, 15*(9), 1264-1278.

Whiteley, K. S., Heggs, T. G., Koch, H., Mawer, R. L., & Immerl, W. (2000). *Polyolefins.* Ullmann's Encyclopedia of Industrial Chemistry.

Workel, M. F., Dowson, D., Ehret, P., & Taylor, C. M. (2000). The influence of mean contact pressure on the friction coefficient of a traction fluid at high pressure. *Proceedings of the Institution of Mechanical Engineers, Part C: Journal of Mechanical Engineering Science, 214*(2), 309-312.

Xue, S. D., Li, X. Y., & Cai, Y. C. (2009). Experiments on a new type of seismic isolation bearing combined with Teflon frictional sliding system and springs. *Beijing*

Gongye Daxue Xuebao/Journal of Beijing University of Technology, 35(2), 168-173.

Yakut, A., & Yura, J. (2002a). Parameters influencing performance of elastomeric bearings at low temperatures. *Journal of Structural Engineering, 128*(8), 986-994.

Yakut, A., & Yura, J. (2002b). Evaluation of low-temperature test methods for elastomeric bridge bearings. *Journal of Bridge Engineering, 7*(1), 50-56.

Yasar, C., Karuk, V., Kaplan, O., Cavdar, E., & Ozdemir, G. (2023b). Amplification in mechanical properties of a lead rubber bearing for various exposure times to low temperature. *Buildings, 13*(2), 478.

Yaşar, C., Karuk, V., Cavdar, E., & Ozdemir, G. (2023a). Variation in mechanical properties of a lead–rubber bearing exposed to low temperature. *Journal of Cold Regions Engineering, 37*(3), 04023012.

Zayas, V. (1987b). Earthquake protective column support. *US patent 4644714*.

Zayas, V., Low, S., & Mahin, S. (1987a). The FPS earthquake resistant system experimental report. UC Berkeley (Report No. UCB/EERC-87/01).

Zayas, V., Low, S., & Mahin, S. (1990). A simple pendulum technique for achieving seismic isolation. *Earthquake Spectra, 6*(2), 317–33.

Zeng, C., Tao, Z., & Bai, J. F. (2013). Research on the Influencing Factors of Friction Coefficient between PTFE and Stainless-Steel of Sliding Isolation Bearings. *Advanced Materials Research, 740*, 624-629.

Zhang, C., & Ali, A. (2021). The advancement of seismic isolation and energy dissipation mechanisms based on friction. *Soil Dynamics and Earthquake Engineering, 146*, 106746.

Zhang, R., & Li, A. (2020). Experimental study on temperature dependence of mechanical properties of scaled high-performance rubber bearings. *Composites Part B: Engineering, 190*.

http-1: https://www.tis.com.tr/urunler (Accessed on: 02.01.2025)

http-2: www.tis.com.tr/wp-content/uploads/2022/11/TDP-Katalog.pdf (Accessed on: 02.01.2025)

http-3: https://peer.berkeley.edu/peer-strong-ground-motion-databases (Accessed on: 02.01.2025)

CURRICULUM VITAE

ORCID ID: 0000-0003-1497-0908

Name Surname **:Esengül ÇAVDAR**

Foreign Language **:English**

Educational Background:

- 2023-2024, University of Politecnico di Milano, Architecture, Built Environment and Construction Engineering Department, Italy, Milano, Visiting PhD
- 2016-2019, Eskişehir Technical University, Institute of Graduate Programs /Engineering Faculty, Civil Engineering Department, Master of Science
- 2011-2016, Anadolu University, Engineering Faculty, Civil Engineering Department, Bachelor of Science

Professional Background:

- 2025-present, R&D Engineer, TIS, Technological Isolation Systems, Ankara.
- 2024-2025, Lecturer, Porsuk Vocational School, Eskişehir Technical University, Eskişehir.
- 2020-2024, Lecturer, ESQUAKE Seismic Isolator Test Laboratory, Eskişehir Technical University, Eskişehir.

Publications and/or Scientific/Artistic Activities:

Projects:

- TÜBİTAK 2214, "Determination of friction properties of a sliding isolation system at low temperatures by means of small-scale slider tests", 2023-2024.
- UDAP-Ç-21-35, "Change in Mechanical Properties of a Double Concave Sliding Isolator Under Different Loading Conditions", 2021-2023.
- TÜBİTAK 1001, "Effect of Exposure Time to Low Air Temperature on both Seismic Isolator Characteristics and Structural Response", 2020-2022.

- TÜBİTAK 1002, “Sensitivity of Scale Factors and Dynamic Analysis Results to Change in Methodology of Scaling”, 2018-2019.
- Anadolu University Research Project, “Sensitivity of Scale Factors Computed for Ground Motions Used in Dynamic Analyses to Ground Motion Orientation”, 2017-2018.
- TÜBİTAK 2209, “Change in Maximum Isolator Displacements of LRBs due to Change in Orientation of Scaled Near Field Ground Motions”, 2015.

Publications in Refereed Journals:

15. **Çavdar** E., Özdemir G., Bruschi E., Quaglini V., Özçamur U. “A unified model for estimation of the friction coefficient of sliding isolators by means of small-scale tests” (*Under review*)

14. **Çavdar** E., Özdemir G., Bruschi E., Quaglini V., Özçamur U. “Dynamic Friction Coefficient of Sliding Isolators at Different Low Temperatures and Exposure Times” (*Under review*)

13. Karuk V., Yaşar C., **Çavdar** E., Özdemir G., 2024. “Combined Effect of Low Temperature and Exposure Time on Seismic Performance of an LRB-Isolated Bridge”, *Journal of Bridge Engineering*, 29(12), p. 04024092.

12. **Çavdar E.**, Özdemir G., Quaglini V., Bruschi E., Özçamur U., 2024. “Friction Coefficient of Sliding Isolators in Icing Conditions”, *Structures*, Vol. 63, p. 106369.

11. Yaşar, C., Karuk, V., **Cavdar, E.**, Ozdemir, G., 2024. “Modifications in both lead and rubber properties of LRBs at low temperatures considering the size effect”, *Engineering Structures*, 307, 117902.

10. Ozturk, H., **Cavdar, E.**, Ozdemir, G., 2023. "Effectiveness of Seismic Isolation in a Reinforced Concrete Structure with Soft Story", *Structural Engineering and Mechanics,* 87(5), 405-418.

9. **Çavdar, E.**, Quaglini, V., Özdemir, G., Karuk, V., Bruschi, E., Özçamur, U., 2023. "Experimental Investigation of Wear Effects on the Friction Coefficient of a Curved Surface Slider: Comparison of Small- and Full-Scale Tests ", *Journal of Earthquake Engineering*, 1-20.

8. Yaşar, C., Karuk, V., **Cavdar, E.**, Ozdemir, G., 2023. "Variation in Mechanical Properties of a Lead–Rubber Bearing Exposed to Low Temperature". *Journal of Cold Regions Engineering*, 37(3), 04023012.

7. Yasar, C., Karuk, V., Kaplan, O., **Cavdar, E**., Ozdemir G., 2023. "Amplification in Mechanical Properties of a Lead Rubber Bearing for Various Exposure Times to Low Temperature", *Buildings*, 13 (2), 478.

6. **Cavdar, E**., Ozdemir G., 2022. "Amplification in Maximum Isolator Displacement of an LRB Isolated Building due to Mass Eccenticity", *Bulletin of Earthquake Engineering*, 20 (1), 607-631.

5. **Çavdar, E**., Ozdemir G., Karuk, V., 2022. "Modification in Response of a Bridge Seismically Isolated with Lead Rubber Bearings Exposed to Low Temperature", *Teknik Dergi*, 33 (5), 1-24.

4. Erdoğdu, H., **Cavdar, E**., Ozdemir G., 2021. "Comparison of Design Spectra in Turkish Earthquake Codes (TEC and TBEC) in terms of Seismic Isolator Design ", *Teknik Dergi*, 32 (5), 11127-11152, doi: 10.18400/tekderg.713068.

3. **Cavdar, E**., Ozdemir G., 2020. "Using Maximum Direction of a Ground Motion in a Code-Compliant Analysis of Seismically Isolated Structures", *Structures*, 28, 2163-2173.

2. **Çavdar, E**., Ozdemir G., Bayhan, B., 2019. "Significance of Ground Motion Scaling Parameters on Amplitude of Scale Factors and Seismic Response of Short- and Long-Period Structures", *Earthquake Spectra*, 35(4), 1663-1688.

1. **Cavdar E**., Ozdemir G., 2018. "Change in Maximum Isolator Displacements due to Change in Orientation of Scaled Near Field Ground Motion Records ", *Journal of the Faculty of Engineering and Architecture of Gazi University*, 33(2), 585-598.

Publications in International Conferences

22. Özdemir G., Yaşar C., Karuk V., Çavdar E., 2024. "Contribution of Lead to Stiffness of an LRB at Low Temperatures with an Emphasis to Size Effect", *18th World Conference on Earthquake Engineering,* 30 Jun- 5 July 2024, Milano, Italy.

21. Çavdar E., Özdemir G., Quaglini V., Özcamur, U., 2024. "Investigation on Static Friction Coefficient of a Double Curved Surface Slider", *18th World Conference on Earthquake Engineering,* 30 Jun- 5 July 2024, Milano, Italy.

20. Özdemir G., Ağlan F., Gelmez A., Dilek B., Çavdar E., 2023. "Effect of Mass Irregularity on Seismic Performance of a Base-Isolated RC Building", *15th International*

Congress on Advances in Civil Engineering, 6-8 September 2023, Famagusta, North Cyprus.

19. Quaglini V., Bruschi E., Çavdar E., Özdemir G., Karuk V., Özçamur U., 2023. “Effects of wear on the friction coefficient of a Curved Surface Slider”, *8th International Symposium on Life-Cycle Civil Engineering*, 2-6 July 2023, Milano, Italy.

18. Karuk V., Yasar C., Cavdar E., Ozdemir G., 2022. “Performance Assessment of a Bridge Seismically Isolated with Lead Rubber Bearings at Low Temperature”, *17th World Conference on Seismic Isolation, Energy Dissipation and Active Vibration Control of Structures*, 11-16 September 2022, Torino, Italy.

17. Cavdar E., Ozdemir G., Ozcamur, U., 2022. “Experimental Investigation on Hysteretic Behavior of a Double Friction Pendulum and Frictional Heating”, *17th World Conference on Seismic Isolation, Energy Dissipation and Active Vibration Control of Structures*, 11-16 September 2022, Torino, Italy.

16. Solenoglu E., Ciftci T., Cavdar E., Ozdemir G., 2021. “Influence of Ground Motion Duration on Response of a Lead Rubber Bearing Isolated Structure”, *14th International Congress on Advances in Civil Engineering*, 6-8 September 2021, İstanbul, Turkey.

15. Yasar C., Karuk V., Cavdar E., Ertas M.C., Sorman A.A., Ozdemir G., 2021. “Assessment of Existing Definitions to Estimate Properties of Lead Rubber Bearings Exposed to Low Temperature”, *14th International Congress on Advances in Civil Engineering*, 6-8 September 2021, İstanbul, Turkey.

14. Yasar C., Karuk V., Cavdar E., Ertas M.C., Sorman A.A., Ozdemir G., 2021. “Examination of Mechanical Properties of a Lead Rubber Bearing in Case of Different Ambient Temperatures and Exposure Times”, *6th International Conference on Earthquake Engineering and Seismology*, 13-15 October 2021, Gebze, Turkey.

13. Cavdar E., Ozdemir G., 2021. “Investigation on Both Experimentally and Analytically Obtained Response of a Double Friction Pendulum”, *6th International Conference on Earthquake Engineering and Seismology*, 13-15 October 2021, Gebze, Turkey.

12. Cavdar E., Karuk V., Ozdemir G., 2021. “Adequecy of Property Modification Factors Used to Estimate LRB Response in Case of Low Temperature”, *6th International Conference on Earthquake Engineering and Seismology*, 13-15 October 2021, Gebze, Turkey.

11. Cavdar E., Karuk V., Ozdemir G., 2021. “Variation in Response of a Bridge Seismically Isolated with LRBs under the Effect of Low Ambient Temperature”, *8th International Conference on Computational Methods in Structural Dynamics and Earthquake Engineering*, 28-30 June 2021, Athens, Greece.

10. Ozdemir G., Cavdar E., Karuk V., 2021. “Effect of Extremely Low Temperature on Mechanical Properties of a Large Size LRB”, *8th International Conference on Computational Methods in Structural Dynamics and Earthquake Engineering*, 28-30 June 2021, Athens, Greece.

9. Cavdar E., Ozdemir G., Kale O., 2020. “Variation of Near Fault Ground Motion Intensity Measures Due to Filtering”, *4th International Symposium on Natural Hazards and Disaster Management*, 24-25 October 2020, Bursa, Turkey.

8. Cavdar E., Ozdemir G., 2020. “Sürtünmeli Yüzeyli Sismik İzolatörler İçin Yeni Bir Kayıcı Yüzey Geliştirilmesi”, *7th International Fiber and Polymer Research Symposium*, 25-26 September 2020, Bursa, Turkey.

7. Cavdar, E., Ozdemir, G., 2019. “On the Seismic Response of a Mass Eccentric Structure Seismically Isolated by LRB”, *International Civil Engineering and Architecture Conference*, 17-20 April 2019, Trabzon, Turkey.

6. Cavdar, E., Ozdemir, G., 2019. “On the Maximum Ground Motion Direction and Response of Seismically Isolated Structures, *16th World Conference on Seismic Isolation, Energy Dissipation and Active Vibration Control of Structures*, 01-06 July 2019, St. Petersburg, Russia.

5. Cavdar, E., Ozdemir, G., 2019. “Sensitivity of Scale Factors to Parameters Used in Ground Motion Scaling Method”, *VI. International Earthquake Conference Kocaeli*, 25-27 September 2019, Kocaeli, Turkey.

4. Karuk, V., Cavdar, E., Ozdemir, G., 2019. “Influence of Ambient Temperature on Properties of a Double-Core Lead Rubber Bearing, 5th International Conference on Earthquake Engineering and Seismology, 08-11 October 2019, Ankara, Turkey.

3. Erdogdu, H., Cavdar, E., Ozdemir, G., 2019. “Comparison of 2007 And 2018 Turkish Earthquake Codes: Design of a Seismically Isolated Structure, 5th International Conference on Earthquake Engineering and Seismology, 08-11 October 2019, Ankara, Turkey.

2. Cavdar E., Ozdemir G., 2017. “On the Orientation of Ground Motions and Their Scaling in Accordance with Code Provisions”, 7th International Conference on Advances in Experimental Structural Engineering, 6-8 Eylül 2017, Pavia, İtalya.

1. Çavdar E., Özdemir G., 2017. “Ölçeklendirilen Deprem Hareketlerinin Farklı Doğrultularda Etkimesi Durumunda Kurşun Çekirdekli Kauçuk İzolatörlerde Gözlenen Maksimum Deplasman Değerlerindeki Değişim”, 4th International Conference on Earthquake Engineering and Seismology, 11-13 Ekim 2017, Eskişehir, Türkiye.

Publications in National Conferences

3.Şimşek A., Çavdar E., Özdemir G., 2022. “Mafsallı Kayıcı Çekirdek Kullanımının Eğri Yüzeyli Sürtünmeli Yalıtım Birimi Davranışı Üzerindeki Etkileri”, 8. Yapı Mekaniği Laboratuvarları Çalıştayı, 14-15 Ekim 2022, Türkiye.

2. Yaşar C., Karuk V., Çavdar E., Özdemir G., 2022. “Kurşun Çekirdekli Kauçuk İzolatör Bileşenlerinin Düşük Sıcaklıklardaki Davranışlarının Ayrı Ayrı Test Edilmesi İçin Deneysel Bir Çalışma”, 8. Yapı Mekaniği Laboratuvarları Çalıştayı, 14-15 Ekim 2022, Türkiye.

1. Çavdar E., Özdemir G., 2019. “Düşük Dış Ortam Sıcaklığına Maruz Kalma Süresinin Sismik İzolatör Mekanik Özellikleri Üzerindeki Etkisi” 7. Yapı Mekaniği Laboratuvarları Çalıştayı, 4-5 Ekim 2019, Türkiye.